

Electrostatic Solitary Waves in Space Plasmas and in Planetary Environments: an overview

Yannis Kourakis

Khalifa University of Science and Technology, Abu Dhabi, UAE
KU Space and Planetary Sciences Center, Abu Dhabi, UAE

ioannisKourakisSci@gmail.com, ioannis.kourakis@ku.ac.ae

Earlier work in collaboration with:

Ibrahem Elkamash, Mansoura University, Faculty of Sciences, Department of Physics, Egypt
and **Brian Reville**, Max-Planck Institute for Nuclear Physics, Heidelberg, Germany

Special thanks: Kuldeep Singh, Steffy Varghese (SPSC), Hans Huybrighs (SPSC), Nikos Lazaridis, (ex) Amaria Javed
(aka the KU joint SPSC/KU-plasma team),
Panos Kevrekidis (Amherst, MA USA), Efstathios Charalampidis (California Polytechnic State U.,US)

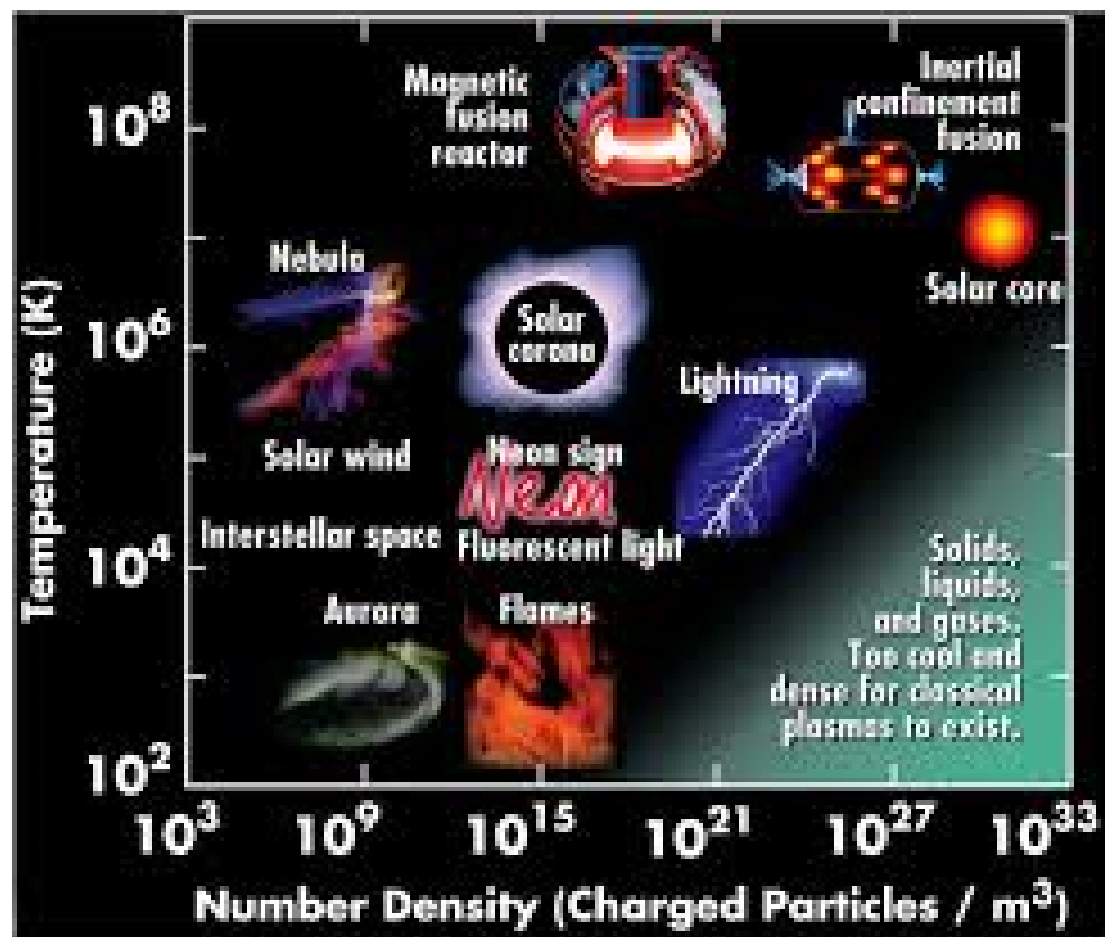
Acknowledgment: projects *ASPIRE* (ex-ADEK) (AARE grant ADEK/HE/157/18) UAE; **FSU-2021-012** (8474000352), **CIRA-2021-064** (8474000412) and **KU-SPSC-8474000336** (*KU Space and Planetary Science Center/SPSC*), funded by Khalifa University of Science & Technology, Abu Dhabi, UAE.

Preamble

- Plasma preliminaries
- Nonlinear modeling: kinetic vs fluid vs computational modeling
- 1D fluid model for electrostatic solitary waves
 - Perturbative vs non-perturbative approach
- 1D fluid model for envelope structures in plasmas
 - Derivation of a nonlinear Schrodinger equation
 - Rogue-waves, parametric investigation
- Summary

Plasma is everywhere! In Nature ...





Multi-ion plasma: basics, fluid modeling

- Large ensemble of charged particles:

- Electrons e^- : charge e mass m_e ($\ll m_i$)
- Ions i^+ : charge $+z_p e$ mass m_p
- Ions i^- : charge $-z_n e$ mass m_n

- Three components (“fluids”); state variables of choice:

- Ions +: finite inertia (dynamic fluid state): density $n_p(x, t)$, speed $\mathbf{u}_p(x, t)$
- Ions -: finite inertia (dynamic fluid state): density $n_n(x, t)$, speed $\mathbf{u}_n(x, t)$
- Electrons: inertia *ignored* (Maxwell-Boltzmann state): density $n_e = n_{e,0} e^{\frac{e\phi}{k_B T_e}}$

- Self-generated electric field: $\mathbf{E} = -\nabla \phi$ ($\phi(x, t)$: electrostatic potential)

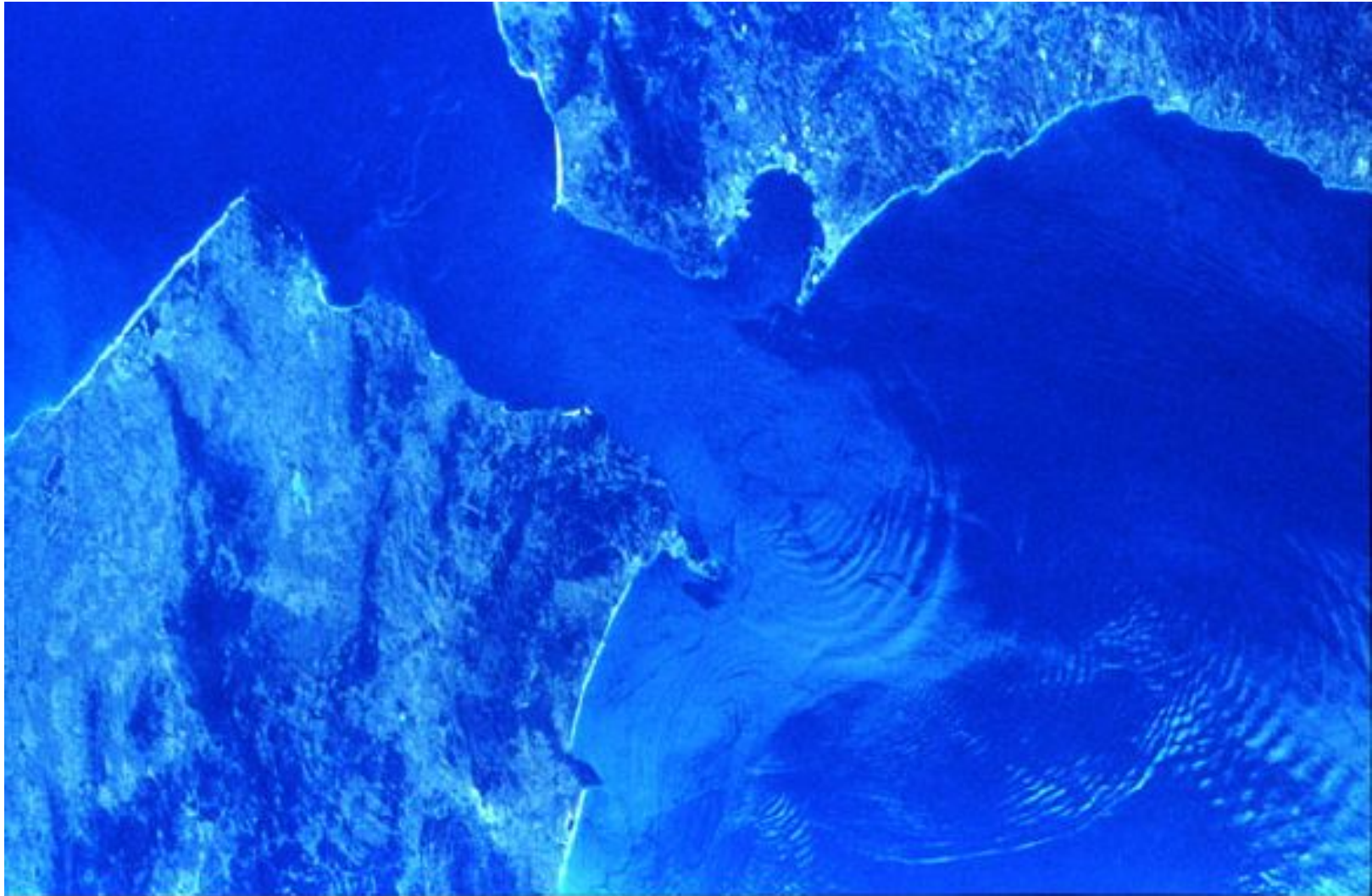
Nonlinear excitations - *Solitary waves (SWs)*

- SWs occur in abundance in Nature, in various physical contexts
- are ***localized coherent structures***, bearing remarkable properties: preserve their shape (stationary profile), are robust, i.e. persist against perturbations and collisions with one another, ...
- represent localized lumps of energy, whose manifestation may be constructive (e.g. signal transmission) or destructive (*tsunami*)
- bear various generic forms and names: ***pulses, kinks, holes, shocks, double layers*** or ***potential dips*** (in plasmas), ...
- may either be non-periodic forms (e.g., pulses) or may possess a quasi-periodic internal structure (e.g., oscillons, envelope pulses, breathers)

Solitary waves crossing on a beach



Ocean solitons east of the Strait of Gibraltar



Internal solitons in the Andaman sea (1)

An Atlas of Oceanic Internal Solitary Waves (February 2004)
by Global Ocean Associates
Prepared for Office of Naval Research – Code 322 PO

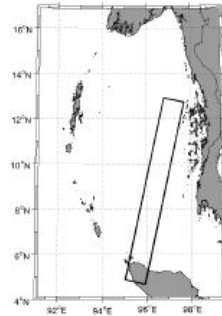
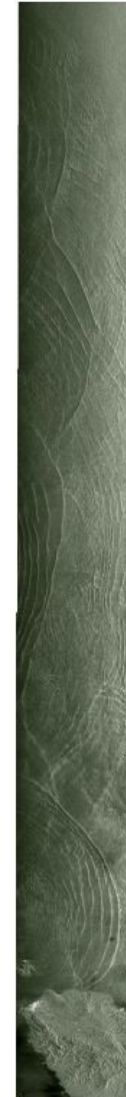
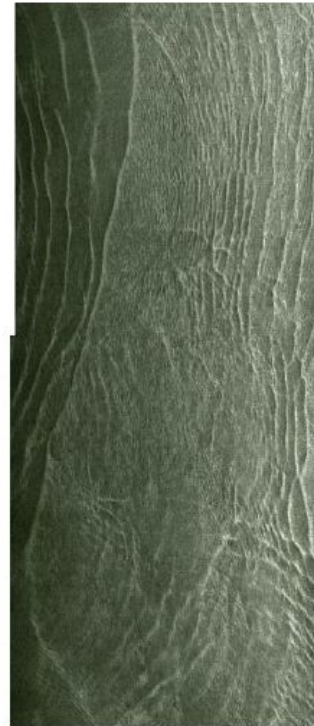


Figure 6. (Right) ERS-2 (C-band, VV) SAR image of the Andaman acquired on 11 February 1997 at 0359 UTC (orbit 9477, frames 3357, 3375, 3393, 3341, 3429, 3447, 3465, 3483, and 3501). The image shows a large number internal wave packets and associated soliton-soliton interaction. Imaged area is 100 km x 900 km. (Below) An enlargement highlighting a middle portion of the image. Imaged area 235 km x 100 km ©ESA 1997.

Andaman Sea



Internal solitons in the Andaman sea (2)

An Atlas of Oceanic Internal Solitary Waves (February 2004)
by Global Ocean Associates
Prepared for Office of Naval Research – Code 322 PO

Andaman Sea

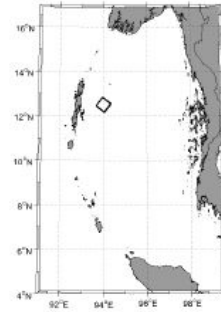
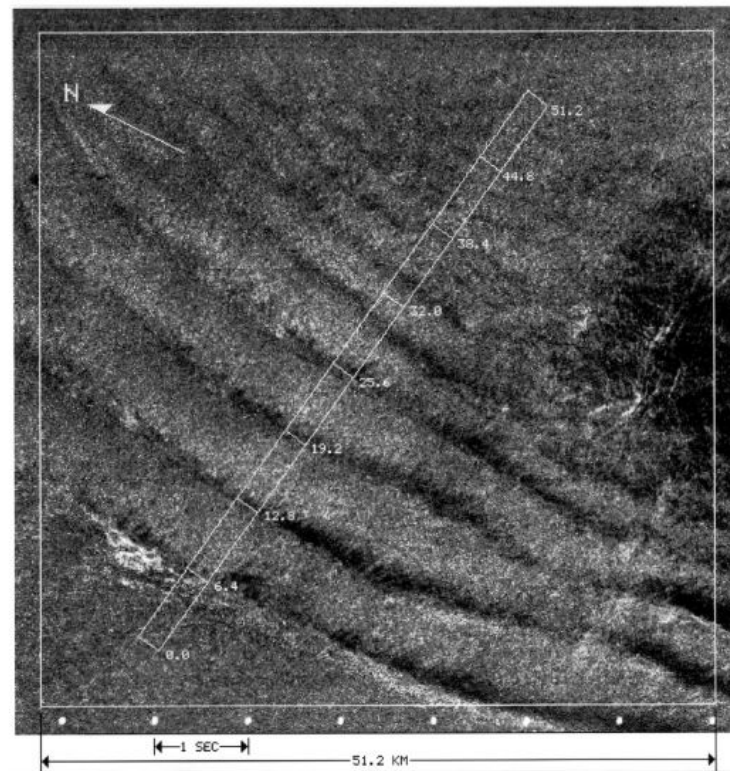
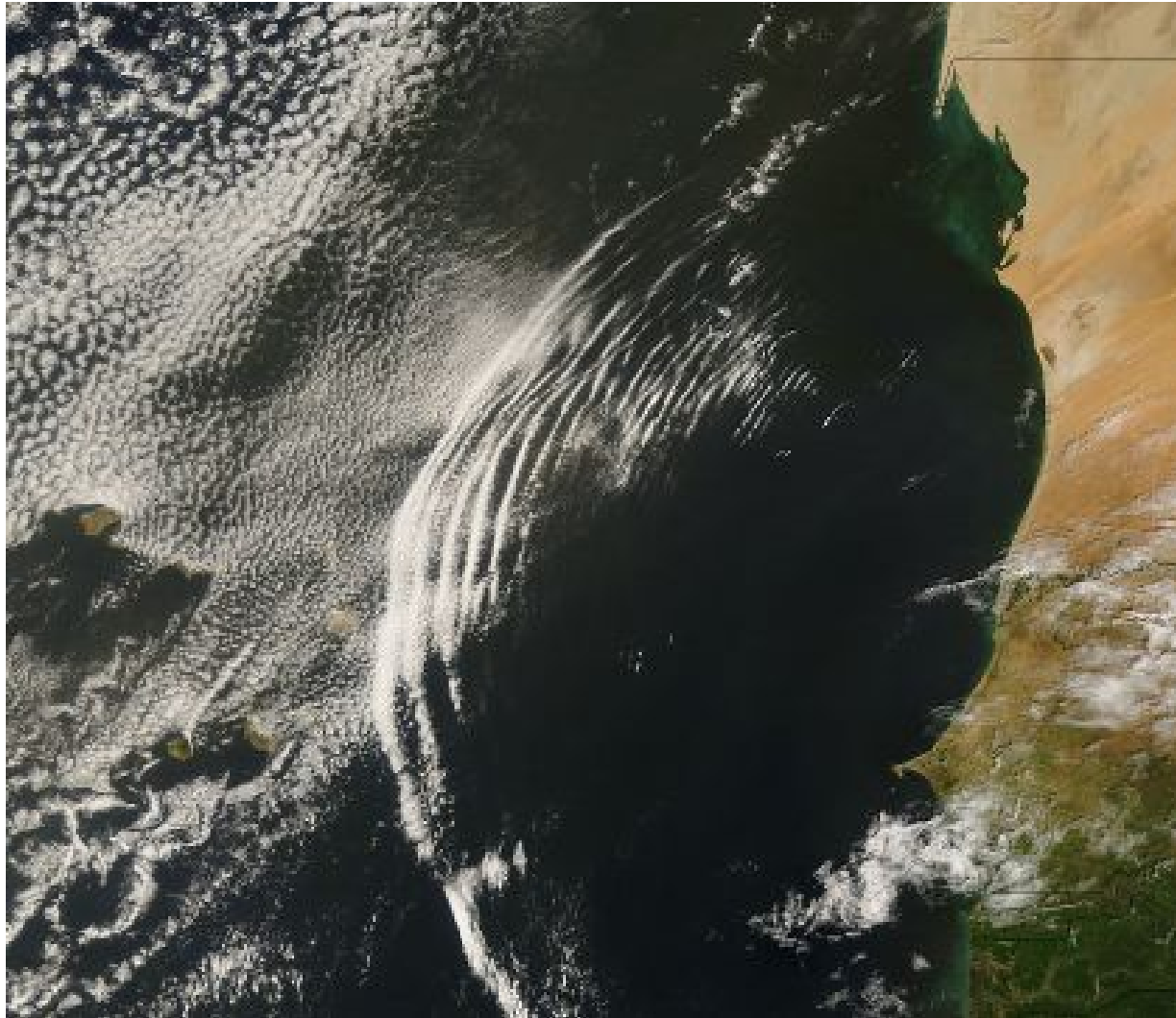


Figure 12. SIR-A (L-band, HH) SAR image near the Andaman Islands acquired on 11 November 1981. The image shows a packet of westward propagating solitons and what is thought to be a rain squall (dark patch at right center). Imaged area is 51.2 km x 51.2 km. [Image courtesy of the Jet Propulsion Laboratory][After Apel et al. 1985]



Solitary clouds west of Africa



Laser plasma experiments on electrostatic waves

PRL 101, 025004 (2008)

PHYSICAL REVIEW LETTERS

week ending
11 JULY 2008

Observation of Collisionless Shocks in Laser-Plasma Experiments

L. Romagnani,^{1,*} S. V. Bulanov,^{2,3} M. Borghesi,¹ P. Audebert,⁴ J. C. Gauthier,⁵ K. Löwenbrück,⁶ A. J. Mackinnon,⁷
P. Patel,⁷ G. Pretzler,⁶ T. Toncian,⁶ and O. Willi⁶

¹*School of Mathematics and Physics, The Queen's University of Belfast, Belfast, Northern Ireland, United Kingdom*

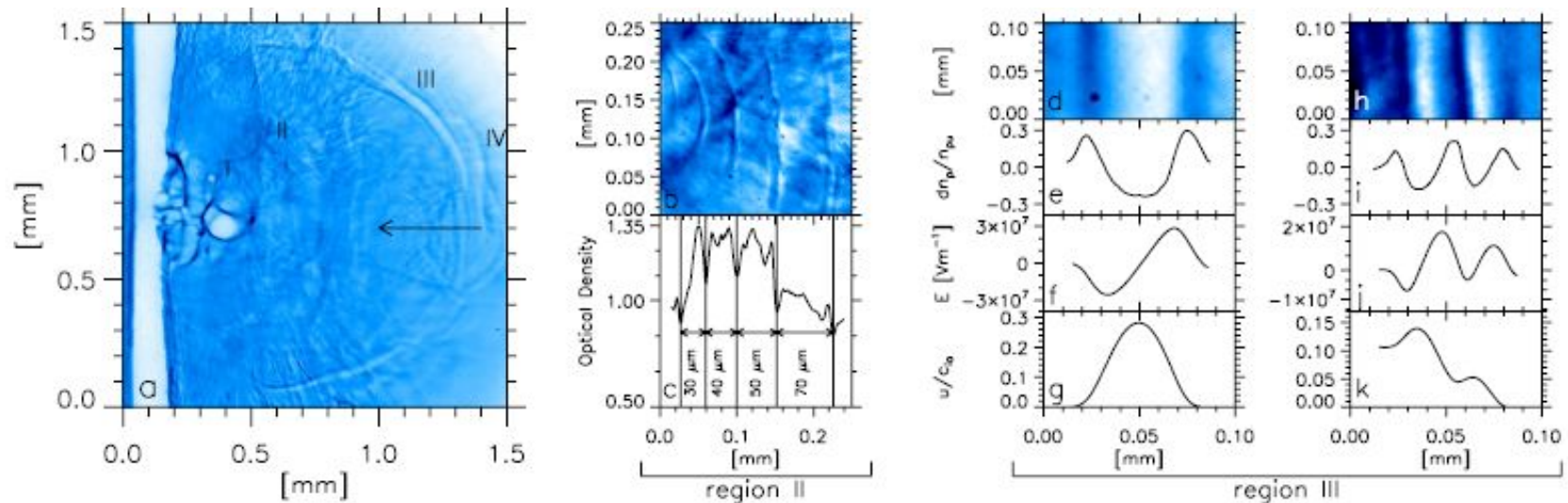


FIG. 1 (color online). (a) Typical proton imaging data taken at the peak of the interaction pulse with protons of 7 MeV energy. Note the strong modulation associated with the ablating plasma in the region I and the modulated pattern ahead of the shock front possibly associated with a reflected ion bunch in the region IV. The arrow indicates the laser beam direction. (b)–(c) Detail and RCF optical density lineout corresponding to the region II showing modulations associated with a train of solitons. (d)–(k) Details of the region III and correspondent lineouts of the probe proton density $\delta n_p/n_{pa}$, reconstructed electric field E , and reconstructed normalized ion velocity u/c_{ia} in the case of an ion acoustic soliton (d)–(g) and of a collisionless shock wave (h)–(k) (the collisionless shock detail corresponds to a different shot not shown here for brevity).

Laser plasma experiments on electrostatic waves (2)

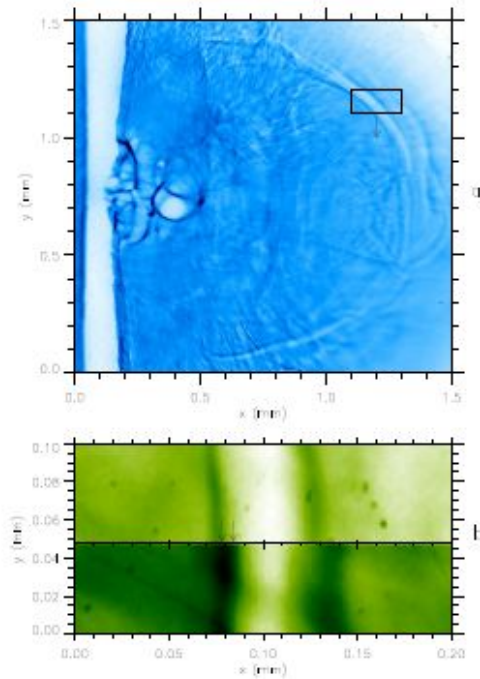


Figure 3.9: a. Proton image showing the ion-acoustic soliton. b Detail of the ion-acoustic soliton at two different times. The relative time between the two frames is ~ 25 ps, and the soliton has moved by $\sim 5 \div 10 \mu\text{m}$.

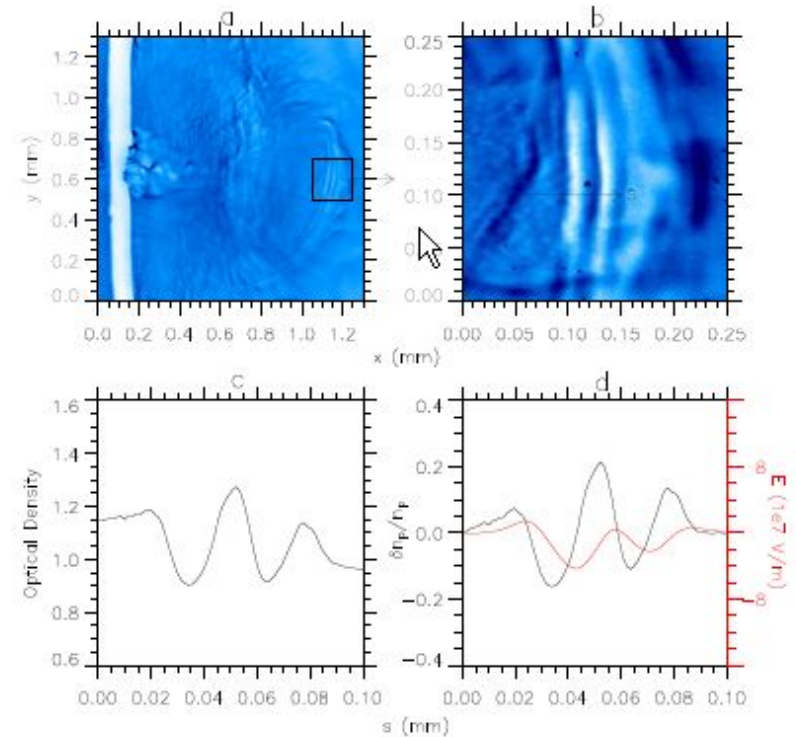


Figure 3.14: a. Proton image taken at the peak of the interaction pulse. b. Detail of the collisionless shock wave. c. Profile of the optical density in the RCF across the collisionless shock. d. Proton density modulation across the shock (black

(courtesy of L Romagnani & M Borghesi, Queen's University Belfast, UK)

Electron-holes observed via proton imaging diagnostics

PHYSICS OF PLASMAS 17, 010701 (2010)

Observation and characterization of laser-driven phase space electron holes

G. Sarri,¹ M. E. Dieckmann,² C. R. D. Brown,³ C. A. Cecchetti,¹ D. J. Hoarty,³ S. F. James,³ R. Jung,⁴ I. Kourakis,¹ H. Schamel,⁵ O. Willi,⁴ and M. Borghesi¹

¹School of Mathematics and Physics, The Queen's University of Belfast, Belfast BT7 1NN, United Kingdom

²ITN, Linköping University, 60174 Norrköping, Sweden

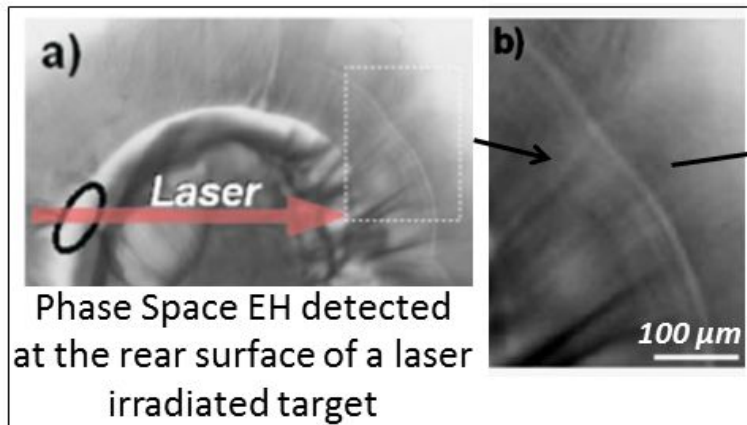
³AWE, Aldermaston, Reading, Berkshire RG7 4PR, United Kingdom

⁴Institute for Laser and Plasma Physics, Heinrich-Heine-University, 40225 Düsseldorf, Germany

⁵Physikalisches Institut, Universität Bayreuth, D-95440 Bayreuth, Germany

(Received 12 November 2009; accepted 15 December 2009; published online 7 January 2010)

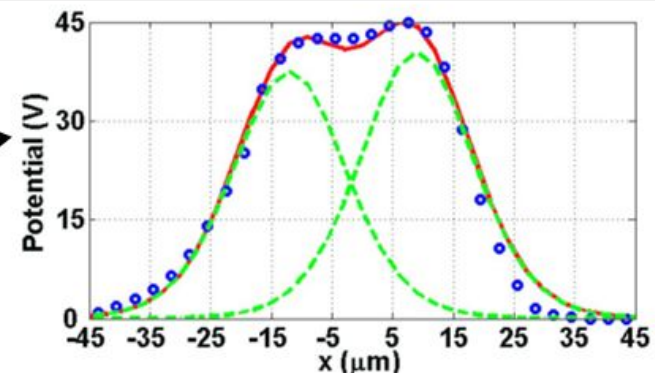
The direct observation and full characterization of a phase space electron hole (EH) generated during laser-matter interaction is presented. This structure, propagating in a tenuous, nonmagnetized plasma, has been detected via proton radiography during the irradiation with a ns laser pulse ($I\lambda^2 \approx 10^{14}$ W/cm²) of a gold *hohlraum*. This technique has allowed the simultaneous detection of propagation velocity, potential, and electron density spatial profile across the EH with fine spatial and temporal resolution allowing a detailed comparison with theoretical and numerical models.



- Incomplete thermalization of the background plasma
- Hot electron population accelerated by the laser



Fit by κ -distributed plasma electron distribution



Potential profile fitted with two bell-shaped, κ -dependent soliton curves:

$$\phi(x) = \phi_{\max} \operatorname{sech}^4 \left(\frac{x}{4\sqrt{\gamma_e}} \right) \quad \kappa\text{-dependent parameter: } \kappa \sim 4$$

Shock creation and particle acceleration driven by plasma expansion into a rarefied medium

G. Sarri,¹ M. E. Dieckmann,² I. Kourakis,¹ and M. Borghesi¹

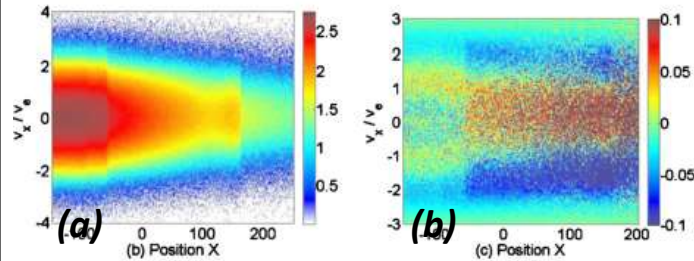
¹Centre for Plasma Physics, The Queen's University of Belfast, Belfast BT7 1NN, United Kingdom

²VITA ITN, Linköping University, 60174 Norrköping, Sweden

(Received 26 March 2010; accepted 6 July 2010; published online 19 August 2010)

The expansion of a dense plasma through a more rarefied ionized medium is a phenomenon of interest in various physics environments ranging from astrophysics to high energy density laser-matter laboratory experiments. Here this situation is modeled via a one-dimensional particle-in-cell simulation; a jump in the plasma density of a factor of 100 is introduced in the middle of an otherwise equally dense electron-proton plasma with a uniform proton and electron temperature of 10 eV and 1 keV, respectively. The diffusion of the dense plasma, through the rarefied one, triggers the onset of different nonlinear phenomena such as a strong ion-acoustic shock wave and a rarefaction wave. Secondary structures are detected, some of which are driven by a drift instability of the rarefaction wave. Efficient proton acceleration occurs ahead of the shock, bringing the maximum proton velocity up to 60 times the initial ion thermal speed. © 2010 American

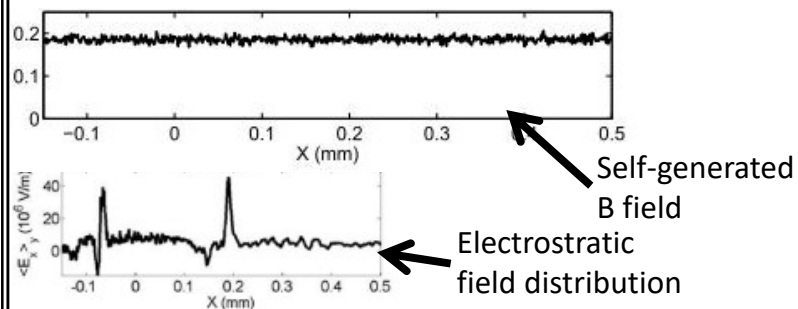
Non-Maxwellian behaviour of the electron density distribution of a plasma expanding into a rarefied medium has been seen in PIC sims



(a) Phase space of the expanding electrons.
(b) Electron distribution function normalised to a Maxwellian with same density and temperature.

Non-thermality generated by the counterstreaming electrons of the rarefied medium.

Suppression of Weibel instability → electrostatic plasma evolution



Clear difference from expansion into vacuum!

ESWs in Space?

It all started with the Northern Lights...

Auroras are the result of disturbances in the magnetosphere caused by the solar wind.

Major disturbances result from enhancements in the speed of the solar wind from coronal holes and coronal mass ejections.

These disturbances alter the trajectories of charged particles in the magnetospheric plasma.

Excerpt from <https://en.wikipedia.org/wiki/Aurora> .

Live visual sample: <https://www.youtube.com/watch?v=izYiDDt6d8s> .

Double Layers in Space observations – history...

- Mozer et al [PRL 1977] were the first to provide an interpretation of S3-3 satellite data *in the aurora* as double layers (DLs):

Observations of Paired Electrostatic Shocks in the Polar Magnetosphere*

F. S. Mozer, C. W. Carlson, M. K. Hudson, R. B. Torbert, B. Parady, and J. Yatteau
Physics Department and Space Sciences Laboratory, University of California, Berkeley, California 94720

and

M. C. Kelley
School of Electrical Engineering, Cornell University, Ithaca, New York 14854
(Received 6 December 1976)

dc and ac plasma-density and vector-electric-field detectors on a polar orbiting satellite have measured spatially confined regions of extremely large ($\sim \frac{1}{2}$ V/m) electric fields in the auroral zone at altitudes below 8000 km. Such regions frequently have double structures of opposing electric fields containing characteristic and different wave spectra internal and external to themselves. These structures are identified as paired electrostatic shocks which are associated with electrostatic ion cyclotron wave turbulence.

The S3-3 satellite was launched during the summer of 1976 into a nearly polar orbit with perigee and apogee altitudes of 260 and 8050 km, respectively. On-board instruments have made the first *in situ* measurements of dc electric fields at auroral latitudes and altitudes where particle-acceleration, kilometeric-radiation-generation,

measured potential differences yield three orthogonal components of the static or fluctuating electric field. Four of the spheres are located at the ends of four 18-m wire booms that are maintained in the satellite spin plane by centrifugal force. The remaining pair of spheres are oriented along the vehicle spin axis on 3-m rigid

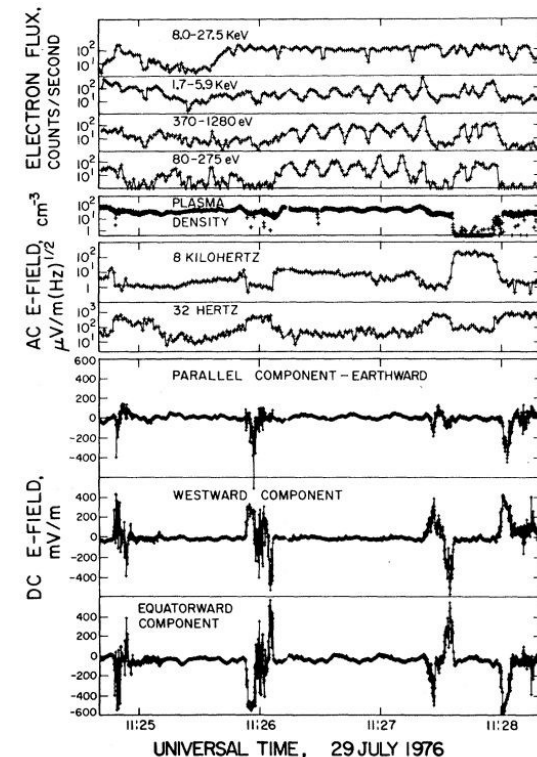


FIG. 1. Field and particle measurements made on a satellite during its poleward-bound passage through extremely large dc-electric-field regions in the northern auroral zone. The particle data are modulated at twice the satellite spin frequency.

DLs vs Electrostatic Shocks & Solitary Waves

- Inspired by Mozer et al [PRL 1977], Witt and Lotko [Phys. Fluids, 1978] modelled pulse-shaped observations as *paired* ion-acoustic shocks:

Ion-acoustic solitary waves in a magnetized plasma with arbitrary electron equation of state

E. Witt and W. Lotko

Space Sciences Laboratory, University of California, Berkeley, California 94720

(Received 17 August 1982; accepted 6 April 1983)

The oblique propagation of fully nonlinear, slow ion-acoustic solitary waves in a collisionless, low-beta, magnetized plasma is examined. The analysis includes the effects of a finite ion pressure, electron trapping, and multicomponent particle populations. The existence of both compressive and rarefactive modes propagating obliquely to the magnetic field in a plasma with two distinct Boltzmann electron populations and cold ions is demonstrated. It is shown that paired electrostatic shocks observed over the Earth's auroral zone may be closely related to the rarefactive modes. As a measure of the collisionless dissipation encountered by the solitary waves, the linear response of the plasma to slow ion-acoustic waves is also examined.

I. INTRODUCTION

Ion-acoustic solitary waves have been observed in laboratory plasmas, and much progress has been made in theory. Unmagnetized versions of these waves have been extensively studied. (See Tran¹ for a review.) It is also of interest to determine how a magnetic field affects the propagation of these waves. One motivation comes from the field of space physics. Recent electric field measurements^{2,3} in space indicate that localized nonlinear plasma waves generally accompany and are possibly responsible for the acceleration of auroral particles to kilovolt energies. The observed waves, referred to as paired electrostatic shocks, propagate at speeds much less than the electron thermal speed, suggesting that they may be related to nonlinear electrostatic waves propagating as slow or intermediate modes.⁴ Numerical studies⁵⁻⁷ of

In this paper we present the first finite-amplitude, magnetized analysis of nonlinear ion-acoustic waves in which $N_e(\Psi)$ is arbitrary and in which the ions may have a finite temperature. As in previous treatments, the nonlinear plasma response is described by time stationary fluid equations for the relatively cold ions and by Poisson's equation in the quasineutral approximation. The quasineutral approximation allows us to study only waves with finite angles of propagation relative to the uniform magnetic field, and the approximation requires the solutions to have "slowly changing" electric fields. This is discussed in more detail in Sec. II. Our treatment, for arbitrary $N_e(\Psi)$, allows us to make general statements about the resulting nonlinear wave solutions. For instance, previous authors have found, using the Boltzmann electron approximation, that waves can exist only when their speed v_p lies in the range $c_s \cos \theta < v_p < c_s$, where θ is the angle of propagation relative to the magnetic

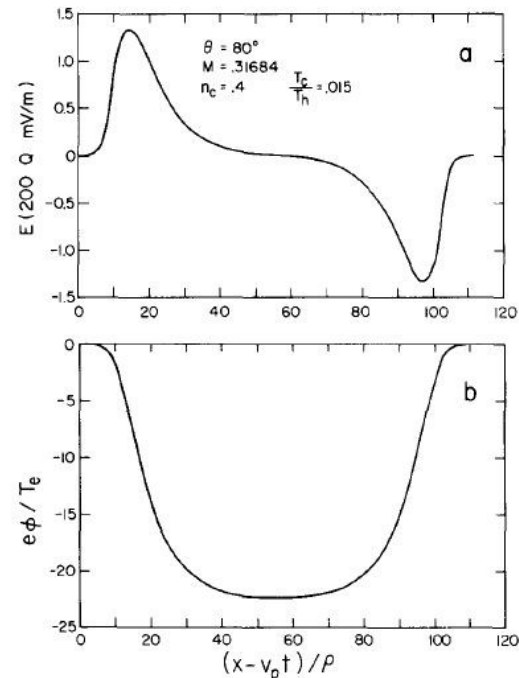


FIG. 7. Numerical solitary wave solution of Eq. (17) for a two-temperature Boltzmann electron and cold ion plasma model. The wave is rarefactive and propagates at $\theta = 80^\circ$ relative to the magnetic field. Other parameters of the solution are indicated in the figure. (a) Electric field in units of $200 Q$ mV/m where $Q = (f_{ei}/100 \text{ Hz})(T_e/10 \text{ eV})^{1/2}$. For example, when $f_{ei} = 100 \text{ Hz}$ and $T_e = 10 \text{ eV}$, the peak electric field is about 280 mV/m . (b) Normalized electric potential profile.

Electrostatic Solitary Waves (ESWs) – history...

- ESWs –to be distinguished from DLs–were first observed in the auroral region in 1982 [Temerin et al, PRL 1982], using satellite S3-3 data...

VOLUME 48, NUMBER 17

PHYSICAL REVIEW LETTERS

26 APRIL 1982

Observations of Double Layers and Solitary Waves in the Auroral Plasma

M. Temerin, K. Cerny, W. Lotko, and F. S. Mozer

Space Sciences Laboratory, University of California, Berkeley, California 94720

(Received 29 January 1982)

Small-amplitude double layers and solitary waves containing magnetic-field-aligned electric field components have been observed for the first time in the auroral plasma between altitudes of 6000 and 8000 km in association with electron and ion velocity distributions that indicate the presence of electric fields parallel to the magnetic field. The double layers may account for a large portion of the parallel potential drop that accelerates auroral particles.

PACS numbers: 53.35.Fp, 52.35.Mw, 94.30.Gm

Double layers, small localized regions of a single electric field polarity, have been studied analytically,¹ but until now have been observed only in computer simulations² and in laboratory plasmas.³ We report the first observation of small-amplitude double layers in a naturally occurring plasma. These double layers differ from the previously reported electrostatic shocks⁴

in that their electric field is much smaller (typically no greater than 15 mV/m), their electrostatic polarization relative to the magnetic field is predominantly parallel rather than perpendicular, and the duration of an individual double layer is much shorter—typically 2–20 ms rather than 0.1–10 s for the electrostatic shocks. The dominant polarity of the electric field through an

ESWs: a common occurrence in Space plasma observations

- ESWs occur in abundance as magnetic-field aligned *bipolar* electric field structures (among other forms), observed in abundance in satellite data (Cluster, FAST, ...)
- Solitary waves: potential pulses, solitons, double layers, flat-topped pulses, ...

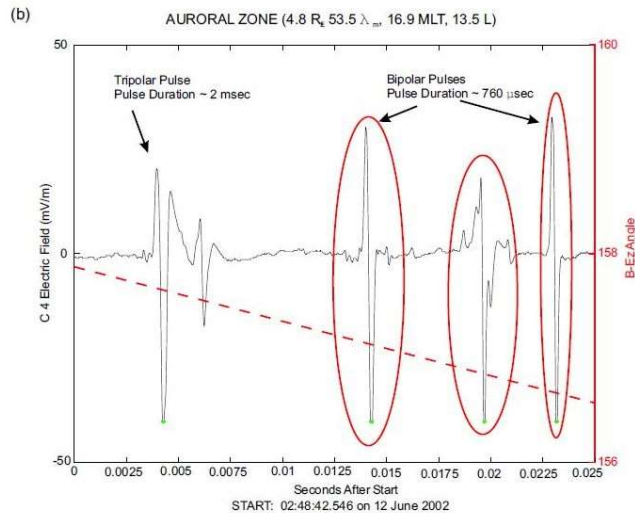


Fig. 1. Cluster WBD data taken on 12 June 2002 in the auroral zone. (a) Spectrogram showing the frequency and power spectral density of the emissions. The broad-band signals ranging up to about 10 kHz are indicative of times when IES are observed. (b) Representative waveform from a time of the broad-band signals, showing the two types of IES: bipolar and tripolar pulses.

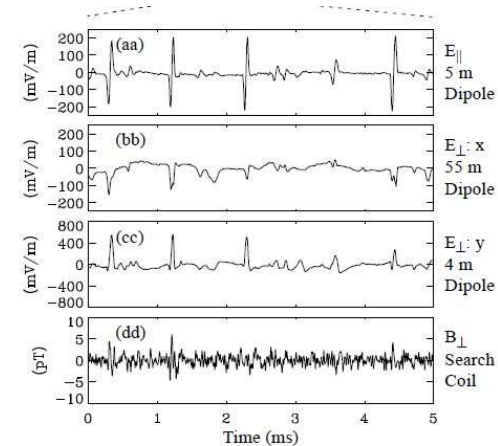


Figure 5. (From [5]) (a) The electric field parallel to B_0 . (b) The electric field perpendicular to B_0 (ΔE_{\perp}) and in the spin plane of the satellite. This signal, measured by a 56 m dipole antenna, appears attenuated, indicating that the structure size may have been < 112 m. (c) ΔE_{\perp} along the spin axis of the satellite. (d) A perturbation magnetic field perpendicular to B_0 (ΔB_{\perp}). ΔB_{\perp} was filtered to a pass band (3 kHz–16 kHz) to expose the weak signals and therefore may not appear unipolar in this figure. (aa)–(dd) An expanded view of this data.

Figures from: Pickett *et al* Ann. Geophys. (2004) (L, Cluster), Ergun *et al*, PPCF (1999) (R, FAST)

ESWs near Saturn (Enceladus) - Cassini mission

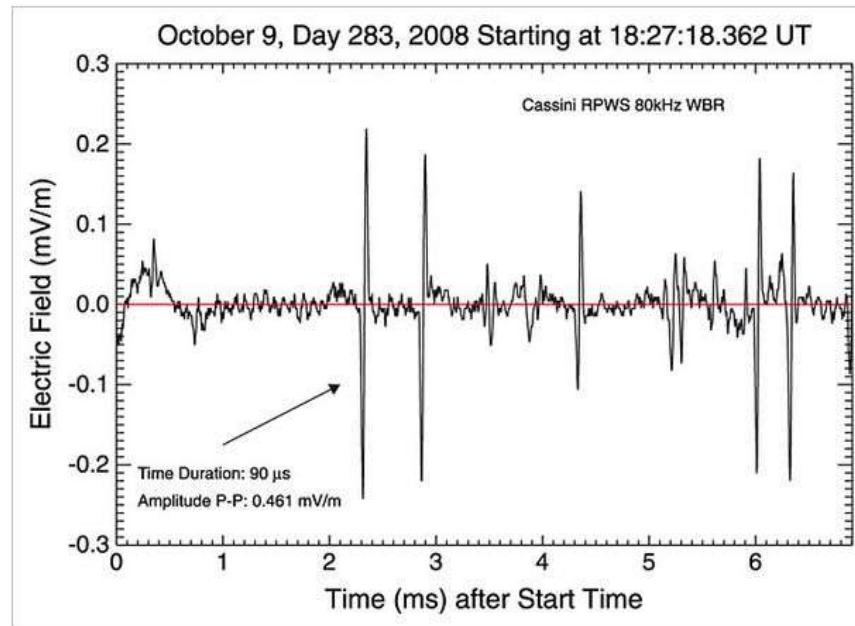


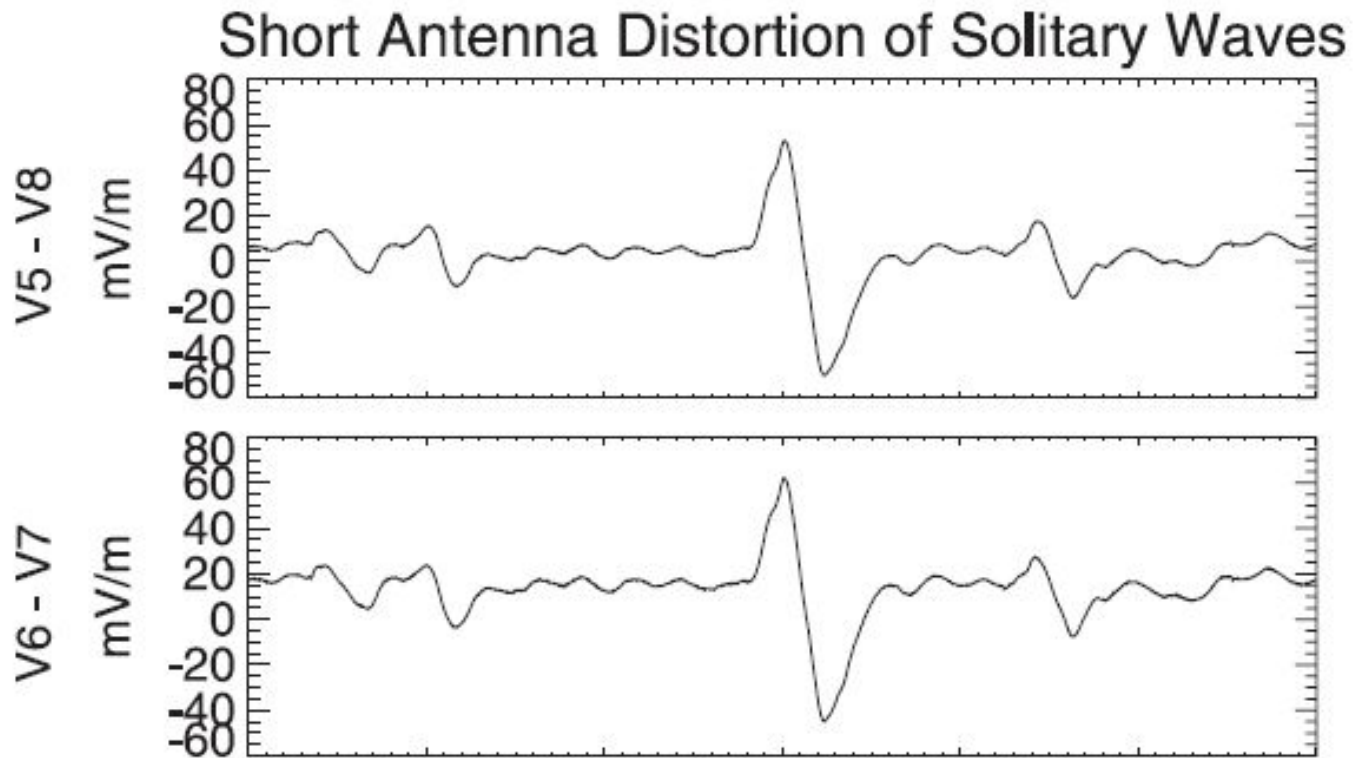
Figure 2

[Open in figure viewer](#) | [PowerPoint](#)

Time series data of the calibrated electric field data over a ≈ 7 ms interval from the Cassini RPWS WBR, 80 kHz filter bandwidth, obtained on 9 October 2008, ~ 0.5 h before crossing the Enceladus dust plume. These data show five well-defined bipolar ESW pulses embedded within a much lower amplitude oscillatory wave. Note that the amplitudes of these ESWs are comparable to those in Figure 1, but their time durations are much shorter.

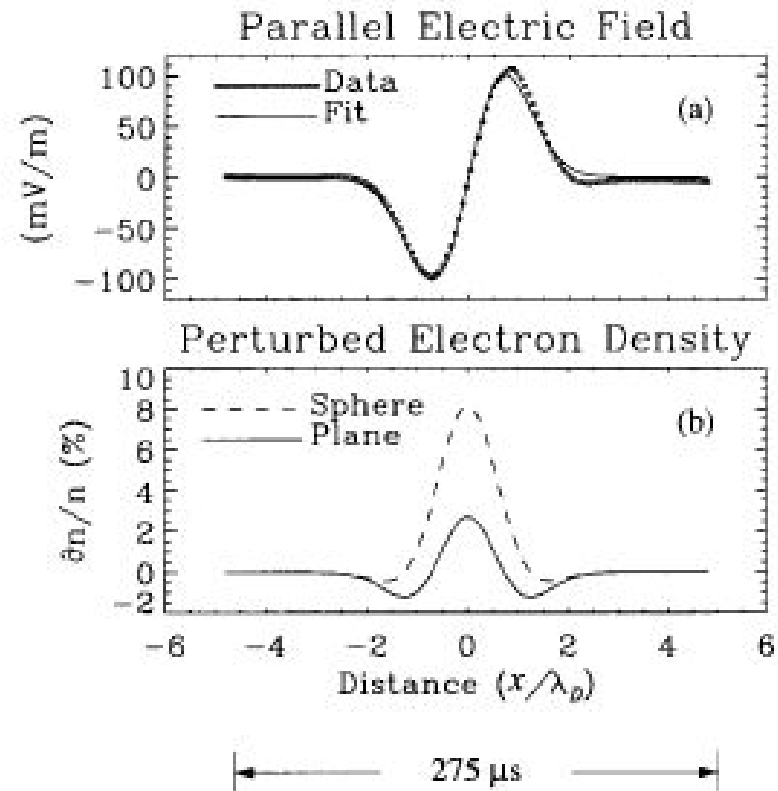
Source: JS Pickett et al, JGR Space Physics **120** (8), 6569 (2015)

FAST satellite observations of large solitary spikes in the Earth's *auroral* region



FAST auroral observations (2)

Ergun, et al.: Properties of fast solitary structures



Nonlinear Processes in Geophysics (1999) 6: 187–194

Properties of fast solitary structures

R. E. Ergun, C. W. Carlson, L. Muschietti, I. Roth, and J. P. McFadden

Space Sciences Laboratory, University of California, Berkeley, CA, 94720, USA

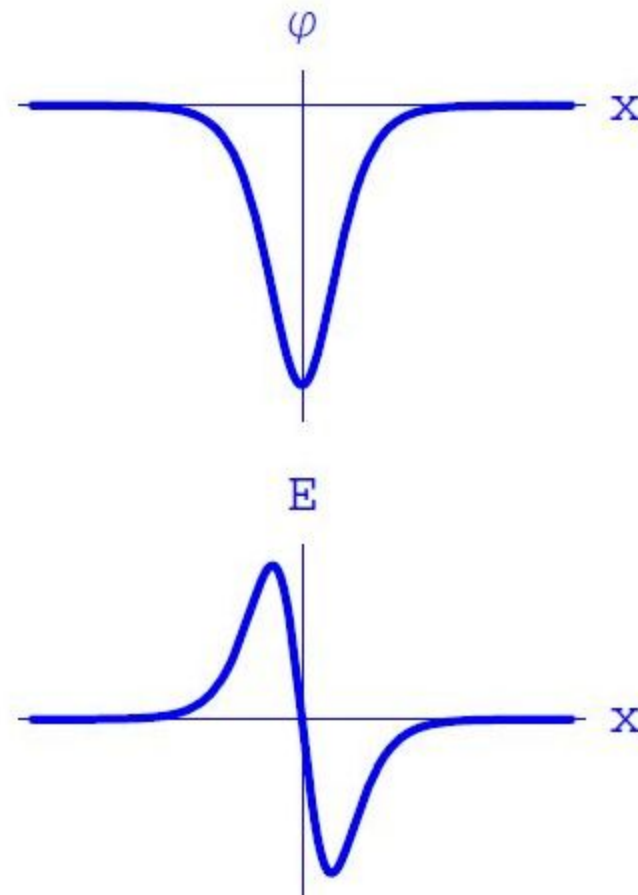
Received: 15 June 1999 – Revised: 6 September 1999 – Accepted: 13 September 1999

Abstract. We present detailed observations of electromagnetic waves and particle distributions from the Fast Auroral SnapshoT (FAST) satellite which reveal many important properties of large-amplitude, spatially-coherent plasma structures known as “fast solitary structures” or “electron phase space holes”. Similar structures have been observed in

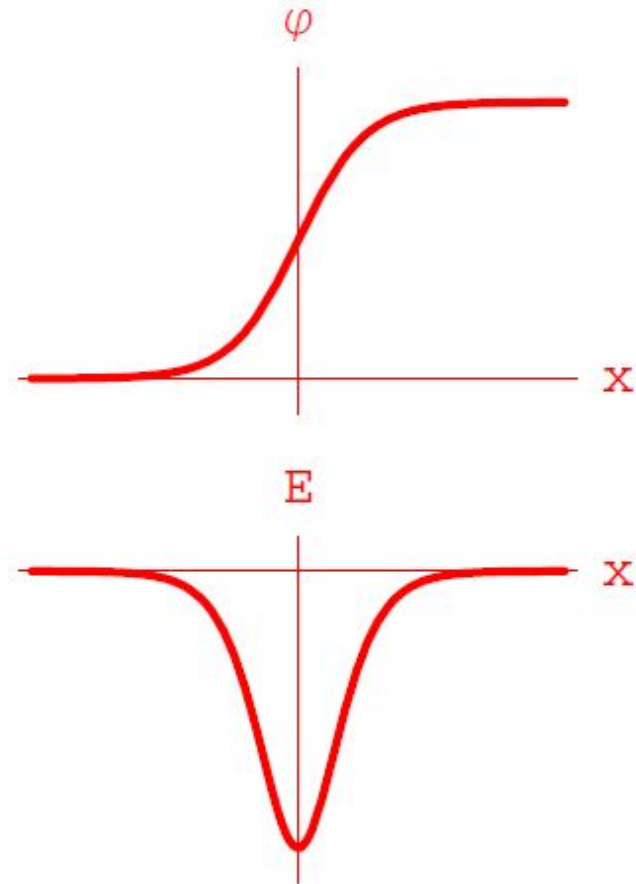
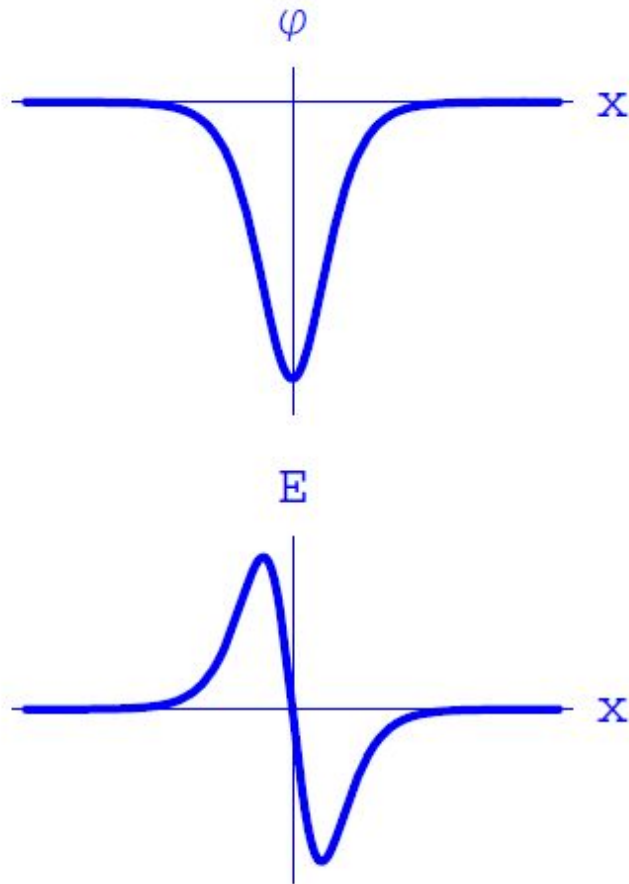
which distinguish acoustic solitons (Ergun et al., 1982). The structure is brief, electrostatic and that FAST has

Fig. 5. (From Ergun et al., 1998c) (a) ΔE_{\parallel} . The dots are the data at $0.5 \mu\text{s}$ resolution translated into Debye lengths assuming a constant parallel velocity, $v_{\text{sol}} = 3.2 \times 10^6$. The smooth trace is the fit to Eq. (2). (b) Calculated charge densities assuming spherical and planar geometry. The plasma conditions were $n_p = 5.7 \pm 2.0 \text{ cm}^{-3}$, $T_{e\parallel} = 704 \pm 145 \text{ eV}$, $v_{\text{sol}} = 3.2 \times 10^6 \pm 1.1 \times 10^6 \text{ m/s}$, $T_{i\perp} = 370 \pm 74 \text{ eV}$, $|B_0| = 11481 \pm 10 \text{ nT}$, $\lambda_D = 82 \pm 30 \text{ m}$, and $\rho_{H^+} = 241 \pm 24 \text{ m}$.

Electrostatic potential and electric field bipolar structures (1)



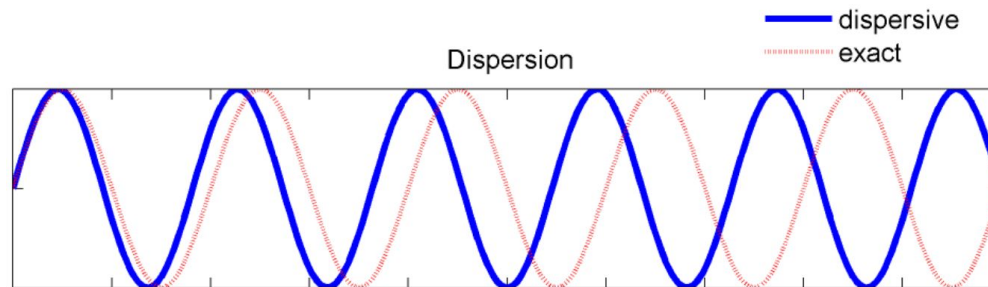
ES potential and E-field: *bipolar* vs *monopolar* structures (2)



Solitary waves require a balance between:

– **Dispersion**, manifested via:

- wave spreading in Fourier space: different modes (\mathbf{k}) travel at different speeds:

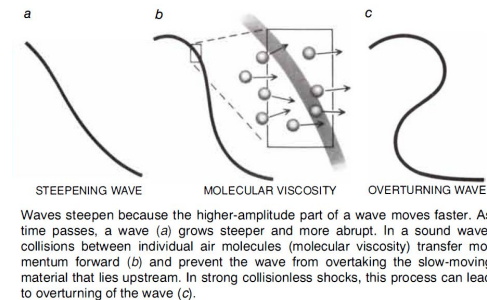


(Source: <http://www.scholarpedia.org>)

- Chromatic dispersion effect in Optics (*rainbow!*)
- Curvature in the dispersion curve $\omega = \omega(k)$, in solid state physics.
- The phase speed $v_{ph} = \frac{\omega}{k} = f(\mathbf{k})$ is a function of the wavenumber \mathbf{k} .

... and **Nonlinearity**, manifested as:

- Amplitude-dependence of the phase speed: larger amplitudes travel faster!
- This results in wave steepening, and eventually wave-breaking:



... a physical phenomenon well-known to seafarers (or *surfers*):



Further traces of nonlinearity include:

- *Secondary harmonic generation.*
- *No superposition principle:* different normal (Fourier) modes do not sum up.
- *Sidebands* appear in the Fourier spectrum.
- ***Energy localization*** (to be discussed later).

Korteweg de Vries (KdV) theory for electrostatic waves

Taniuti and Wei [J. Phys. Soc. Jpn. **24**, 941 (1968)] propose their *reductive perturbation technique*, for long-wavelength ES *acoustic modes* in plasmas.

We review the basic qualitative aspects of this technique below.

- Dispersion relation (*acoustic mode*):

$$\omega \simeq v_{ph}k + Ak^3 + \dots ,$$

(where A is to be determined, for a given plasma composition), thus

$$kx - \omega t \simeq k(x - v_{ph}t) - Ak^3t + \dots$$

- Appropriate space/time stretching

$$\xi = \epsilon^{1/2}(x - Vt), \quad \tau = \epsilon^{3/2}t \quad (V \in \mathfrak{R})$$

- $n \simeq n_0 + \epsilon n_1 + \epsilon^2 n_2 + \dots$; $u \simeq \epsilon u_1 + \epsilon^2 u_2 + \dots$; $\phi \simeq \epsilon \phi_1 + \epsilon \phi_2 + \dots$

Plasma fluid *toy-model* for electrostatic waves (1D)

Continuity (for plasma species s , e.g. *ions*):

$$\frac{\partial n_s}{\partial t} + \frac{\partial \phi}{\partial x} (n_s u_s) = 0$$

Mean velocity u_s equation:

$$\frac{\partial u_s}{\partial t} + u_s \frac{\partial u_s}{\partial x} = -\frac{q_s}{m_s} \frac{\partial \phi}{\partial x}$$

The potential Φ obeys *Poisson's eq.*:

$$\frac{\partial^2 \phi}{\partial x^2} = -4\pi \sum_s q_s n_s = 4\pi e (n_e - Z_i n_i + \dots)$$

- At a given dynamical scale for species s ($= e, i, d$, i.e. electrons, ions, dust, ...), the state of other species may be prescribed by simplifying assumptions;
- Typical paradigm: for ion-acoustic waves ($s = i$), *ions* are inertial, so *electrons* are assumed at equilibrium (e.g. Maxwellian: $n_e \sim e^{e\phi/k_B T_e}$).

- The method is rather tedious yet straightforward; details are omitted here.
- *Korteweg-de Vries (KdV) equation:*

$$\frac{\partial \psi}{\partial \tau} + A \psi \frac{\partial \psi}{\partial \xi} + B \frac{\partial^3 \psi}{\partial \xi^3} = 0.$$

- ★ $\psi = \phi_1$ denotes a small ($\sim \epsilon \ll 1$) correction to the electric potential,
- ★ Constraint: $V = c_s \rightarrow$ propagation at (or slightly above) the sound speed.
- ★ The coefficients A and B incorporate the physics of the particular problem considered, as they contain the dependence on relevant plasma parameters (lengthy expressions omitted here).
- ★ The *dispersion coefficient* B is positive;
- ★ The *nonlinearity coefficient* A determines the soliton polarity, i.e., the sign (positive/negative) of the soliton pulse (\rightarrow next slide).

- The soliton solution of the KdV equation above reads:

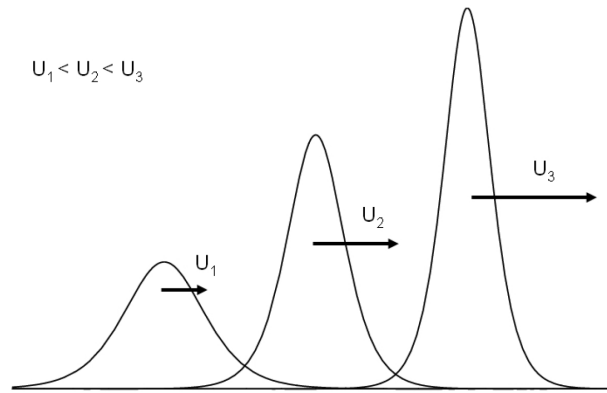
$$\psi = \psi_0 \operatorname{sech}^2 \left(\frac{\xi - U\tau}{L} \right)$$

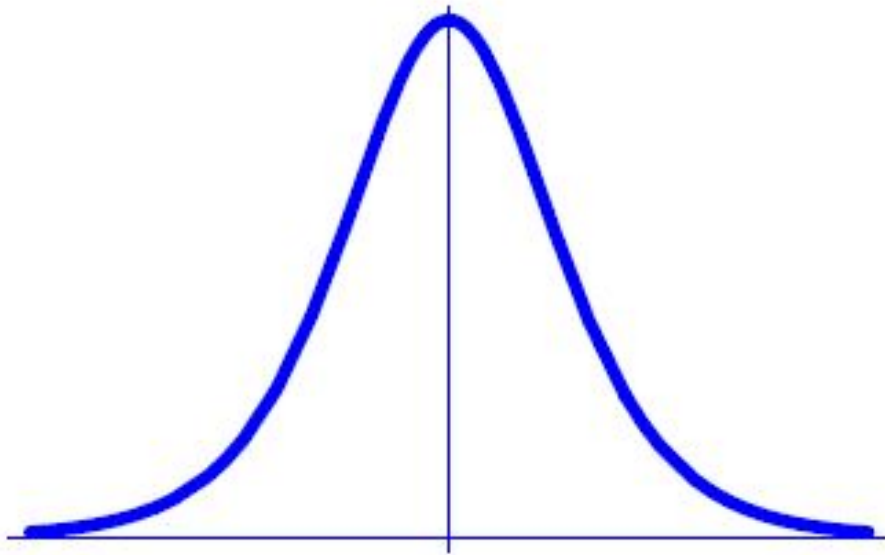
which represents a propagating pulse.

Here:

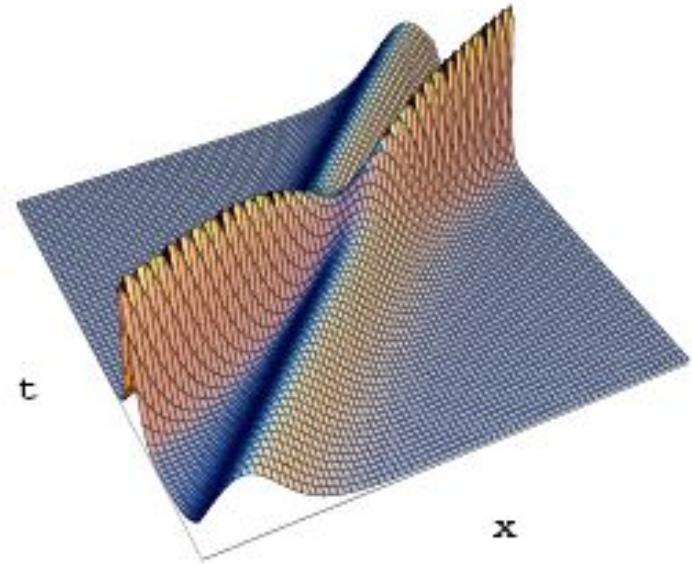
- ★ U is the soliton velocity increment (total soliton speed = $c_s + \epsilon U$)
 - ★ $\psi_0 = \frac{3U}{A}$ is the maximum *soliton amplitude*, and
 - ★ $L = 2\sqrt{B/U}$ is the *soliton width*.
- **Width-amplitude relation:** $\psi_0 L^2 = 12B/A = \text{constant}$, thus *faster* solitons

are *taller* and *narrower*:



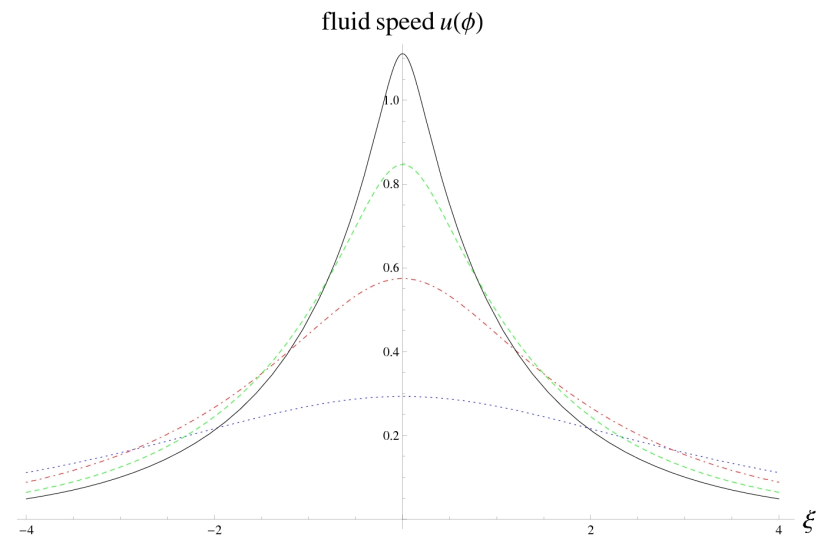
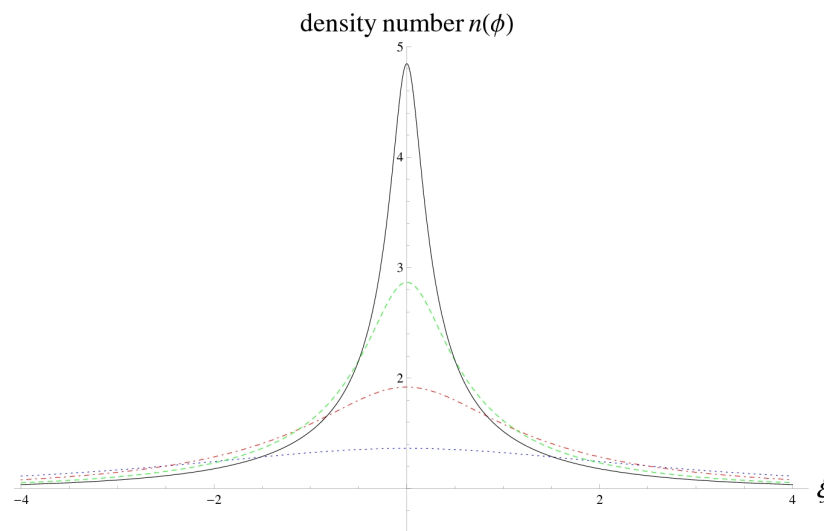
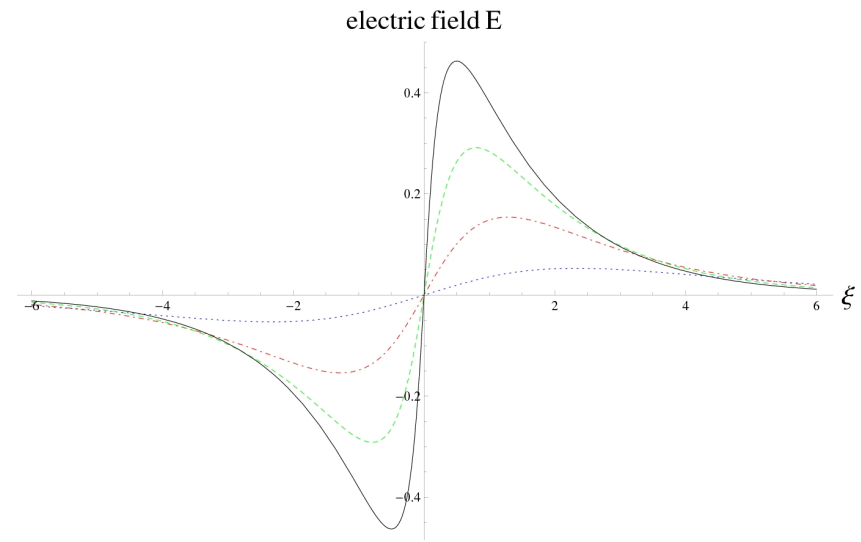
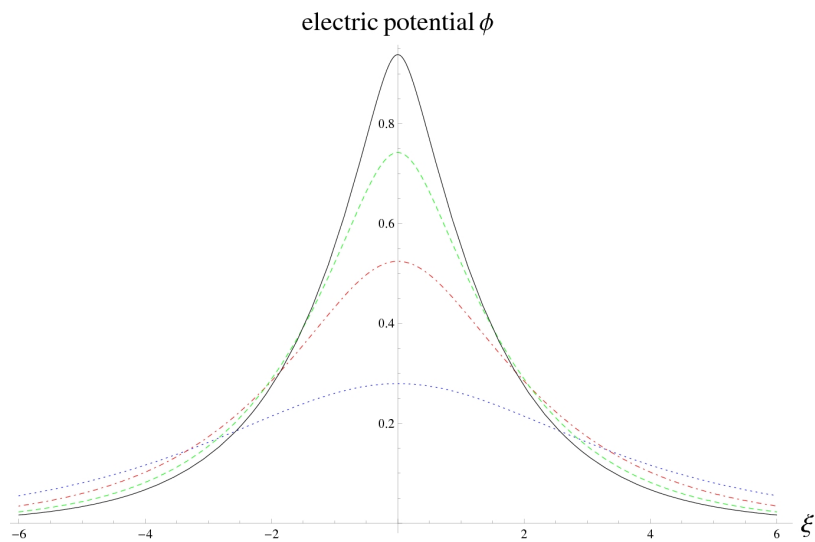


*Typical shape of positive potential
KdV soliton (in arbitrary units)*



*Typical interaction between two
positive potential KdV solitons*

Solution in terms of ϕ + ambipolar field $E = -\nabla\phi$ and fluid variables n, u



Mind the gap...

Restricted validity: The KdV theory obeys certain constraints & limitations

- It is a *small-amplitude* theory: not suitable for strong excitations (off equilibrium);
- Solutions are *weakly* super-acoustic;
- The methodology only works for *acoustic*-type modes (frequency = zero for infinite wavelength); optical modes (or e.g. Langmuir waves in plasmas) are not covered!

Electrostatic solitary waves

A “toy-model”: cold ion fluid + kappa-distributed electrons

Continuity:
$$\frac{\partial n}{\partial t} + \frac{\partial(nu)}{\partial x} = 0$$

Momentum:
$$\frac{\partial u}{\partial t} + u \frac{\partial u}{\partial x} = - \frac{\partial \phi}{\partial x}$$

Poisson Eq.:
$$\frac{\partial^2 \phi}{\partial x^2} = -n + n_e$$

S/thermal electrons:
$$n_e = n_{e,0} \left(1 - \frac{\phi}{\kappa - 3/2}\right)^{-\kappa + 1/2}$$

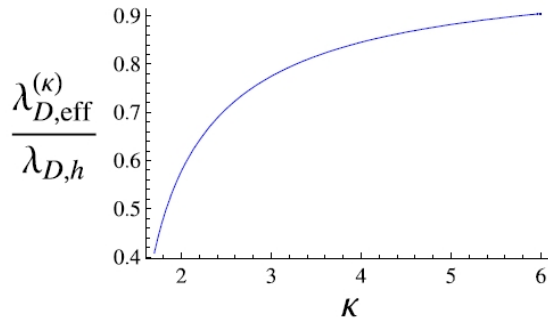
Scaling:
$$n = \frac{n_i}{n_{i0}}, \quad u = \frac{u_i}{c_s}, \quad x = \frac{x}{\lambda_D}, \quad \phi = \frac{e\phi}{k_B T_e}, \quad t = \omega_{pi} t$$

$$c_s = \left(\frac{k_B T_e}{m_i}\right)^{1/2}, \quad \omega_{pi} = \left(\frac{4\pi n_{i0} e^2}{m_i}\right)^{1/2}, \quad \lambda_D = \left(\frac{k_B T_e}{4\pi n_{i0} e^2}\right)^{1/2}$$

[Work in collaboration with: NS Saini, S Sultana, T Baluku, M Hellberg]

Linear regime: modified linear dispersion relation

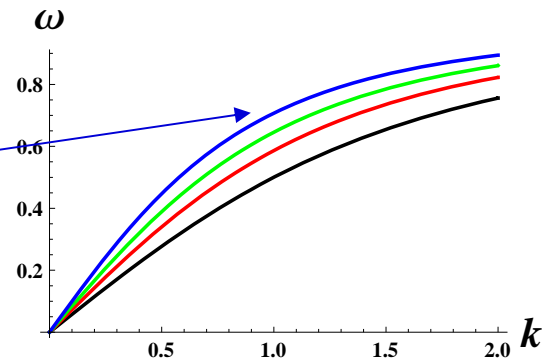
$$\omega^2 = \frac{k^2}{k^2 + c_1} \rightarrow c_1 = \frac{2\kappa - 1}{2\kappa - 3}$$



*κ-modified Debye screening:
Shorter Debye length for small κ!*

Figure 1. Variation of the electrostatic screening (effective Debye) length (scaled) with the superthermality parameter κ . See that the curve approaches unity at the infinite κ limit.

Blue: $\kappa = \infty$ (Maxwellian)
Green: $\kappa = 4$
Red: $\kappa = 2.6$
Black: $\kappa = 2$



(*) [Agreement with Bryant JPP (1996), Mace & Hellberg (PoP 1995)]

Pseudopotential formalism for ion-acoustic travelling waves

[Vedenov & Sagdeev 1961, Sagdeev 1966, Verheest & Hellberg 2009 (review)]

- stationary frame, single travelling coordinate $\xi = x - Mt$
- * reduction of the fluid model PDEs in $\{x, t\}$ to an ODE in ξ
- * **pseudo-energy-balance equation** (for *e-i plasma*):

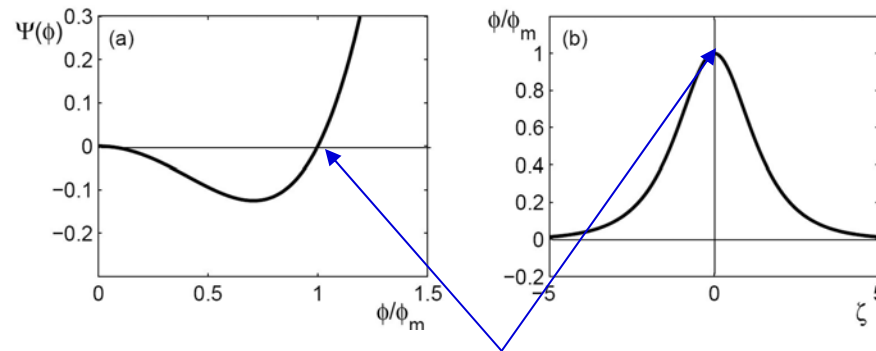
$$\frac{1}{2} \left(\frac{d\phi}{d\xi} \right)^2 + V(\phi) = 0$$

$$V(\phi) = M^2 \left(1 - \sqrt{1 - \frac{2\phi}{M^2}} \right) + 1 - \left(1 - \frac{\phi}{\kappa - 3/2} \right)^{-\kappa + 3/2}$$

- * solution obtained (numerically) for the electric potential ϕ
- * density and fluid velocity given by

$$n = \frac{1}{\sqrt{1 - 2\phi/V^2}} \quad v = V - \sqrt{V^2 - 2\phi}$$

The generic solitary wave (pulse) solution bears the form:

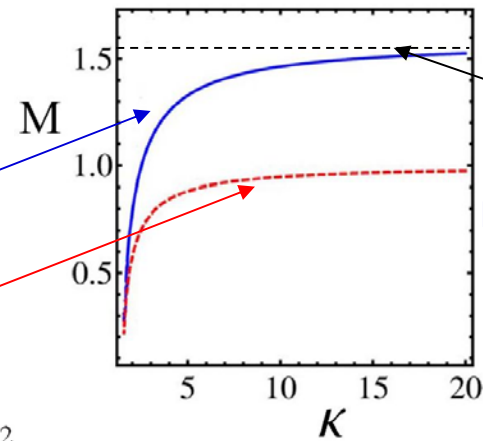


potential pulse amplitude = root of V

Slower “supersonic” (but no subsonic!) solitons
for smaller kappa values:

M_2 : infinite compression point
(choked flow)

M_1 : κ -dependent “sound speed” $M_1 \equiv \left(\frac{\kappa - 3/2}{\kappa - 1/2} \right)^{1/2}$



Known asymptotic limit 1.58
for infinite κ
i.e. for Maxwellian electrons

FIG. 1. (Color online) IA soliton existence domain in the parameter space of κ and Mach number, M . Solitons may be supported in the region between the two curves. The lower, dashed curve represents the minimum (soliton) condition, M_1 , and the upper, solid curve the infinite compression limit, M_2 .

Ion-Acoustic Super Solitary Waves in Dusty Multispecies Plasmas

Alexander E. Dubinov and Dmitry Yu. Kolotkov

Abstract—The concept of a new form of solitary waves—super solitary waves—is proposed, specific for embracing one or several interior separatrices on their wave phase portraits. The super solitary waves of an ion-acoustic type exist, for example, in non-magnetized plasma containing five species of charged particles. For such plasma, electrostatic potential for ion-acoustic super solitary waves is calculated. The super solitary waves can be easily identified among usual solitons, e.g., in differential circuits installed into the measuring channel.

Manuscript received November 20, 2011; revised February 7, 2012; accepted February 20, 2012. Date of publication April 6, 2012; date of current version May 9, 2012. This work was supported in part by a grant of the foundation “Dynasty” and in part by Grant RFBR# 10-02-90418-Ukr_a.

A. E. Dubinov is with the Russian Federal Nuclear Center—All-Russian Scientific and Research Institute of Experimental Physics (RFNC-VNIIEF), 607188 Sarov, Russia, and also with Sarov Institute of Physics and Technology (SarFTI), National Research Nuclear University “MEPhI,” 607188 Sarov, Russia (e-mail: dubinov@ntc.vniief.ru).

D. Y. Kolotkov is with Sarov Institute of Physics and Technology (SarFTI), National Research Nuclear University “MEPhI,” 607188 Sarov, Russia (e-mail: molotok300@gmail.com).

Digital Object Identifier 10.1109/TPS.2012.2189026

separatrices and a number of equilibrium points. Then, there is a new form of a solitary wave, never described before—a super solitary wave corresponding to the exterior separatrix.

Can super solitary waves exist in plasma? In this paper, it is proven that super solitary wave can exist, for instance, in the case of ion-acoustic waves in dusty multispecies plasmas containing electrons, positrons, and two types of ions of the different signs of charge and dust particles. Notably, various

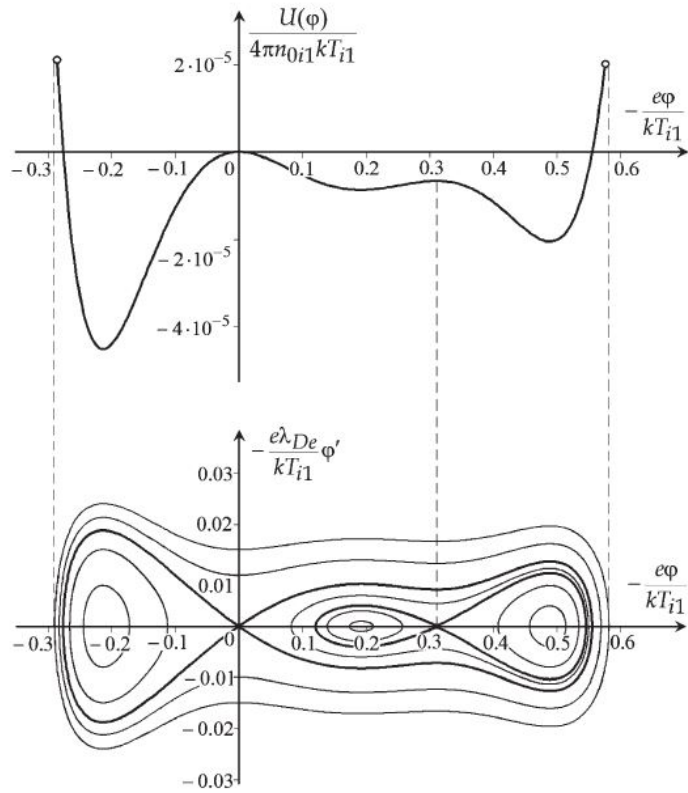


Fig. 2. Plot of pseudopotential (the upper end points, corresponding to the reflection of ions from the potential barrier in the wave, are shown by circles) and the phase wave portrait (in the lower part, separatrices are shown by heavy line). λ_{De} is the electron Debye length.

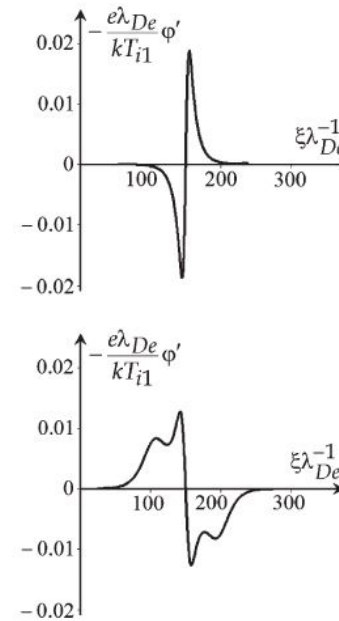


Fig. 4. Profile of the derivatives of (top) a normal soliton and (bottom) a super solitary wave.

Super solitary waves exist in plasma consisting **no fewer than four charged species** of particles (in our case, there are five species). In simpler two- or three-species plasmas, the Sagdeev pseudopotential has no more than one or two minima, and the case when one separatrix is embraced by another external separatrix is not possible; so, super solitary waves do not exist with such a set of parameters.

GENERAL ASPECTS
OF HIGH ENERGY CHEMISTRY

Interpretation of Ion–Acoustic Solitons of Unusual Form
in Experiments in SF₆–Ar Plasma

A. E. Dubinov and D. Yu. Kolotkov

Sarov Physicotechnical Institute, Branch of “Moscow Engineering Physics Institute” National Nuclear Research University,
ul. Dukhova 6, Sarov, Nizhni Novgorod oblast, 607188 Russia
e-mail: dubinov-ae@yandex.ru

Received May 2, 2012; in final form, May 23, 2012

Abstract—The emergence in SF₆–Ar plasma of ion–acoustic solitons with angular profiles or profiles with several maxima has been explained. It has been shown that the cause of these profiles is that the phase trajectories of the solitons of this type in the phase portrait cover one or more separatrices, which in turn can appear only in plasma with a complex chemical composition.

DOI: 10.1134/S0018143912060033

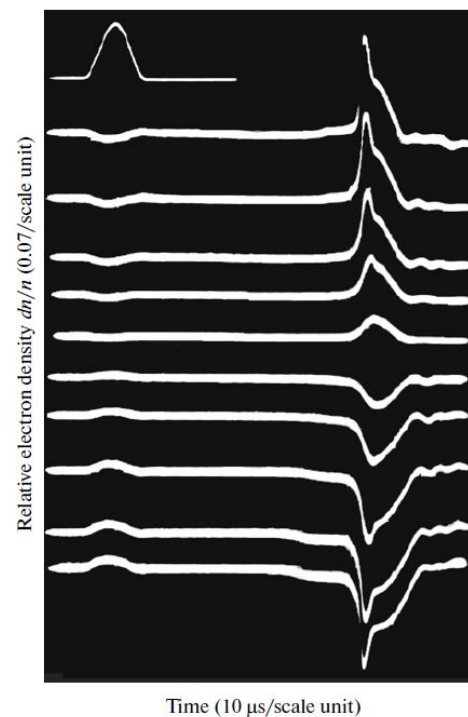


Fig. 1. Oscilloscope traces of the electron density in ion–acoustic solitons in SF₆–Ar plasma obtained at various excitation amplitudes; given at the top left is the profile of the solitons of this type in the phase portrait cover one or more separatrices, which in turn can appear only in plasma with a complex chemical composition.

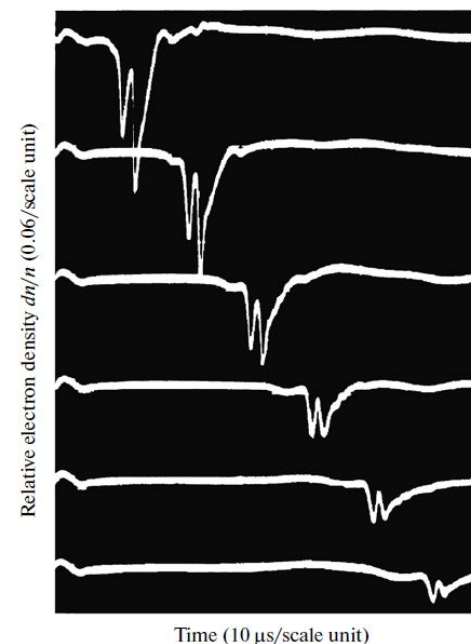


Fig. 2. Oscilloscope traces of the electron density in rarefactive ion–acoustic solitons in Ar–SF₆ plasma obtained at various distances from the excitation site, all the traces exhibit several pronounced minima (notations are as given in [10]).

where $e < 0$ is the charge of the electron and the negative ions; $(-e) > 0$ is the charge of the positive ions; all

Electrostatic supersolitons in three-species plasmas

Frank Verheest,^{1,2,a)} Manfred A. Hellberg,^{2,b)} and Ioannis Kourakis^{3,c)}

¹Sterrenkundig Observatorium, Universiteit Gent, Krijgslaan 281, B-9000 Gent, Belgium

²School of Chemistry and Physics, University of KwaZulu-Natal, Durban 4000, South Africa

³Department of Physics and Astronomy, Centre for Plasma Physics, Queen's University Belfast, BT7 1NN Northern Ireland, United Kingdom

(Received 13 December 2012; accepted 21 December 2012; published online 10 January 2013)

Superficially, electrostatic potential profiles of supersolitons look like those of traditional solitons. However, their electric field profiles are markedly different, having additional extrema on the wings of the standard bipolar structure. This new concept was recently pointed out in the literature for a plasma model with five species. Here, it is shown that electrostatic supersolitons are not an artefact of exotic, complicated plasma models, but can exist even in three-species plasmas and are likely to occur in space plasmas. Further, a methodology is given to delineate their existence domains in a systematic fashion by determining the specific limiting factors. © 2013 American Institute of Physics. [<http://dx.doi.org/10.1063/1.4775085>]

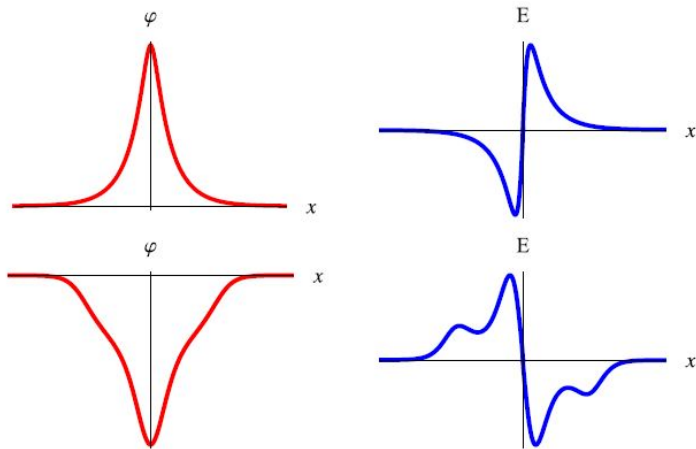


FIG. 1. *Upper panels*: Example of a standard positive soliton and its associated electric field. *Lower panels*: A negative supersoliton and its associated electric field.

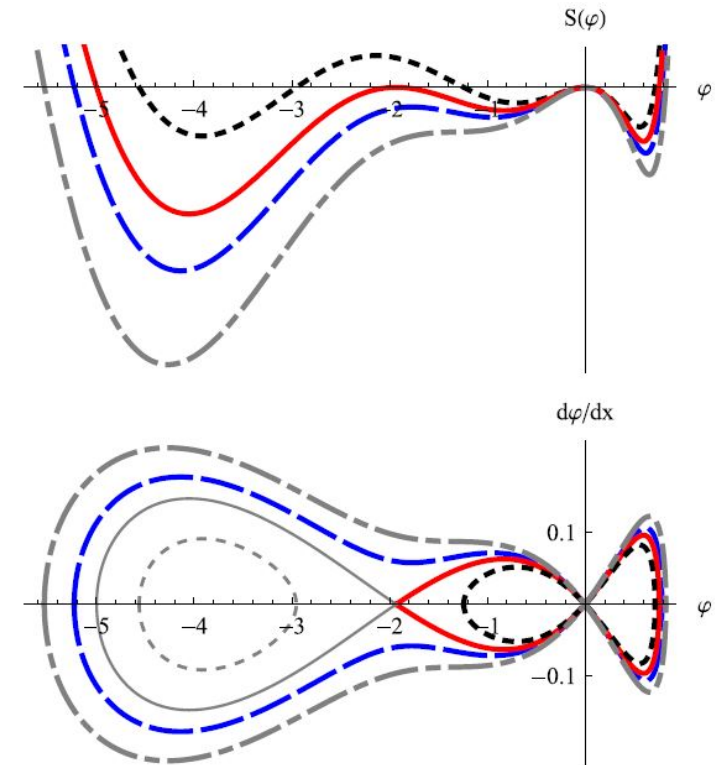


FIG. 3. *Upper panel*: Graphs of $S(\varphi)$ for $\beta = 0.3$, $\mu = 10$, $f = 0.3$ and $M/M_s = 1.023$ (dotted curve), $M/M_s = 1.027$ (solid curve), $M/M_s = 1.030$ (dashed curve) and $M/M_s = 1.035$ (dotted-dashed curve). *Lower panel*: Here the hodographs are presented, with the same curve coding. Thin dotted and solid curves in gray indicate ranges which are not accessible from the undisturbed conditions and thus physically irrelevant.

Dust-ion-acoustic supersolitons in dusty plasmas with nonthermal electrons

Frank Verheest*

Sterrenkundig Observatorium, Universiteit Gent, Krijgslaan 281, B-9000 Gent, Belgium & School of Chemistry and Physics, University of KwaZulu-Natal, Durban 4000, South Africa

Manfred A. Hellberg†

School of Chemistry and Physics, University of KwaZulu-Natal, Durban 4000, South Africa

Ioannis Kourakis‡

Centre for Plasma Physics, Department of Physics and Astronomy, Queen's University Belfast, BT7 1NN Northern Ireland, United Kingdom (Received 26 February 2013; published 15 April 2013)

Supersolitons are a recent addition to the literature on large-amplitude solitary waves in multispecies plasmas. They are distinguished from the usual solitons by their associated electric field profiles which are inherently distinct from traditional bipolar structures. In this paper, dust-ion-acoustic modes in a dusty plasma with stationary negative dust, cold fluid protons, and nonthermal electrons are investigated through a Sagdeev pseudopotential approach to see where supersolitons fit between ranges of ordinary solitons and double layers, as supersolitons always have finite amplitudes. They therefore cannot be described by reductive perturbation treatments, which rely on a weak amplitude assumption. A systematic methodology and discussion is given to distinguish the existence domains in solitary wave speed and amplitude for the different solitons, supersolitons and double layers, in terms of compositional parameters for the plasma model under consideration.

DUST-ION-ACOUSTIC SUPERSOLITONS IN DUSTY ...

PHYSICAL REVIEW E 87, 043107 (2013)

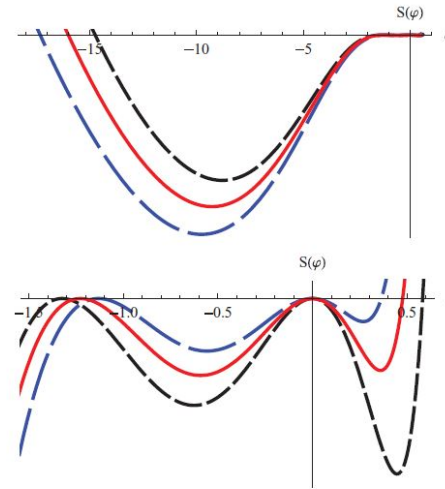


FIG. 4. (Color online) Upper panel: Pseudopotentials with a negative double layer for $f = 0.31$ (blue curve with longer dashes), $f = 0.320$ (red solid curve, at the precise polarity crossover), and $f = 0.33$ (black curve with shorter dashes). Lower panel: Focus on the φ range closer to the undisturbed conditions. Both panels together show that as f is increased, the absolute values of the large negative root decrease, whereas the amplitudes of the negative double layers and the positive soliton increase.

double layers. For a given value of f , the lower limit in M of the supersoliton existence domain is then governed by the

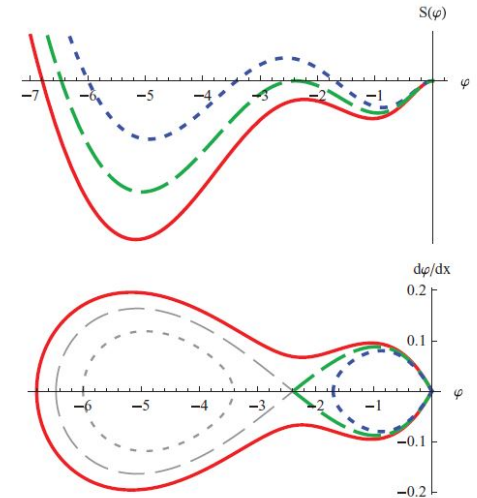


FIG. 5. (Color online) Upper panel: Pseudopotentials with a standard soliton (blue dotted curve, $M/M_s = 1.057$), a double layer (green dashed curve, $M/M_s = 1.061$), and a supersoliton (red solid curve, $M/M_s = 1.065$) for $\beta = 0.3$ and $f = 0.43$. For graphical clarity, the positive soliton domain has been omitted, because the well on this side is very deep and would flatten the important details on the negative side. Lower panel: Here the hodographs are presented, plotting $d\varphi/dx$ as functions of φ , with the same curve coding. Thin dotted and dashed curves in gray indicate ranges which are not accessible from the undisturbed conditions.

* From: NS Saint, I Kourakis and M Hellberg, PoP 16, 062903 (2009) |

Supersolitons in Space plasma observations?

- ESWs occur in abundance as magnetic-field aligned *bipolar* electric field structures (among other forms), observed in abundance in satellite data (Cluster, FAST, ...)
- Solitary waves: potential pulses, solitons, double layers, flat-topped pulses, ...

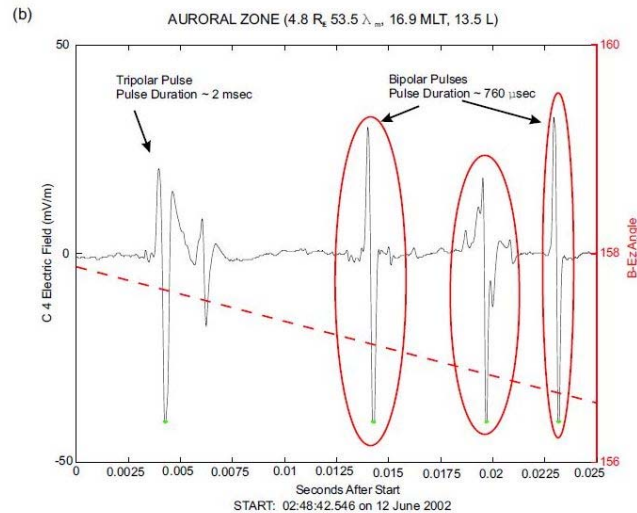


Fig. 1. Cluster WBD data taken on 12 June 2002 in the auroral zone. (a) Spectrogram showing the frequency and power spectral density of the emissions. The broad-band signals ranging up to about 10 kHz are indicative of times when IES are observed. (b) Representative waveform from a time of the broad-band signals, showing the two types of IES: bipolar and tripolar pulses.

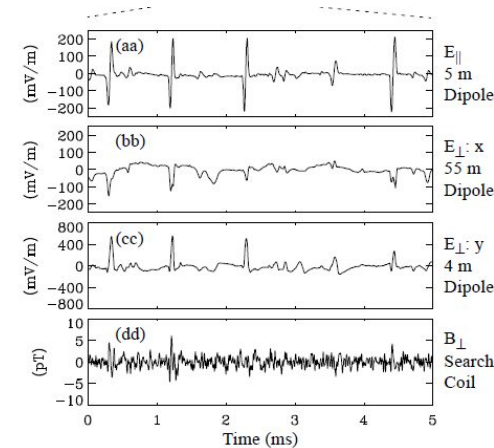


Figure 5. (From [5]) (a) The electric field parallel to B_0 . (b) The electric field perpendicular to B_0 (ΔE_{\perp}) and in the spin plane of the satellite. This signal, measured by a 56 m dipole antenna, appears attenuated, indicating that the structure size may have been < 112 m. (c) ΔE_{\perp} along the spin axis of the satellite. (d) A perturbation magnetic field perpendicular to B_0 (ΔB_{\perp}). ΔB_{\perp} was filtered to a pass band (3 kHz–16 kHz) to expose the weak signals and therefore may not appear unipolar in this figure. (aa)–(dd) An expanded view of this data.

Figures from: Pickett *et al* Ann. Geophys. (2004) (L, Cluster), Ergun *et al*, PPCF (1999) (R, FAST)

One-Dimensional Fluid Code

Plasma Model

(Fluid ions, cold & hot kappa distributed electrons)

$$\frac{\partial N_i}{\partial t_n} + \frac{\partial(N_i U_i)}{\partial x_n} = 0$$

$$\frac{\partial U_i}{\partial t_n} + U_i \frac{\partial U_i}{\partial x_n} = -\frac{\partial \Phi}{\partial x_n}$$

$$N_{he} = \left[1 - \frac{\Phi}{(\kappa_{he} - 3/2)} \right]^{-\kappa_{he} + 1/2}$$

$$N_{ce} = \left[1 - \frac{\Phi}{\tau(\kappa_{ce} - 3/2)} \right]^{-\kappa_{ce} + 1/2}$$

$$\frac{\partial^2 \Phi}{\partial x_n^2} = f N_{ce} + (1 - f) N_{he} - N_i$$

4th order finite difference scheme

Spatial derivative

4th order finite difference scheme

$$\frac{\partial F_h}{\partial x} = \frac{8(F_{h+1} - F_{h-1}) - F_{h+2} + F_{h-2}}{12\Delta x} \quad O(\Delta x)^4$$

$F_h \rightarrow$ represent a physical quantity defined at grid "h"
 $\Delta x \rightarrow$ Grid Spacing

Time derivative

Leap-frog method

$$\frac{\partial n}{\partial t} = f, \quad \frac{n(j+1,i) - n(j,i)}{\Delta t} = f(j+1/2,i) \quad O(\Delta t)^2$$

Here, $\Delta t \rightarrow$ Time step

Kakad, Omura & Kakad et al PoP, 2013

- (a) Memory allocation
- (b) Initialising N_i, N_e, U_i, Φ

INTEGRATING

- (1) Momentum equation of ions

$$U_i = - \int_{\Delta t} \left[U_i \frac{\partial U_i}{\partial x} + \frac{\partial \Phi}{\partial x} \right] dt$$

- (2) Continuity equation of ions

$$N_i = - \int_{\Delta t} \frac{\partial(N_i U_i)}{\partial x} dt$$

Δt

POISSON SOLVER

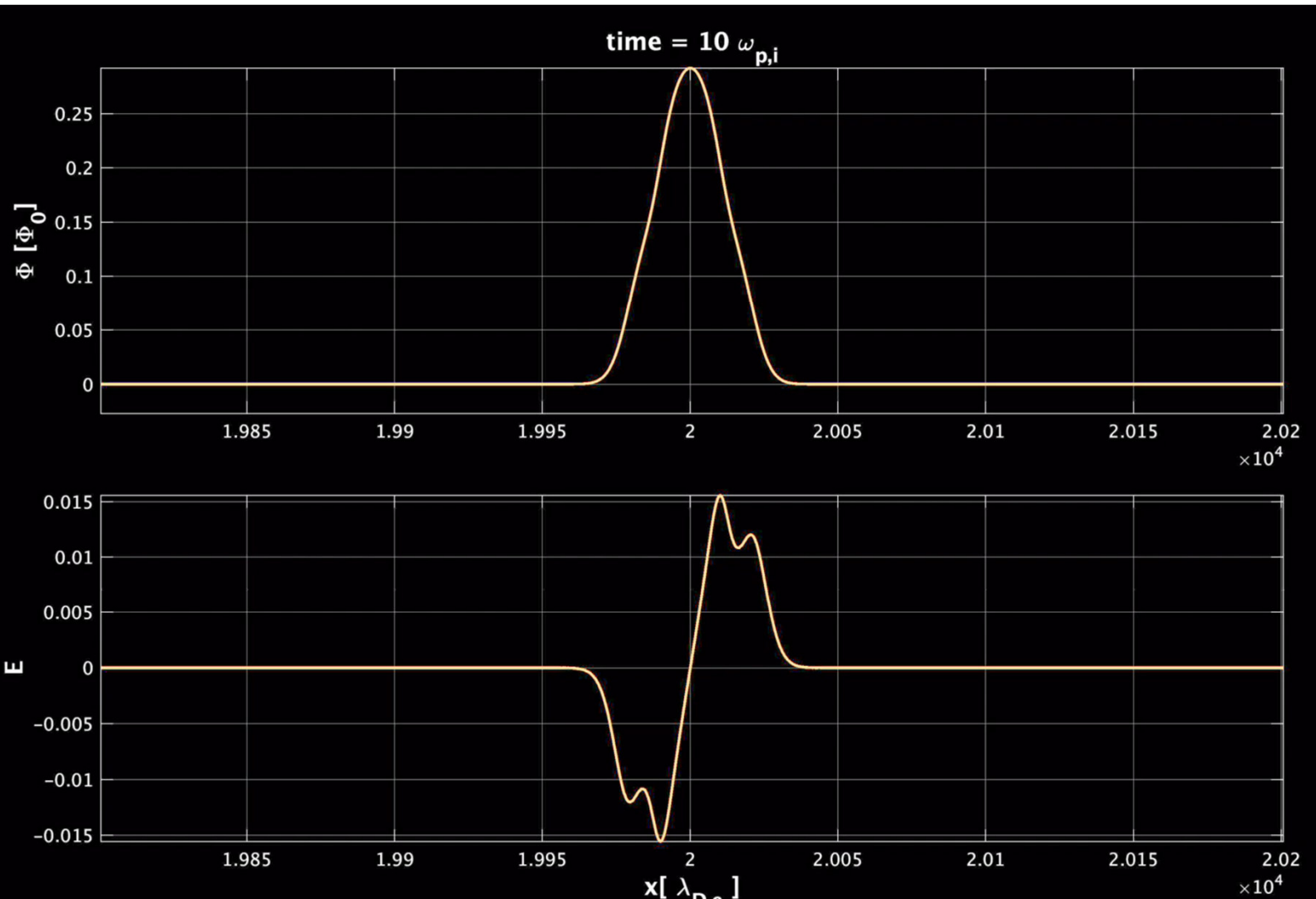
$$\Phi = \int_L \left[\int_L (N_e - N_i) dx \right] dx$$

$$N_e = \left[1 - \frac{\Phi}{\kappa - 3/2} \right]^{-\kappa + 1/2}$$

Successive Over Relaxation method best for simulating plasma with kappa distributions

Lotekar, Kakad, Kakad et al, CNSNS, 2019

Evolution of Supersolitons through density perturbation



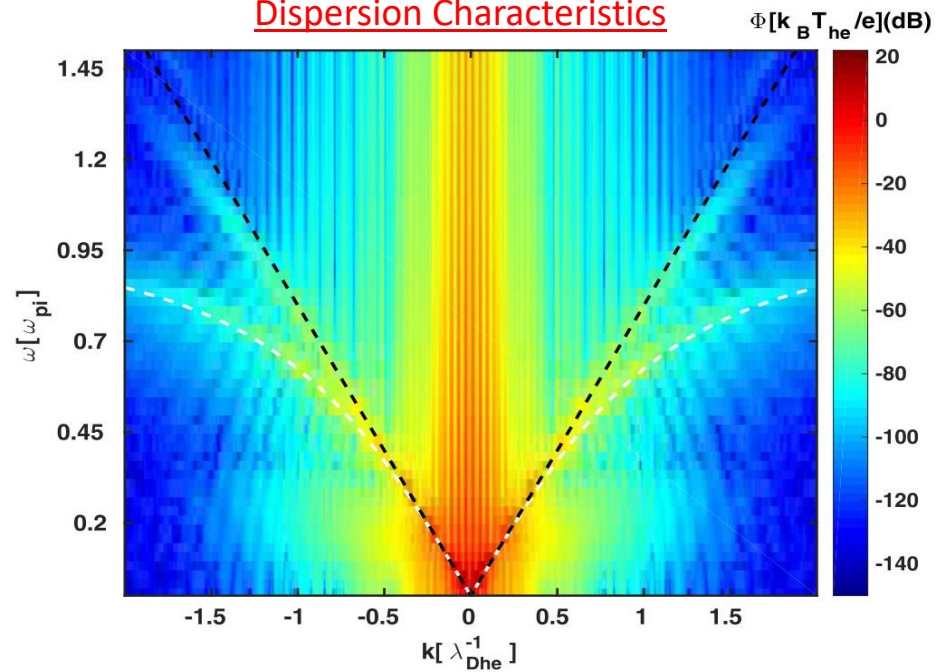
First-ever model simulation of the new subclass of solitons "Supersolitons" in plasma

Kakad+Lotekar+ Kakad, *Physics of Plasmas*, 2016

->>> See movie 1 by Amar Kakad

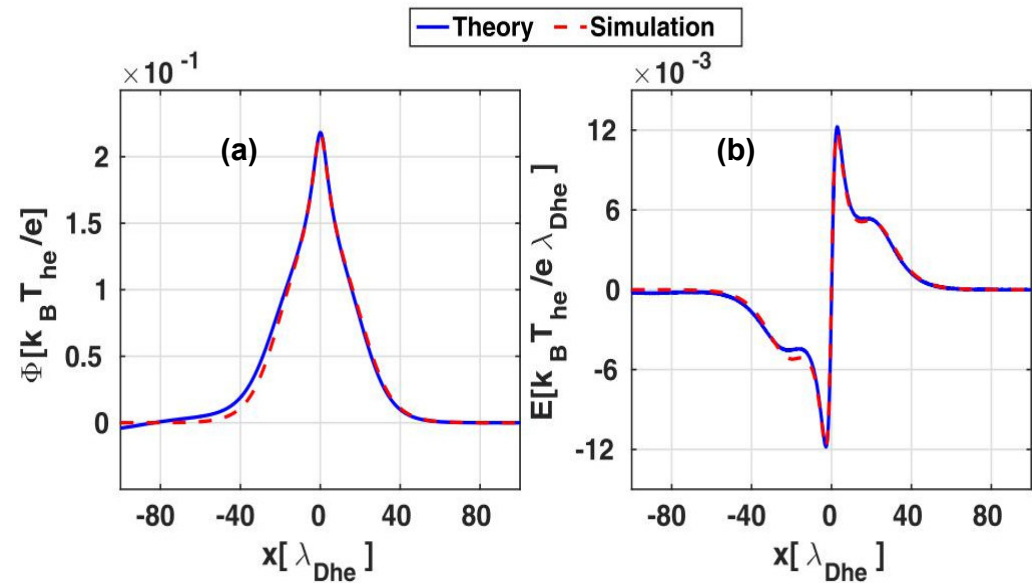
Supersolitons: Characteristics

Dispersion Characteristics



ω - k diagram during time = 0–200 from the simulation

Simulation vs Theory

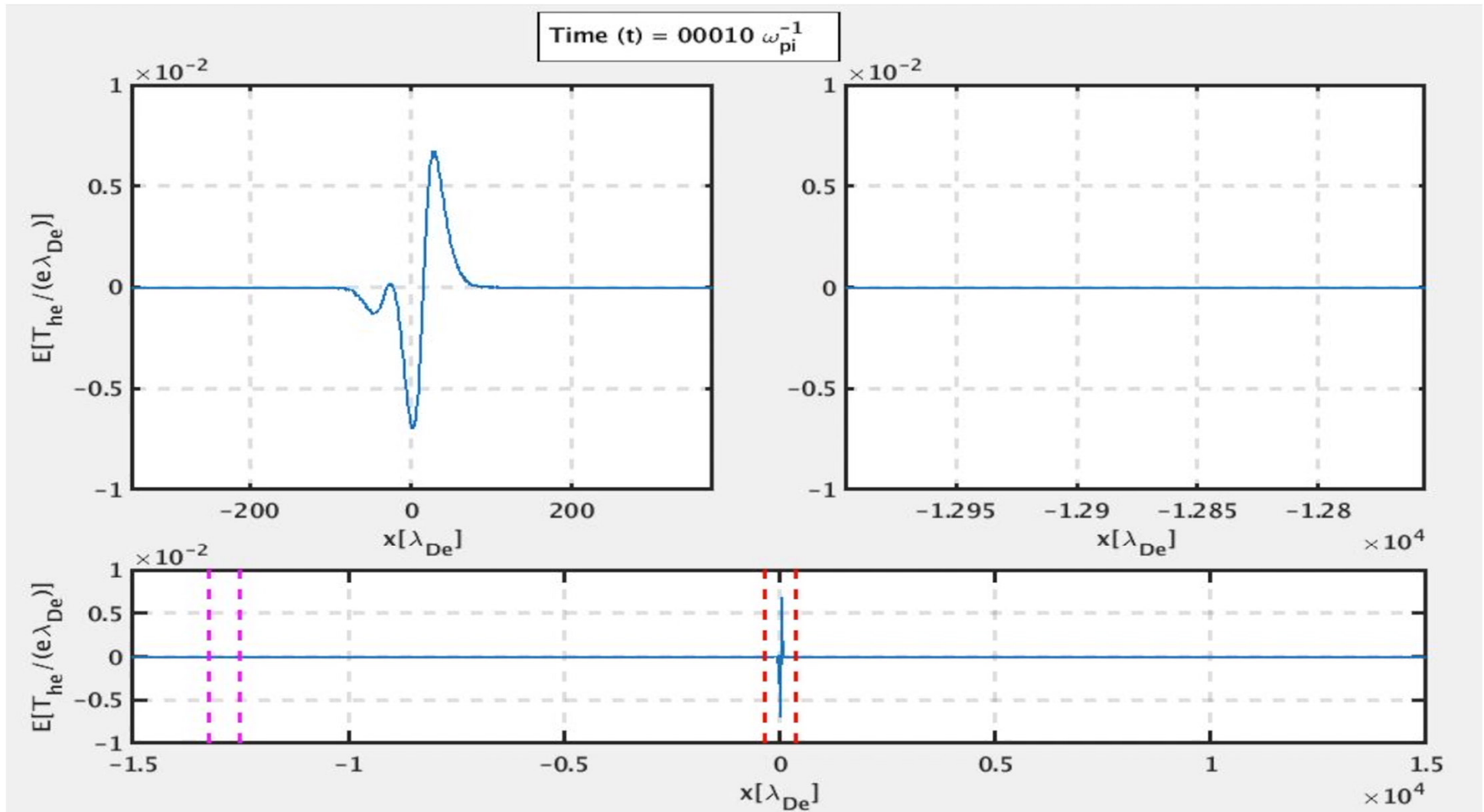


(a) potential (ϕ) and (b) electric field (E_n) profiles of IA supersoliton from simulation and theory

Kakad + Lotekar + Kakad,
Physics of Plasmas, 2016

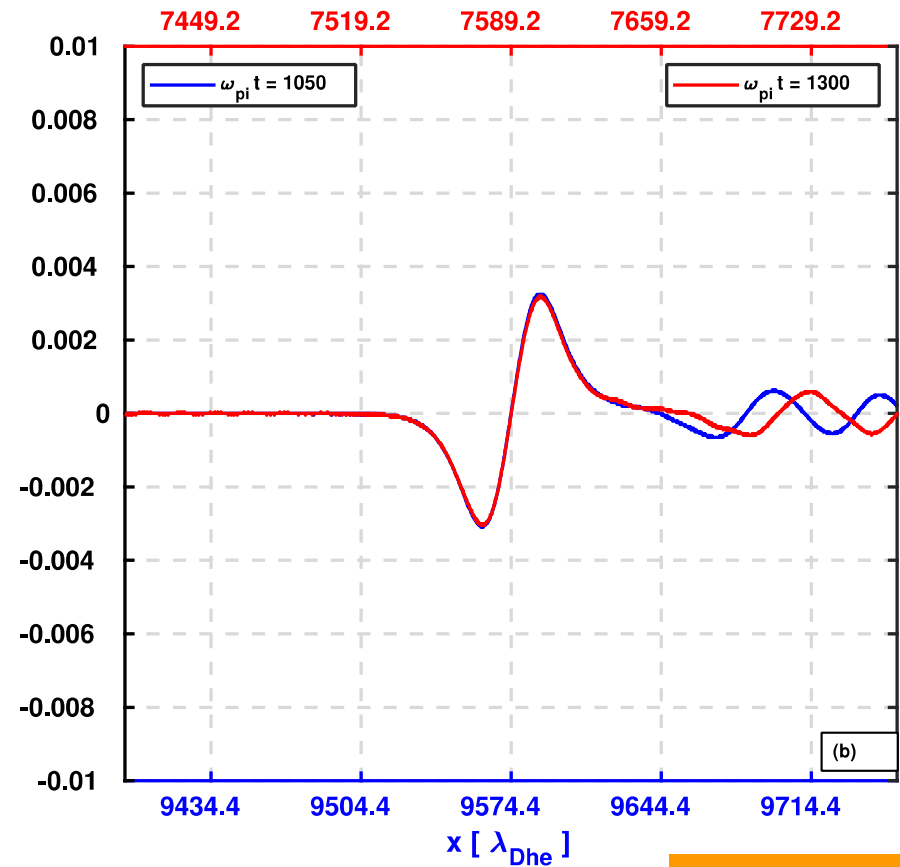
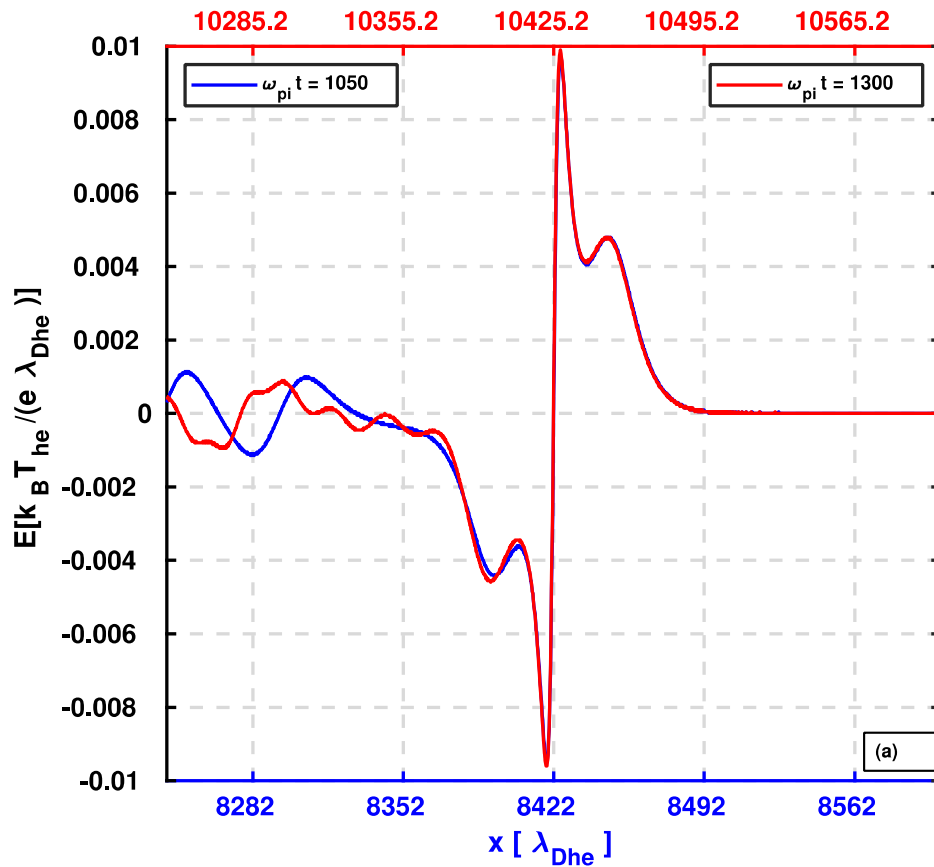
Collision of Supersolitons with Regular Soliton

Lotekar+Kakad+Kakad,
Physics of Plasmas, 2016



->>> See movie 2 by Amar Kakad

SSW and RSW before & after collision



Part B - Envelope Structures

Rogue waves – an emerging paradigm

- *Rogue waves* are localized excitations (events) of extreme amplitude, exceeding twice the average strength of background turbulence level;

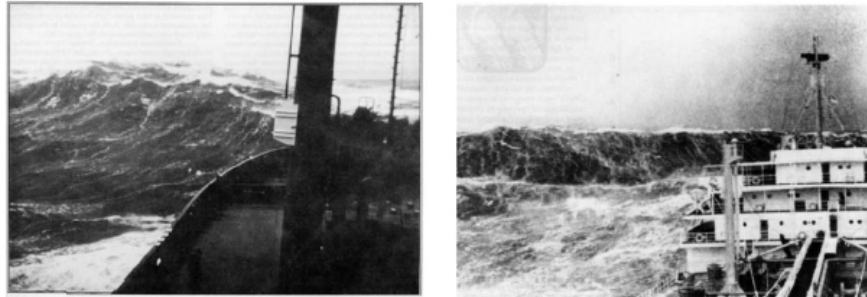
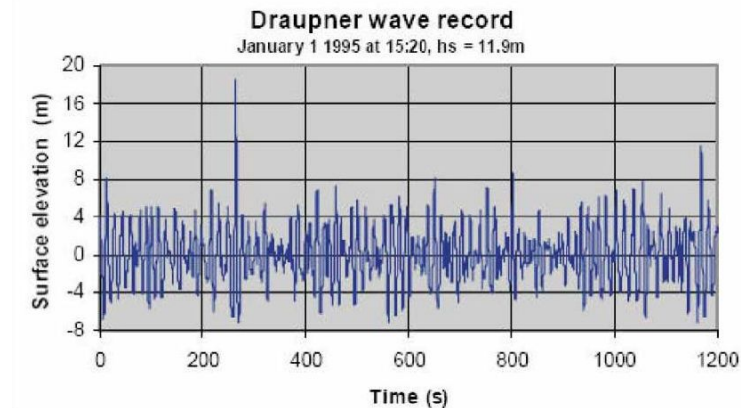


Fig. 2. Various photos of rogue waves.



Data from the Draupner platform event in Norway (Jan. 1995).

Credit: Kharif & Pelinovsky, Eur. Journal of Mechanics B/Fluids **22**, 603 (2003).

Theoretical attempts to explain freak wave formation

... via water surface envelope mode interaction:

PRL 97, 094501 (2006)

PHYSICAL REVIEW LETTERS

week ending
1 SEPTEMBER 2006

Instability and Evolution of Nonlinearly Interacting Water Waves

P. K. Shukla,^{1,2} I. Kourakis,² B. Eliasson,² M. Marklund,¹ and L. Stenflo¹

¹Centre for Nonlinear Physics, Department of Physics, Umeå University, SE-90187 Umeå, Sweden

²Institut für Theoretische Physik IV and Centre for Plasma Science and Astrophysics, Fakultät für Physik und Astronomie, Ruhr-Universität Bochum, D-44780 Bochum, Germany

(Received 16 February 2006; published 30 August 2006)

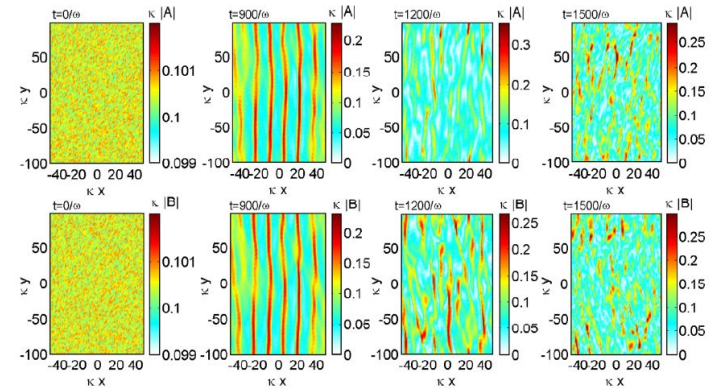


FIG. 4 (color online). The interaction between two waves, initially with equal amplitudes $|A| = |B| = 0.1\kappa^{-1}$ and a propagation angle of $\theta = \pi/8$ relative to the dichotome. Added to the initially homogeneous wave envelopes is a low-amplitude noise of order $10^{-3}/\kappa$ to give a seed to the modulational instability.

EPL, 86 (2009) 24001
doi: 10.1209/0295-5075/86/24001

www.epljournal.org

Evolution of rogue waves in interacting wave systems

A. GRÖNLUND^{1,2(a)}, B. ELIASSON³ and M. MARKLUND³

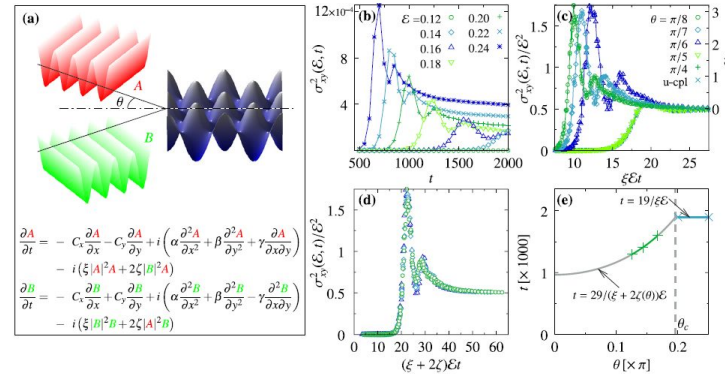
¹Department of Mathematics, Uppsala University - SE-751 06 Uppsala, Sweden, EU

²Umeå Plant Science Center, Department of Forest Genetics and Plant Physiology,

Swedish University of Agricultural Sciences - SE-901 83 Umeå, Sweden, EU

³Department of Physics, Umeå University - SE-901 87 Umeå, Sweden, EU

received 4 December 2008; accepted in final form 16 March 2009



[Credit: M. Onorato, A.R. Osborne and M. Serio, Phys. Rev. Lett., **96** 014503 (2006);
P. K. Shukla, I. Kourakis, B. Eliasson, M. Marklund and L. Stenflo, Phys. Rev. Lett. **97**, 094501 (2006);
A. Grönlund, B. Eliasson and M. Marklund, EPL, **86** 24001 (2009).]

Rogue Wave Observation in a Water Wave Tank

A. Chabchoub,^{1,*} N. P. Hoffmann,¹ and N. Akhmediev²

¹*Mechanics and Ocean Engineering, Hamburg University of Technology, Eißendorfer Straße 42, 21073 Hamburg, Germany*

²*Optical Sciences Group, Research School of Physics and Engineering, The Australian National University, Canberra ACT 0200, Australia*

(Received 28 February 2011; published 16 May 2011)

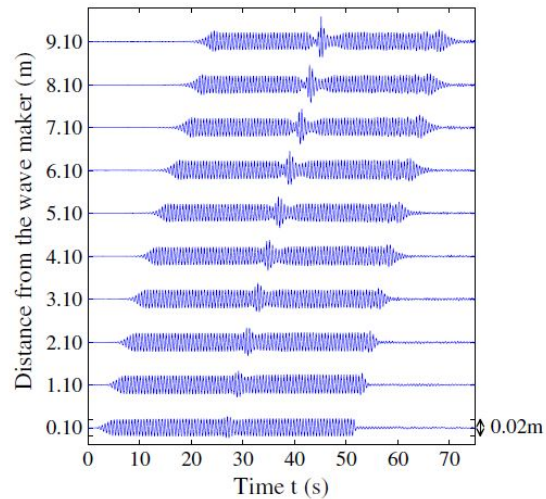
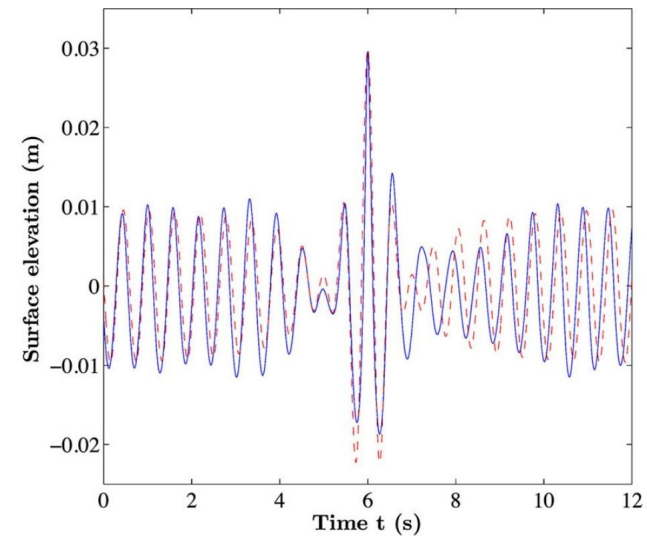


FIG. 3 (color online). Temporal evolution of the water surface height at various distances from the wave maker.



[Credit: A. Chabchoub *et al*, Phys. Rev. Letters **106**, 204502 (2011); (right plot) A. Chabchoub/Hamburg University of Technology (online).]

LETTERS

Optical rogue waves

D. R. Solli¹, C. Ropers^{1,2}, P. Koonath¹ & B. Jalali¹

Recent observations show that the probability of encountering an extremely large rogue wave in the open ocean is much larger than expected from ordinary wave-amplitude statistics^{1–3}. Although considerable effort has been directed towards understanding the physics behind these mysterious and potentially destructive events, the complete picture remains uncertain. Furthermore, rogue waves have not yet been observed in other physical systems. Here, we introduce the concept of optical rogue waves, a counterpart of

Although the physics behind rogue waves is still under investigation, observations indicate that they have unusually steep, solitary or tightly grouped profiles, which appear like “walls of water”¹⁰. These features imply that rogue waves have relatively broadband frequency content compared with normal waves, and also suggest a possible connection with solitons—solitary waves, first observed by J. S. Russell in the nineteenth century, that propagate without spreading in water because of a balance between dispersion and nonlinearity. As

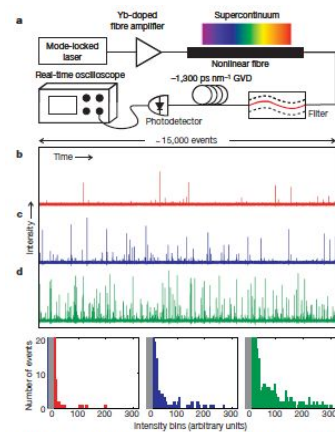


Figure 1 | Experimental observation of optical rogue waves. a, Schematic of experimental apparatus. b–d, Single-shot time traces containing roughly 15,000 pulses each and associated histograms (bottom of figure: left, middle, c; right, d) for average power levels $0.8 \mu\text{W}$ (red), $3.2 \mu\text{W}$ (blue) and $12.8 \mu\text{W}$ (green), respectively. The grey shaded area in each histogram demarcates the noise floor of the measurement process. In each measurement, the vast majority of events (>99.5% for the lowest power) are buried in this low intensity range, and the rogue events reach intensities of at least 30–40 times the average value. These distributions are very different from those encountered in most stochastic processes.

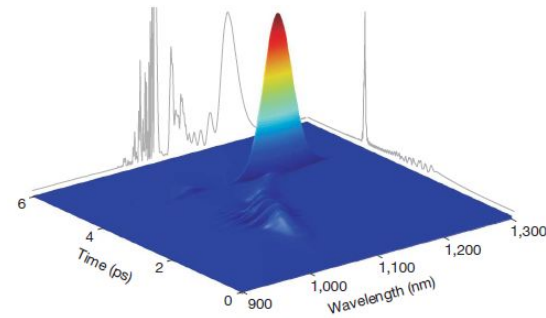


Figure 3 | Time-wavelength profile of an optical rogue wave obtained from a short-time Fourier transform. The optical wave has broad bandwidth and has extremely steep slopes in the time domain compared with the typical events. It appears as a ‘wall of light’ analogous to the ‘wall of water’ description of oceanic rogue waves. The rogue wave travels a curved path in time-wavelength space because of the Raman self-frequency shift and group velocity dispersion, separating from non-solitonic fragments and remnants of the seed pulse at shorter wavelengths. The grey traces show the full time structure and spectrum of the rogue wave. The spectrum contains sharp spectral features that are temporally broad and, thus, do not reach large peak power levels and do not appear prominently in the short-time Fourier transform.

Credit: D.R. Solli, C. Ropers, P. Koonath, B. Jalali, Nature **450**, 1054 (2007).

The Peregrine soliton in nonlinear fibre optics

B. Kibler¹, J. Fatome¹, C. Finot¹, G. Millot¹, F. Dias^{2,3}, G. Genty⁴, N. Akhmediev⁵ and J. M. Dudley⁶★

The Peregrine soliton is a localized nonlinear structure predicted to exist over 25 years ago, but not so far experimentally observed in any physical system¹. It is of fundamental significance because it is localized in both time and space, and because it defines the limit of a wide class of solutions to the nonlinear Schrödinger equation (NLSE). Here, we use an analytic

Our experiments are designed using the breather formalism of ref. 2. With dimensionless field $\psi(\xi, \tau)$, the self-focusing NLSE is:

$$i\frac{\partial\psi}{\partial\xi} + \frac{1}{2}\frac{\partial^2\psi}{\partial\tau^2} + |\psi|^2\psi = 0 \quad (1)$$

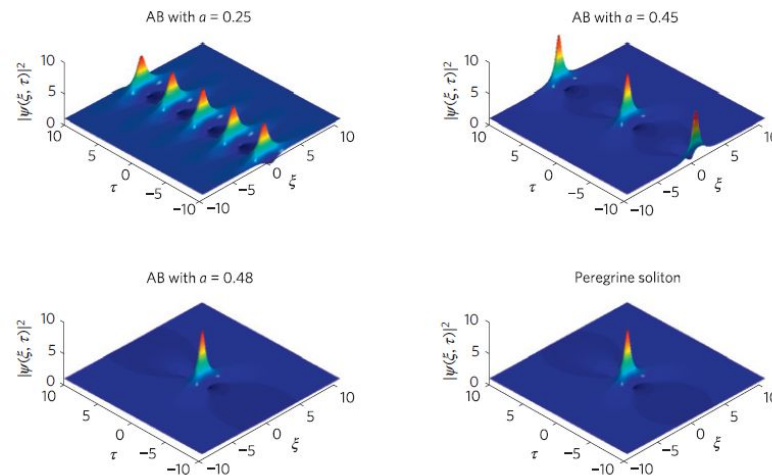


Figure 1 | Plotted Akhmediev breather solutions using equation (2) for modulation parameter $a = 0.25$, $a = 0.45$ and $a = 0.48$, as well as the ideal Peregrine soliton of equation (3), the limiting case of the Akhmediev breather as $a \rightarrow 1/2$. Maximum temporal compression occurs at normalized distance $\xi = 0$. The differences between the Akhmediev breather (AB) with $a = 0.48$ and the Peregrine soliton can be seen with close inspection of the decay of the peak to the wings; they are shown more clearly in Fig. 2.

[B. Kibler, J. Fatome, C. Finot, G. Millot, F. Dias, G. Genty, N. Akhmediev & JM Dudley, Nat. Phys. **6**, 790 (2010)]

Freak waves everywhere ?

- Rogue wave formation has been investigated in various frameworks, including:
 - * **oceanic freak waves** (or *ghost waves*, or rogons, or WANDTs “*Waves that Appear from Nowhere and Disappear without a Trace*”)
[Akhmediev et al, PLA (2009); Kharif & Pelinovsky, Eur. J. Mech. B/Fluids (2003)]
 - * **surface waves** generated in water tank experiments [Chabchoub, PRL (2011)]
 - * extreme intensity events (“**rare solitons**”) in *nonlinear optics*
[Solli et al, Nature (2007); Kibler et al, Nat. Phys. (2010) & Nature/Sci.Rep. (2012)]
 - * **errors in data communications** [Savory et al, J. Lightwave Technol. (2006)]
 - * **anomalous acoustic turbulence** in superfluid Helium [Ganshin et al, PRL (2008)]
 - * **rogue cells** – forerunners of metastatic cancer [Kaiser, Science (2010)]
 - * **stock market dynamics**: crashes, asset pricing (*Black-Scholes* theory) ...
- Unlike solitary waves (which are propagating excitations which are localized in space), rogue waves may be localized in space *and* in time (“*ghost waves*”).

What about ... freak waves in plasmas? (1)

- The *freak wave* paradigm was employed in plasmas as a possible mechanism for magnetic hole generation by *Michael Ruderman* (*), who considered the generation of Alfvén type freak waves by adopting a *Derivative Nonlinear Schrödinger (DNLS)* equation model.

Eur. Phys. J. Special Topics 185, 57–66 (2010)
© EDP Sciences, Springer-Verlag 2010
DOI: 10.1140/epjst/e2010-01238-7

THE EUROPEAN
PHYSICAL JOURNAL
SPECIAL TOPICS

Regular Article

Freak waves in laboratory and space plasmas

Freak waves in plasmas

M.S. Ruderman^a

School of Mathematics and Statistics, University of Sheffield, Hounsfield Road, Hicks Building, Sheffield
S3 7RH, UK

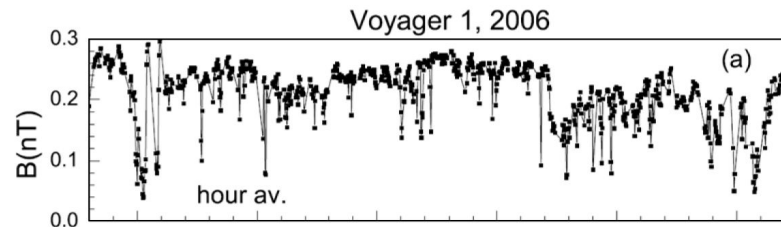


Fig. 1. Voyager 1 observations of hour averages of the magnetic field strength B in the heliosheath. The magnetic field magnitude shows many spike-like dips that are too narrow to be resolved in the hour average. Figure taken from Ref. [10].

[(*)] MS Ruderman, Eur. Phys. J. Special Topics **185**, 57 (2010)]

Freak waves in plasmas (2)

Rogue waves have been considered recently in various plasma contexts:

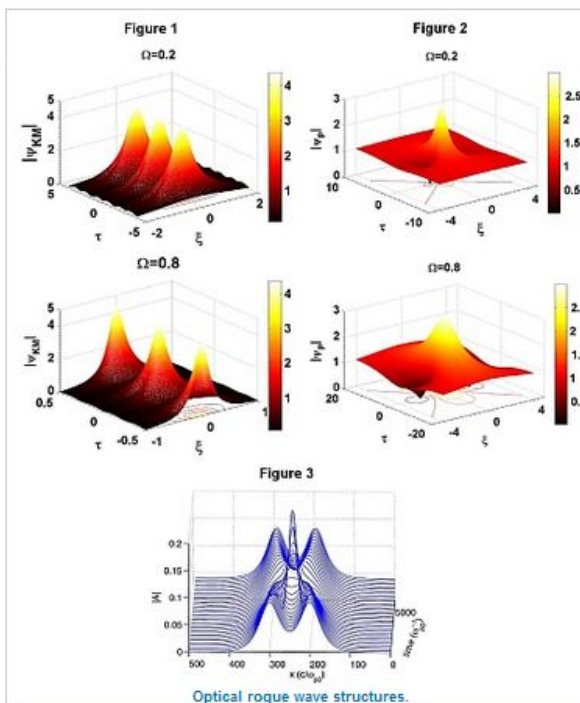
- *Alfvén-type rogue waves* [Shukla et al, Physics Letters A (2012)]
- *Langmuir rogue waves in electron-positron plasmas*
[Moslem, PoP 2011]
- *Electrostatic waves in e-p-i plasmas*
[El-Awady & Moslem, Phys. Plasmas 2011; El-Labany et al, Astrophys. Space Sci. 2012]
- *Dusty plasmas*
[Abdelsalam, et al, Phys. Plasmas 2011; Moslem et al, PRE 2011]
- *Surface plasma waves* [Moslem, Shukla and Eliasson, Europhys. Lett. 2011].
- Most of these studies have relied on a phenomenological analogy between rogue waves and large amplitude solutions of nonlinear model PDEs, e.g. KdV/mKdV or NLS equations (families).

Monster waves in a laser beam: myth or reality?

How can ultra-strong electromagnetic excitations be formed during the interaction of a laser beam with a plasma?

The unexpected occurrence of a huge water-wall (generally termed a rogue wave, or freak wave) has been a nightmare for seafarers (Onorato *et al* 2001 *Phys. Rev. Lett.* **86** 5831; Shukla *et al* 2006 *Phys. Rev. Lett.* **97** 094501) and a fascinating subject of research for nonlinear physicists (Akhmediev *et al* 2009 *Phys. Rev. A* **80** 043818). The amplitude of these giant waves is often reported to exceed twice or thrice the average height of surrounding waves (background turbulence), a fact suggesting a nonlinear description should be adopted as a model. This is a hot topic of current research, both in ocean physics and in other areas, including nonlinear optics, photonics and, more recently, in plasma physics. A better understanding of the formation of such destructive waves in the ocean would lead to the possibility of predicting, or even suppressing their occurrence. On the other hand, in nonlinear optics they can be used to generate high amplitude pulses when required. Significant research effort is being invested in elucidating the conditions for such excitations to occur, and in identifying their spatial and temporal characteristics.

In charged matter (plasma), by now recognized as the fourth state of matter and as the main



Related links

- [Electromagnetic rogue waves in beam-plasma interactions](#)
- [Special issue on Optical Rogue Waves](#)

Most recent Most read

- 
[Enhanced transmission under evanescent incidence](#)
Apr 25, 2014
 - 
[Low refractive index sensing](#)
Apr 25, 2014
 - 
[Simultaneous measurement of refractive index and thickness](#)
Apr 22, 2014
- [More LabTalk](#)

[*Electromagnetic Rogue Waves in Beam-Plasma Interactions*, G.P. Veldes, J. Borhanian, M. McKerr, V. Saxena, D.J. Frantzeskakis and I. Kourakis, *J. Optics* **15** (Special issue on Optical Rogue Waves), 064003 (2013);

IoP LabTalk article (online, 2013): *Monster waves in a laser beam: myth or reality?*]

Freak waves observed in plasma experiments?

- Random events – hard to observe in the laboratory!
- First experiment on negative-ion plasmas (NIPs):

PRL 107, 255005 (2011)

PHYSICAL REVIEW LETTERS

week ending
16 DECEMBER 2011

Observation of Peregrine Solitons in a Multicomponent Plasma with Negative Ions

H. Bailung,¹ S. K. Sharma,¹ and Y. Nakamura^{1,2}

¹Plasma Physics Laboratory, Physical Sciences Division, Institute of Advanced Study in Science and Technology, Paschim Boragaon, Guwahati-35, India

²On leave from Yokohama National University, Yokohama, Japan

(Received 29 July 2011; published 16 December 2011)

The experimental observation of Peregrine solitons in a multicomponent plasma with the critical concentration of negative ions is reported. A slowly amplitude modulated perturbation undergoes self-modulation and gives rise to a high amplitude localized pulse. The measured amplitude of the Peregrine soliton is 3 times the nearby carrier wave amplitude, which agrees with the theory. The numerical solution of the nonlinear Schrödinger equation is compared with the experimental results.

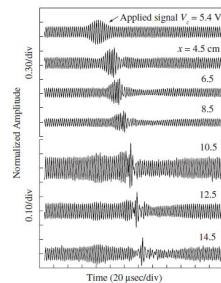


FIG. 2. Observed signals of the electron density perturbation at different probe positions from the separation grid. The top trace is the applied signal with carrier and modulation frequencies 350 and 31 kHz, respectively. Peak to peak amplitude of the applied carrier wave (V_c) is fixed at 5.4 V. Signals observed at 10.5 to 14.5 cm are shown with different amplitude scale (0.10/div) for better resolution.

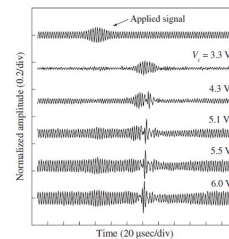


FIG. 3. Signals recorded for different excitation amplitudes of the carrier wave. The probe is fixed at 13.6 cm from the separation grid. Top trace represents the applied signal with carrier and modulation frequencies 350 and 31 kHz, respectively.

[9]. The slight shift in the phase of the carrier part with theory is probably due to the presence of pseudowave in front of the solitons [15]. However, detailed investigation is necessary for confirmation. We analyzed the wave signals

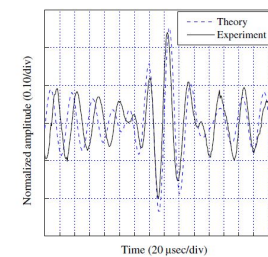


FIG. 4 (color online). Comparison of the time series signal (solid line) observed at 13.6 cm with the theoretical Peregrine soliton (dashed line) obtained by using Eq. (3). The applied carrier and modulation frequencies are 350 and 31 kHz, respectively. $V_c = 5.9$ V. The parameters used for numerical calculations are $\omega = 0.7\omega_{pi}$, ($\omega_{pi} = 492$ kHz), $k = 0.74k_D$, $k_D = 1/\lambda_D = 20.0$ cm⁻¹.

– Second experiment (in dusty plasmas) announced Feb. 2016!

nature
physics

LETTERS

PUBLISHED ONLINE: 29 FEBRUARY 2016 | DOI: 10.1038/NPHYS3669

Generation of acoustic rogue waves in dusty plasmas through three-dimensional particle focusing by distorted waveforms

Ya-Yi Tsai, Jun-Yi Tsai and Lin I*

Rogue waves—rare uncertainly emerging localized events with large amplitudes—have been experimentally observed in many nonlinear wave phenomena, such as water waves^{1–6}, optical waves^{7,8}, second sound in superfluid He II (ref. 9) and ion acoustic waves in plasmas¹⁰. Past studies have mainly focused on one-dimensional (1D) wave behaviour through modulation instabilities^{1,3–5,7,11}, and to a lesser extent on higher-dimensional behaviour^{5,6,8,11,12}. The question whether rogue waves also exist in nonlinear 3D acoustic-type plasma waves, the kinetic origin of their formation and their correlation with surrounding 3D waveforms are unexplored fundamental issues. Here we report the direct experimental observation of dust acoustic rogue waves in dusty plasmas and construct a picture of 3D particle focusing by the surrounding tilted and ruptured wave crests, associated with the higher probability of low-amplitude holes for rogue-wave generation.

Modulation instability (MI) which makes the wave modulation envelope unstable has been well accepted as a mechanism for rogue-wave or envelope soliton generation in systems governed by nonlinear equations, such as the nonlinear Landau–Ginzburg or Schrödinger equations^{1,3–5,7,11,12}. On the other hand, recent studies in nonlinear water, chemical and dust acoustic waves, also demonstrated that MI causes 3D waveform undulation, rupture

(refs 15,16,19,29) are the few examples giving experimental evidence of the ubiquitous behaviour in many other nonlinear media. The advantages of direct video imaging large-area dust density evolution and tracking individual particle motion at the discrete level also make it a good platform to construct an Eulerian–Lagrangian picture as a means of understanding dynamics in nonlinear density wave systems^{18,19,28}. Nevertheless, RWEs have been demonstrated theoretically only in 1D dust acoustic waves²².

The experiment is conducted in a cylindrical radiofrequency (rf) dusty-plasma system, as sketched in Fig. 1a (also see Methods)¹⁶. Figure 1b shows a typical temporal waveform of n_d , the normalized local dust density, in the disordered state of the self-excited downward propagating DAW. The irregular amplitude modulation evidences MI and causes the broadening of the fundamental and higher harmonic peaks in its power spectrum (Fig. 1c).

Figure 1d shows the histogram of the wave height H measured from 12,000 images. As commonly used for oceanic RWEs, the stretched tail beyond $2H_s$ signifies RWEs, where H_s ($=2$) is the significant wave height, defined as the average of the highest third of all wave heights^{1,2}. Figure 1e shows the highly localized and randomly distributed RWEs in the xyt space over 120 wave cycles. The averaged wavelength λ and wave period τ_0 are 1 mm and 32 ms, respectively.

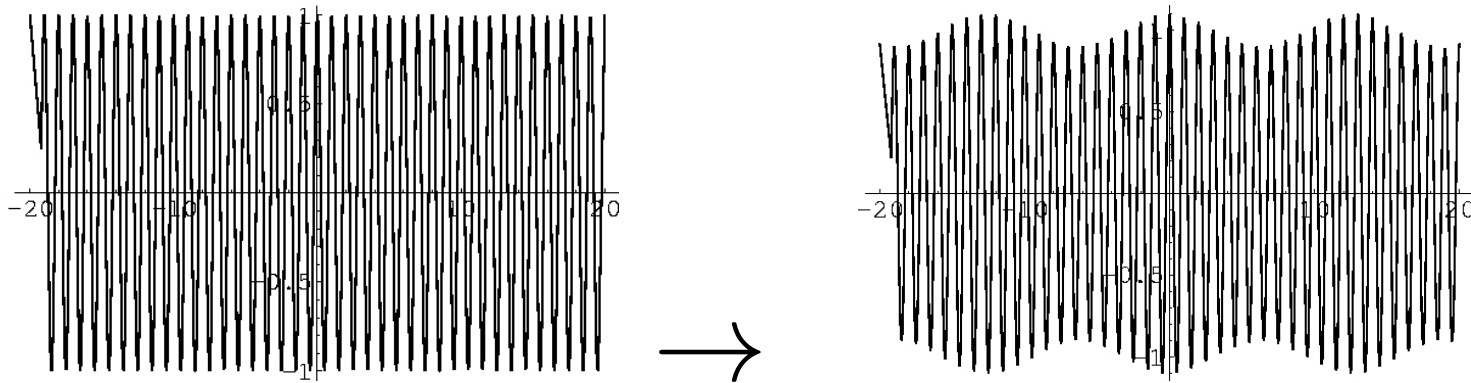
[Ya-Yi Tsai, Jun-Yi Tsai and Lin I, Nature (Physics) (2016) - DOI: 10.1038/NPHYS3669 .]

Intro #2: Nonlinear Amplitude Modulation (prerequisites)

- Harmonic variation of the amplitude of a plasma wavepacket
- Amplitude not constant, may vary weakly in space and time
- Ubiquitous nonlinear mechanism, associated with
 - * *secondary harmonic generation*
 - * *modulational instability*
 - * *envelope solitons*: localized forms with periodic internal structure
 - * *freak waves???*
- **Energy localization**: lumps of energy are formed and propagate in the plasma; dynamics to be harnessed for applications

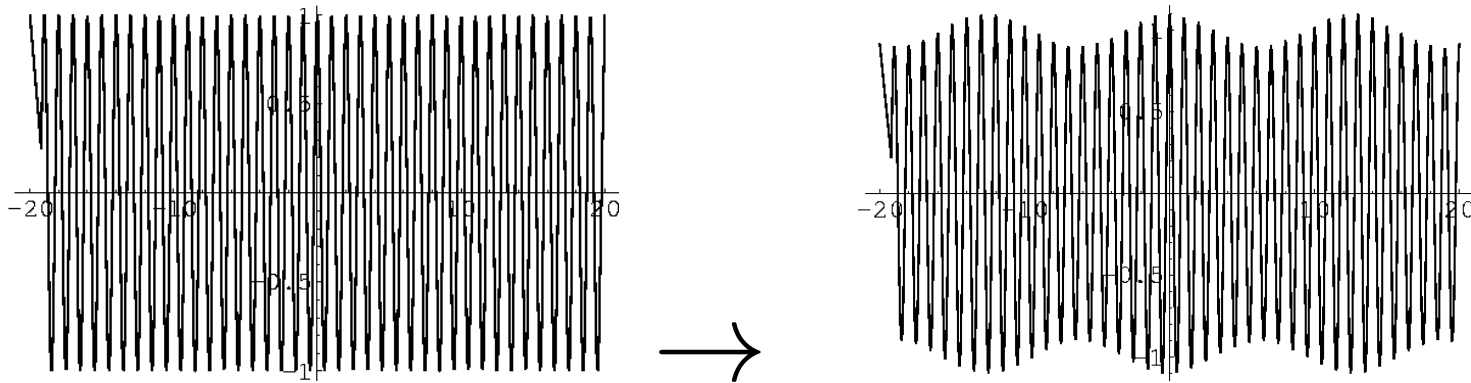
Intro: Prerequisites (*continued*)

The *amplitude* of a harmonic wave may vary in space and time:

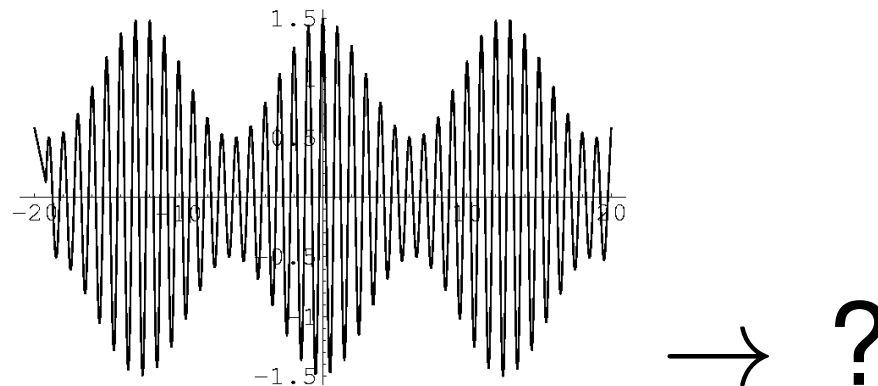


Intro: Prerequisites (*continued*)

The *amplitude* of a harmonic wave may vary in space and time:

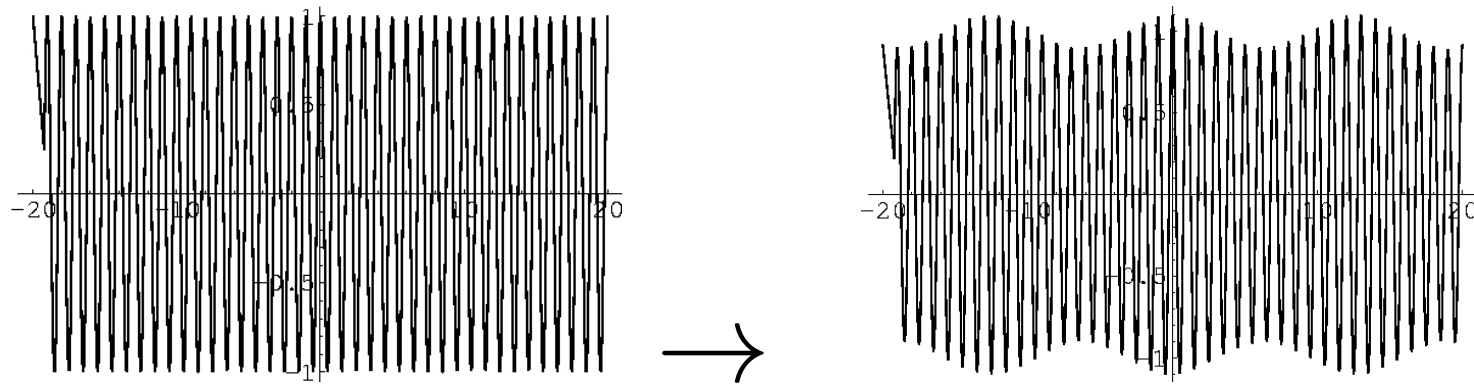


This *modulation* (due to nonlinearity) may be *strong* enough to lead to wave *collapse* (**modulational instability**) or ...

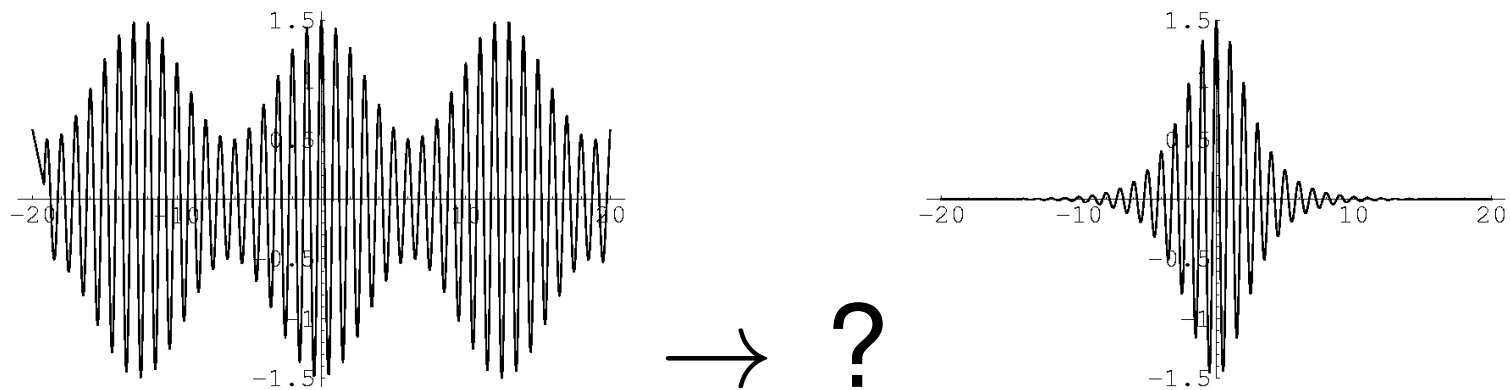


Intro: Prerequisites (*continued*)

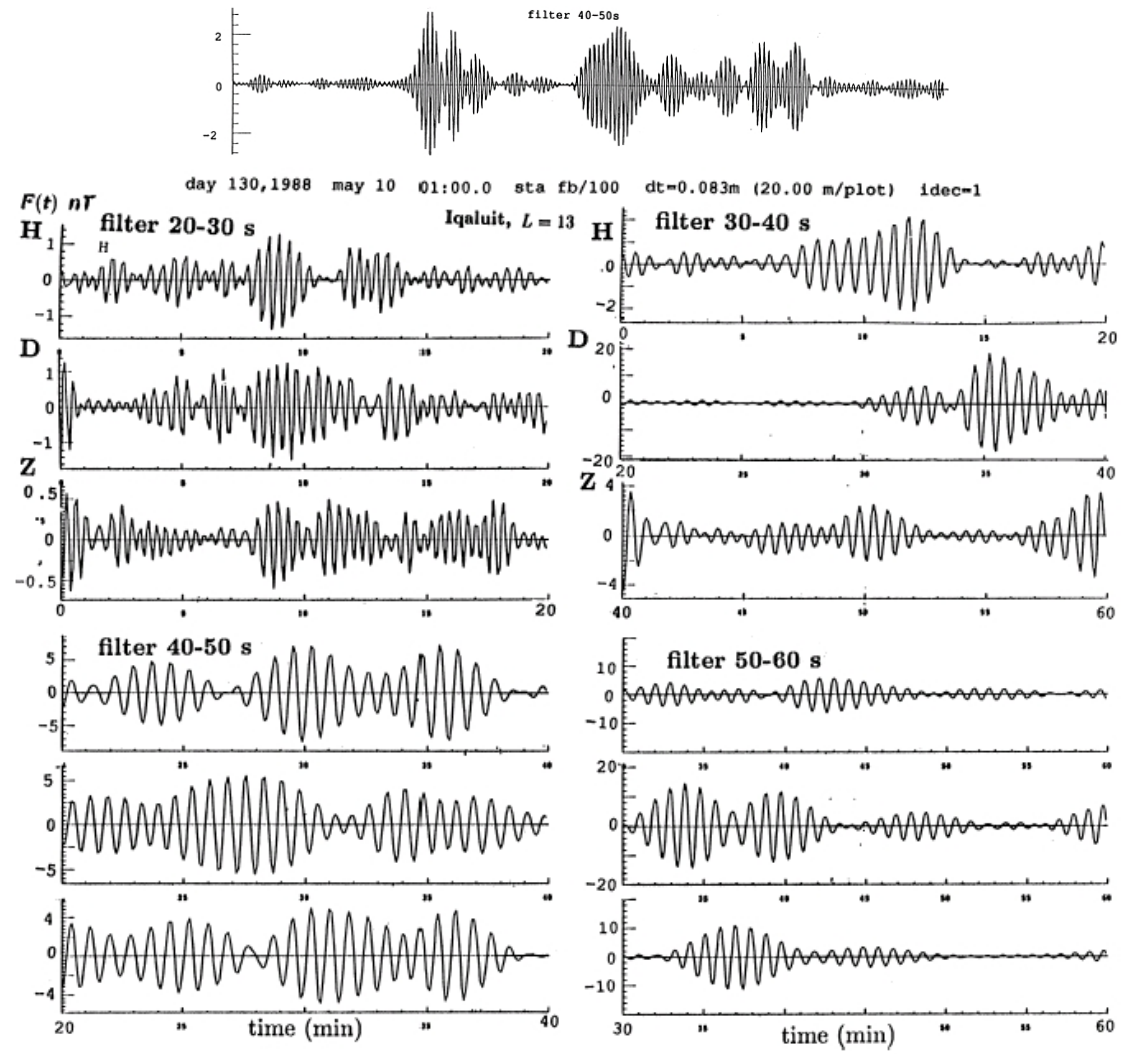
The *amplitude* of a harmonic wave may vary in space and time:



This *modulation* (due to nonlinearity) may be *strong* enough to lead to wave *collapse* (**modulational instability**) or to the formation of **envelope solitons**:



**Modulated structures occur widely,
e.g. in EM field measurements in the magnetosphere, ...**



(from: [Ya. Alpert, Phys. Reports **339**, 323 (2001)])

Inspiration: modulation of EM modes in negative-ion plasmas

- Saito *et al* (1984) considered the modulation instability mechanism in NIP, based on a Korteweg - de Vries (KdV) equation approach;
- M Ruderman *et al* (2008) considered the modulation instability mechanism in negative-ion plasmas, by using a Gardner equation approach at ***near-critical* plasma configuration**:

2 Modulationally unstable ion-acoustic waves in plasmas with negative ions

2.1 Gardner equation for nonlinear waves

Nonlinear ion-acoustic waves in plasmas have been studied for a very long period of time. It was shown that the Korteweg-de Vries (KdV) equation can be used to describe waves with moderate amplitudes [16–18]. The KdV-type ion-acoustic solitons in plasmas consisting of electrons and positive ions were then studied experimentally [19–23].

The behaviour of ion-acoustic waves becomes more complicated when the plasma contains not only positive but also negative ions. When the concentration of negative ions is equal to the critical value, the coefficient at the nonlinear term in the KdV equation is equal to zero, which implies that the cubic non-linearity has to be taken into account. As a result, nonlinear ion-acoustic waves in plasmas with the critical concentration of negative ions are described by the modified Korteweg-de Vries (mKdV) equation [24–28]. The mKdV solutions were also observed in the experiment [29].

When the negative ion concentration is not exactly equal to the critical value, but close to it, both the quadratic and cubic non-linearity has to be taken into account. In that case the dynamics of nonlinear ion-acoustic waves is described by the Gardner equation [30,31],

$$\frac{\partial \psi}{\partial \tau} - a\psi \frac{\partial \psi}{\partial \xi} + g\psi^2 \frac{\partial \psi}{\partial \xi} + \chi \frac{\partial^3 \psi}{\partial \xi^3} = 0. \quad (1)$$

The Bailung-Sharma-Nakamura- experiment:

PRL 107, 255005 (2011)

PHYSICAL REVIEW LETTERS

week ending
16 DECEMBER 2011

Observation of Peregrine Solitons in a Multicomponent Plasma with Negative Ions

H. Bailung,¹ S. K. Sharma,¹ and Y. Nakamura^{1,2}

¹Plasma Physics Laboratory, Physical Sciences Division, Institute of Advanced Study in Science and Technology, Paschim Boragaon, Guwahati-35, India

²On leave from Yokohama National University, Yokohama, Japan

(Received 29 July 2011; published 16 December 2011)

The experimental observation of Peregrine solitons in a multicomponent plasma with the critical concentration of negative ions is reported. A slowly amplitude modulated perturbation undergoes self-modulation and gives rise to a high amplitude localized pulse. The measured amplitude of the Peregrine soliton is 3 times the nearby carrier wave amplitude, which agrees with the theory. The numerical solution of the nonlinear Schrödinger equation is compared with the experimental results.

DOI: 10.1103/PhysRevLett.107.255005

PACS numbers: 52.35.Fp, 52.27.Cm

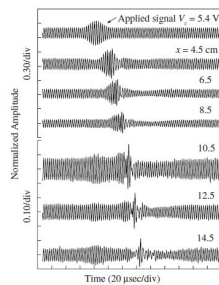


FIG. 2. Observed signals of the electron density perturbation at different probe positions from the separation grid. The top trace is the applied signal with carrier and modulation frequencies 350 and 31 kHz, respectively. Peak to peak amplitude of the applied carrier wave (V_c) is fixed at 5.4 V. Signals observed at 10.5 to 14.5 cm are shown with different amplitude scale (0.10/div) for better resolution.

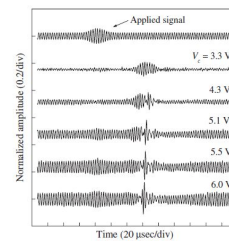


FIG. 3. Signals recorded for different excitation amplitudes of the carrier wave. The probe is fixed at 13.6 cm from the separation grid. Top trace represents the applied signal with carrier and modulation frequencies 350 and 31 kHz, respectively.

[9]. The slight shift in the phase of the carrier part with theory is probably due to the presence of pseudowave in front of the solitons [15]. However, detailed investigation is necessary for confirmation. We analyzed the wave signals

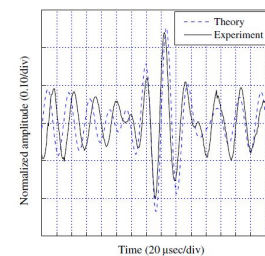


FIG. 4 (color online). Comparison of the time series signal (solid line) observed at 13.6 cm with the theoretical Peregrine soliton (dashed line) obtained by using Eq. (3). The applied carrier and modulation frequencies are 350 and 31 kHz, respectively. $V_c = 5.9$ V. The parameters used for numerical calculations are $\omega = 0.7\omega_{pe}$, $(\omega_{pe} = 492 \text{ kHz})$, $k = 0.74k_D$, $k_D = 1/\lambda_D = 20.0 \text{ cm}^{-1}$.

Read the fingerprint: a number of hypotheses underlies the earlier treatments (by Saito *et al*, Ruderman *et al*, and later Bailung *et al*):

- NIP **near-critical plasma concentration**, so that the quadratic nonlinearity term in the KdV equation is *nearly zero*;
- Gardner equation, i.e.
 - ★ **small-amplitude** ES potential excitation ($\phi \ll kT_e/m$),
 - ★ **small-wavenumber** $k \ll \lambda_D^{-1}$ (long wavelength $\lambda \gg \lambda_D$),
 - ★ **weakly-superacoustic** ($v_{sol} \simeq c_s + \epsilon\delta v$) approximation.
- Questions:
 - ★ Are these requirements **necessary conditions** for freak wave formation?
 - ★ Could freak waves be generated in NIPs in different conditions ... ?
 - ★ ... and, in particular, in more general (non“critical”) plasma configurations?

Multifluid model + multiple-scale analysis

- We consider a three component collisionless unmagnetized plasma consisting of:
 - ★ electrons (mass m_e , charge e), thermalized (inertialess)
 - ★ positive ions (mass m_p , charge $q_p = Z_p e$)
 - ★ negative ions (mass m_n , charge $q_n = -Z_n e$)
- Electrostatic approximation + three-ion fluid model + Poisson's equation:

$$\partial_t n_p + \nabla(n_p u_p) = 0, \quad (1)$$

$$\partial_t u_p + u_p \nabla(u_p) = -\frac{q_p}{m_p} \nabla \phi, \quad (2)$$

$$\partial_t n_n + \nabla(n_n u_n) = 0, \quad (3)$$

$$\partial_t u_n + u_n \nabla(u_n) = -\frac{q_n}{m_n} \nabla \phi, \quad (4)$$

$$\nabla^2 \phi = 4\pi [en_e - q_p n_p - q_n n_n], \quad (5)$$

- Quasi-neutrality assumption: at equilibrium, $n_{e0}e - q_n n_{n0} - q_p n_{p0} = 0$.

- The model equations are cast in a dimensionless form as

$$\partial_t n_p + \nabla(n_p u_p) = 0, \quad (6)$$

$$\partial_t u_p + u_p \nabla(u_p) = -\nabla\phi, \quad (7)$$

$$\partial_t n_n + \nabla(n_n u_n) = 0, \quad (8)$$

$$\partial_t u_n + u_n \nabla(u_n) = \delta \nabla\phi, \quad (9)$$

$$\nabla^2 \phi = -n_p + \beta n_n + (1 - \beta) f(\phi), \quad (10)$$

where $f(\phi) = \exp\left(\frac{e\phi}{k_B T_e}\right) \simeq 1 + c_1 \phi + c_2 \phi^2 + c_3 \phi^3$ (Maxwellian assumption).

- T_e is the electron temperature; $c_1 = 2c_2 = 6c_3 = 1$.
- Dimensionless parameters: $\beta = \frac{Z_n n_{0n}}{Z_p n_{0p}}$, $\delta = \frac{Z_n/m_n}{Z_p/m_p}$.
- Scaling: $T_0 = \omega_{p,+}^{-1} = (4\pi e^2 n_{p,0} Z_p^2 / m_p)^{-1/2}$, $\phi_0 = k_B T_e / e$
 $\lambda_{D,+} = (k_B T_e / 4\pi Z_p e^2 n_{p,0})^{1/2}$, $C_s = V_0 = (Z_p k_B T_e / m_p)^{1/2}$.

The boring part: *multiscale technique for envelope dynamics*

- Following the multiple scales (reductive perturbation) technique of Taniuti and coworkers (JMP & JPSJ 1969), we consider the stretched variables

$$X_n = \epsilon^n x ; \quad T_n = \epsilon^n t ; \quad n = 0, 1, 2, \dots$$

- We define the state vector $\mathbf{S} = (n_p, u_p; n_n, u_n; \phi)$, and
- proceed by expanding near the equilibrium state $\mathbf{S}^{(0)} = (1, 0; 1, 0; 0)$ as

$$\mathbf{S} = \mathbf{S}^{(0)} + \sum_{n=-\infty}^n \epsilon^n \mathbf{S}^{(n)}$$

where

$$\mathbf{S}^{(n)} = \sum_{l=-n}^n \mathbf{S}_l^{(n)} e^{il(kx - \omega t)}$$

denotes the amplitude of the n -th order contribution, as a series of the l -th harmonic amplitude(s) $\mathbf{S}_{(l)}^{(n)} = \mathbf{S}_{(l)}^{(n)}(X_j, T_j)$ (slow, for $j \geq 1$).

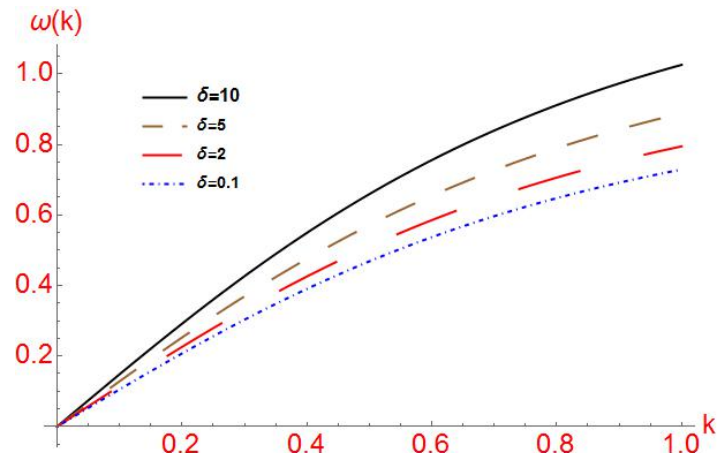
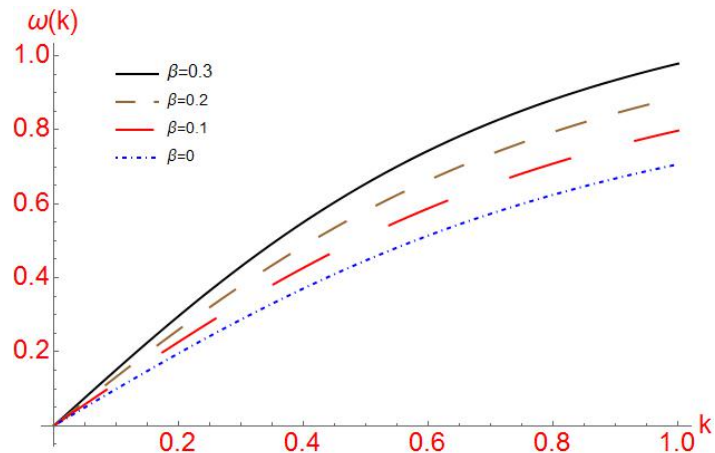
Perturbative scheme – results

- *Dispersion relation:*

$$\omega^2 = \frac{(1 + \delta\beta)k^2}{k^2 + (1 - \beta)}$$

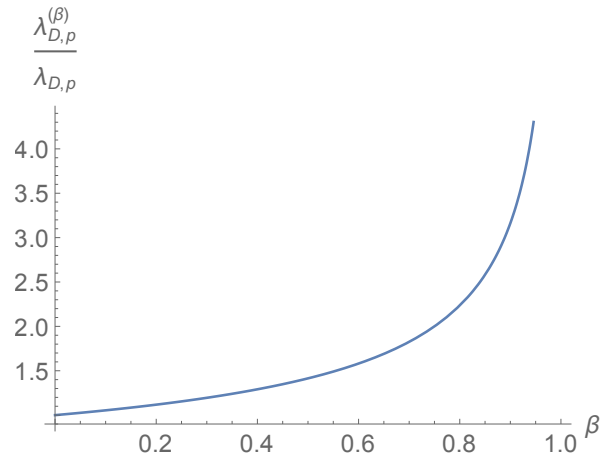
Or, restoring dimensions,

$$\omega^2 = \frac{\omega_{p,p}^2 (1 + \delta\beta) (k\lambda_{D,p})^2}{(k\lambda_{D,p})^2 + (1 - \beta)}$$

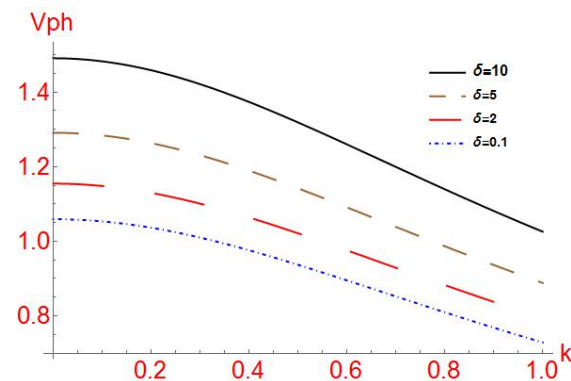
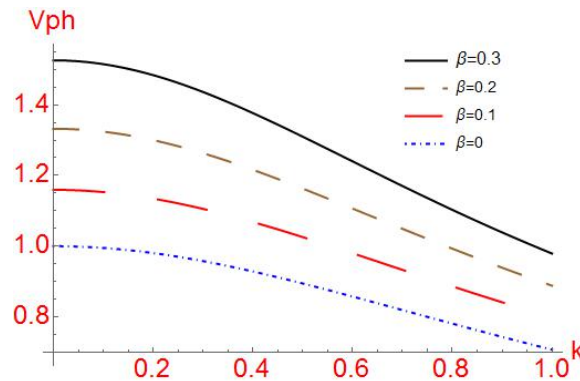


Modified charge (Debye) screening length versus β :

$$\lambda_{D,p}^{(\beta)} = 1/\sqrt{(1-\beta)} \lambda_{D,p}.$$



Modified phase speed: $v_{ph} = \frac{(1-\beta)\sqrt{1+\beta\delta}}{[k^2+(1-\beta)]^{3/2}} \simeq \left(\frac{1+\beta\delta}{1-\beta}\right)^{1/2}$ (for $k \ll 1$).

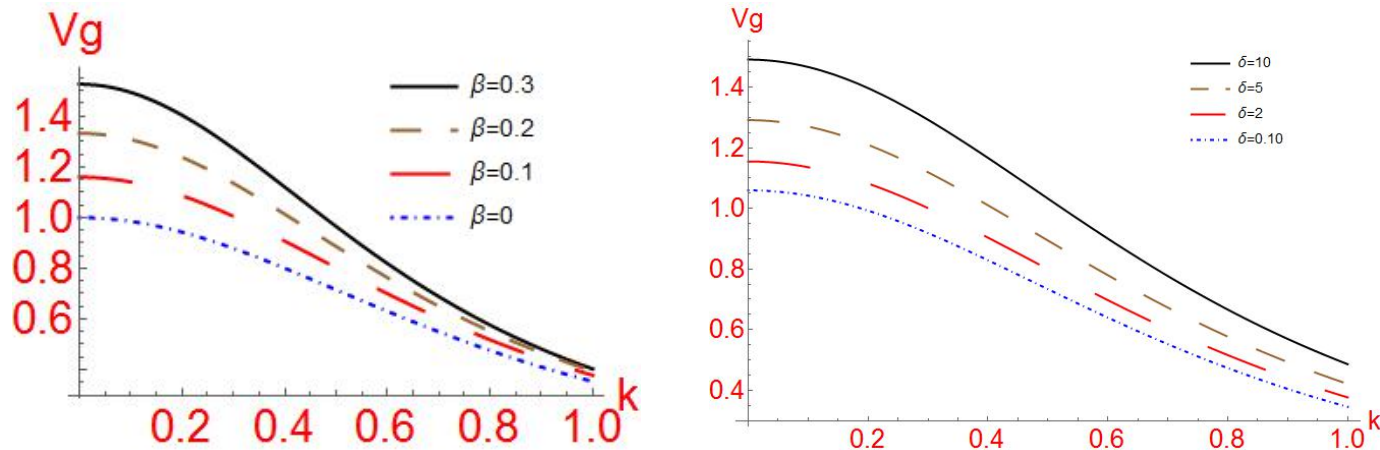


- In order $\sim \epsilon^2$:

$$\partial_1 \phi_1^{(1)} + v_g \nabla_1 \phi_1^{(1)} = 0.$$

- The envelope $\phi_1^{(1)} = \phi_1^{(1)}(X_1 - v_g T_1)$ moves at the *group velocity*:

$$v_g = \frac{d\omega}{dk} = \frac{(1 - \beta)(1 + \delta\beta)^{\frac{1}{2}}}{[k^2 + (1 - \beta)]^{\frac{3}{2}}}.$$



- Increasing the charge-density and mass ratios makes ion acoustic structures faster, i.e., increases the group velocity.

NLS equation for the vector potential (amplitude) $A_1^{(1)}$

- In order $\sim \epsilon^3$:
- This analytical requirement can be expressed in the form

$$i \left(\frac{\partial A_1^{(1)}}{\partial T_2} + v_g \frac{\partial A_1^{(1)}}{\partial X_2} \right) + P \frac{\partial^2 A_1^{(1)}}{\partial X_1^2} + Q |A_1^{(1)}|^2 A_1^{(1)} = 0$$

- Dispersion coefficient P : $P = \frac{1}{2} \left[\frac{3v_g^2}{\omega} + \frac{\omega}{k^2} - \frac{4v_g}{k} - \frac{\omega^3}{\gamma(1+\delta\beta)k^2} \right]$
- Nonlinearity coefficient Q :

$$Q = \frac{(1 - \beta)\omega^3}{2(1 + \delta\beta)k^2} [2c_2(A + B) + 3c_3] - \frac{(1 - \delta^2\beta)}{(1 + \delta\beta)} \left[\frac{Bk}{v_g} + \frac{B\omega}{2v_g^2} + \frac{3Ak^2}{2\omega} \right] - \frac{(1 + \delta^3\beta)}{(1 + \delta\beta)} \left[\frac{k^2}{2\omega v_g^2} + \frac{2k^3}{\omega^2 v_g} + \frac{5k^4}{4\omega^3} \right].$$

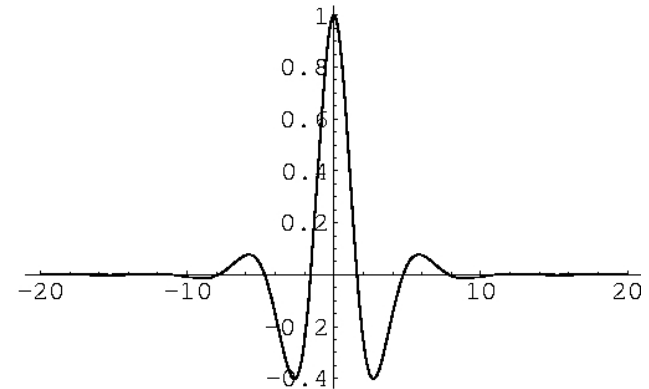
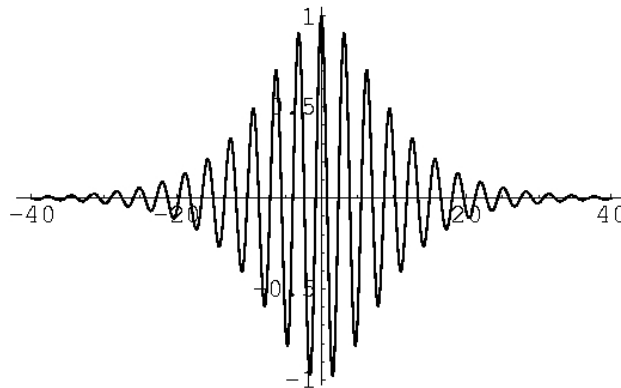
Localized envelope excitations (*bright solitons*) for $PQ > 0$

- The NLSE accepts various solutions in the form: $\psi = \rho e^{i\Theta}$;
the *total* electric potential is then: $\phi \approx \epsilon \rho \cos(\mathbf{k}\mathbf{r} - \omega t + \Theta)$
where the *amplitude* ρ and *phase correction* Θ depend on ζ, τ .
- Bright-type envelope soliton (pulse):

$$\rho = \rho_0 \operatorname{sech}\left(\frac{\zeta - v\tau}{L}\right), \quad \Theta = \frac{1}{2P} \left[v\zeta - \left(\Omega + \frac{1}{2}v^2\right)\tau \right].$$

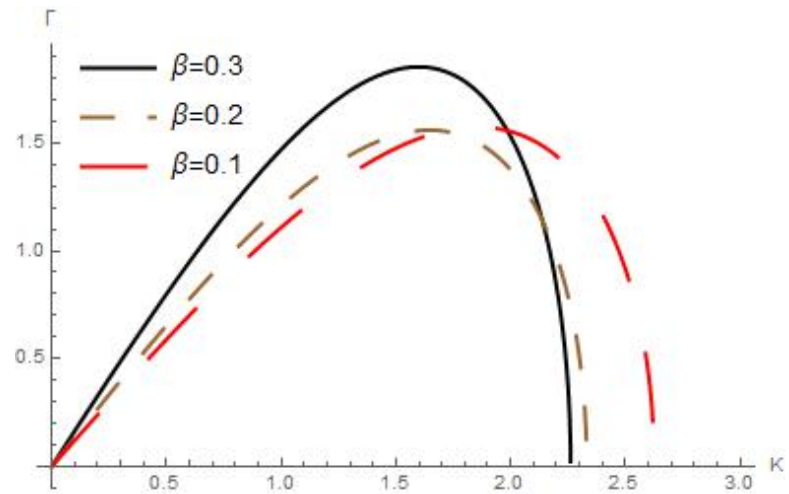
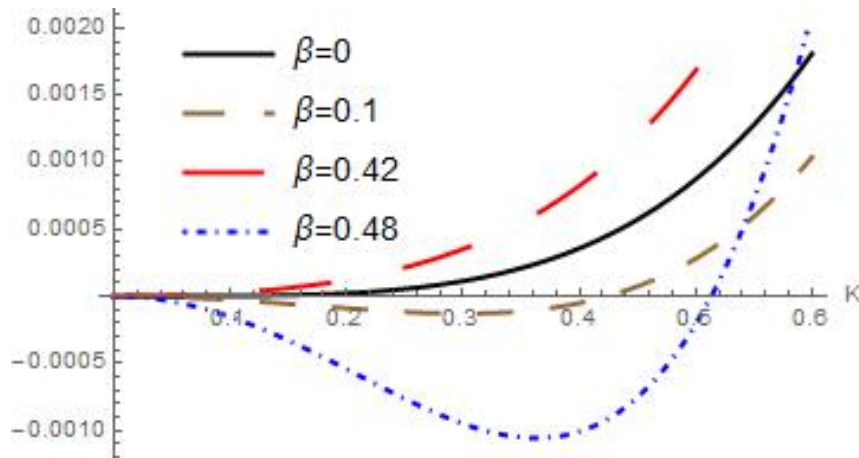
$$L = \sqrt{\frac{2P}{Q}} \frac{1}{\rho_0}$$

This is a
propagating
(and *oscillating*)
localized **pulse**:

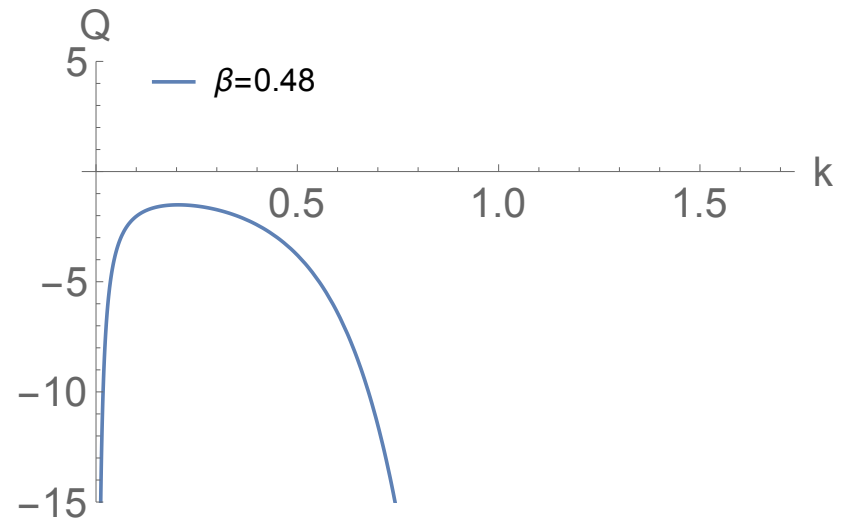
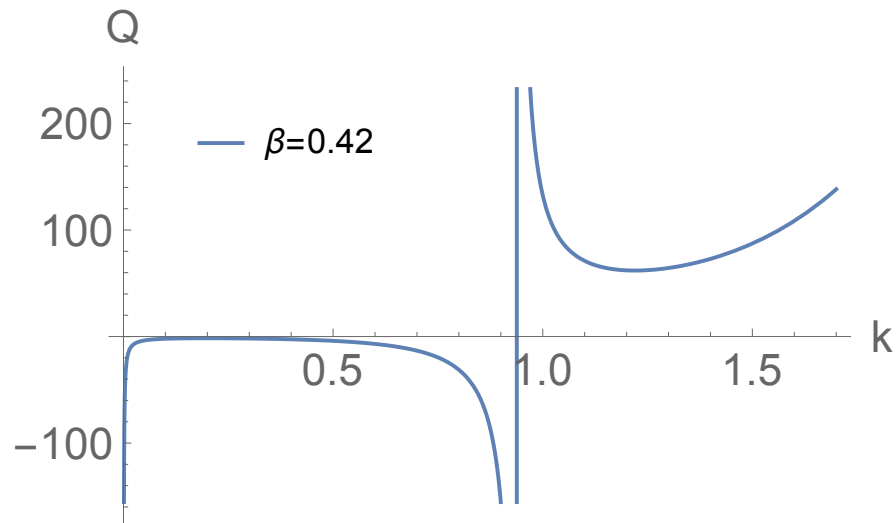
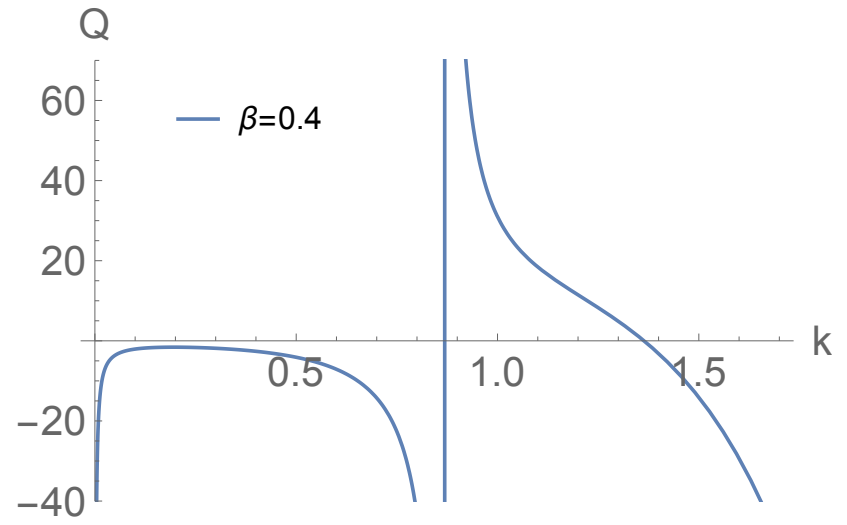
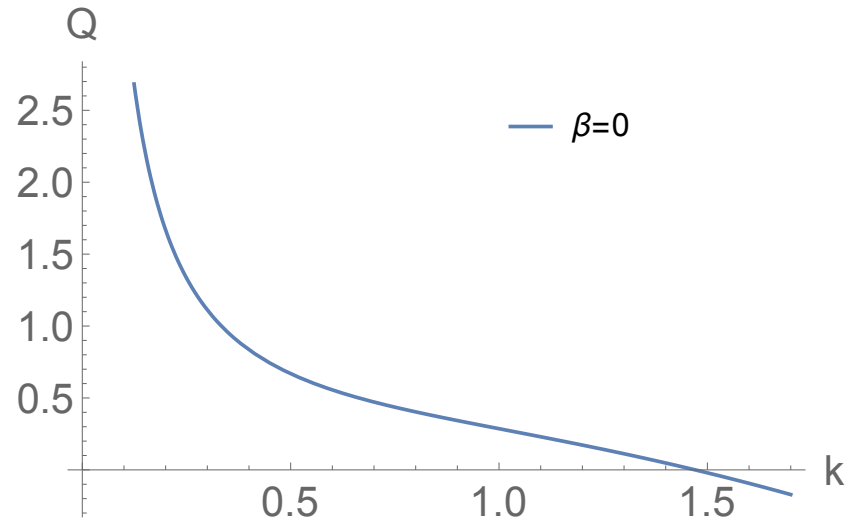


Modulational (in)stability: parametric dependence

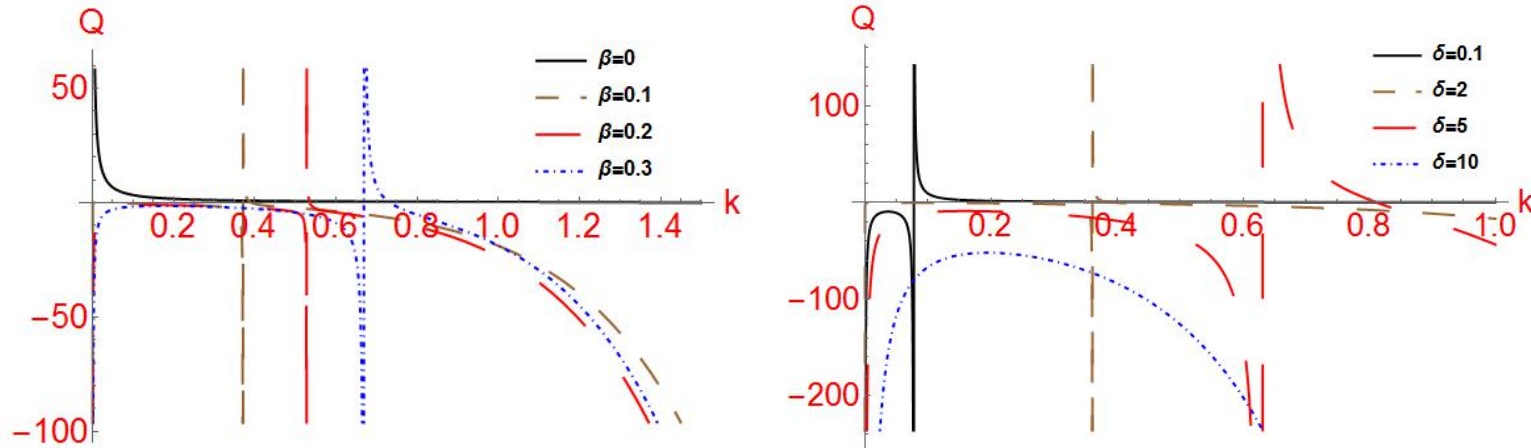
- If $PQ > 0$: the amplitude ψ is *unstable* for $\tilde{k} < \sqrt{2 \frac{Q}{P}} |\psi_{1,0}|$.
- Maximum (instability) growth rate: $\sigma = Q |\psi_{1,0}|^2$, occurs at $\tilde{k}_m < \sqrt{\frac{Q}{P}} |\psi_{1,0}|$
- Both the *instability growth rate* and *threshold* $k_{critical}$ depend on the plasma parameters in a non-trivial (and non-monotonic) manner:



Nonlinearity coefficient: parametric dependence



Nonlinearity coefficient: parametric dependence



- In the long-wavelength limit $k \ll 1$: $P \simeq p_0 k$ and $Q \simeq q_0 k^{-1}$, where:

$$p_0 = -\frac{3\sqrt{1+\delta\beta}}{2(1-\beta)^{3/2}}, \quad q_0 = -\frac{\sqrt{1-\beta} [2 + 2\delta^2\beta^2 - \beta(3 + 2\delta + 3\delta^2)]^2}{12 + (1 + \delta\beta)^{7/2}}.$$

- Recall that the ratio P/Q determines the geometry of envelope solitons ($L \sim (P/Q)^{1/2}$), as well as the criterion for their existence.

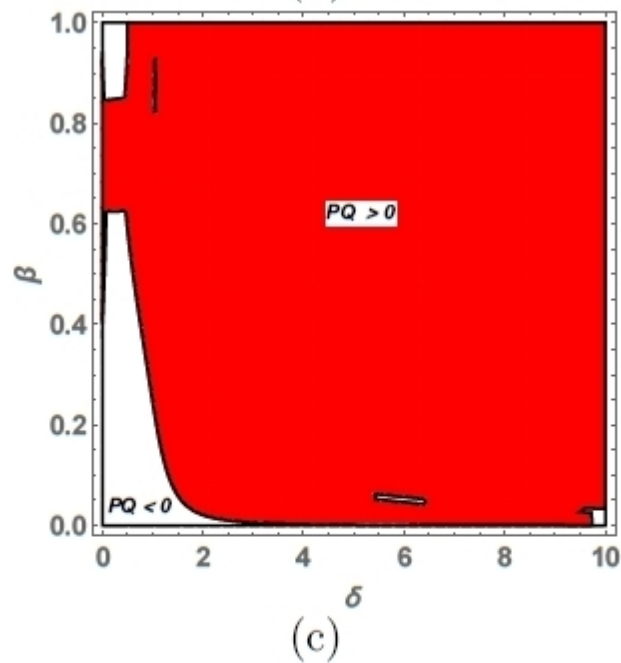
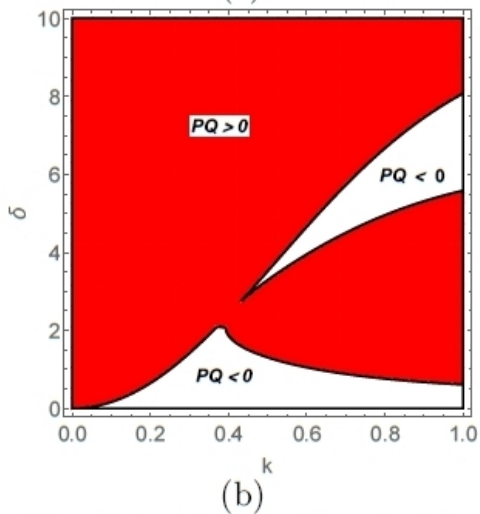
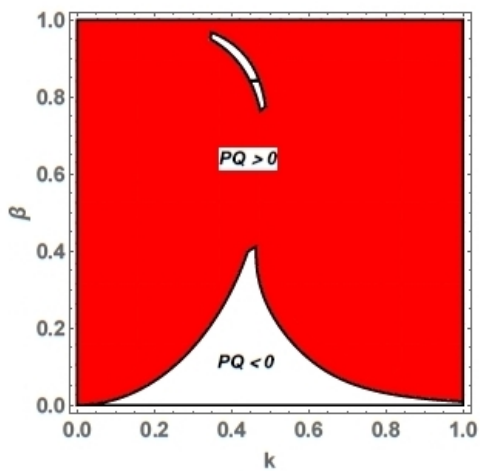
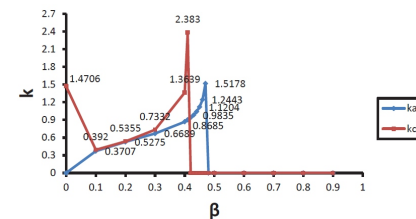
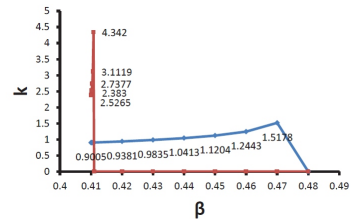
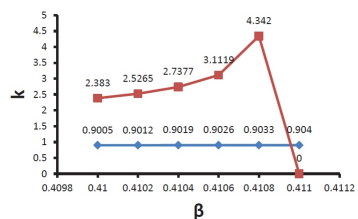
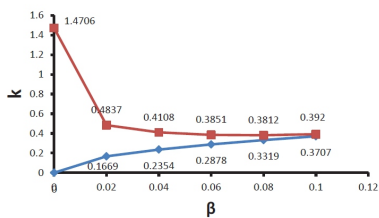


FIG. 9: (Color online) Region for $PQ < 0$ (white region) and $PQ > 0$ (red region) as functions of the wave number k and (a) β when $\delta = 1$, (b) δ when $\beta = 0.1$. (c) β and δ when $k = 0.5$.



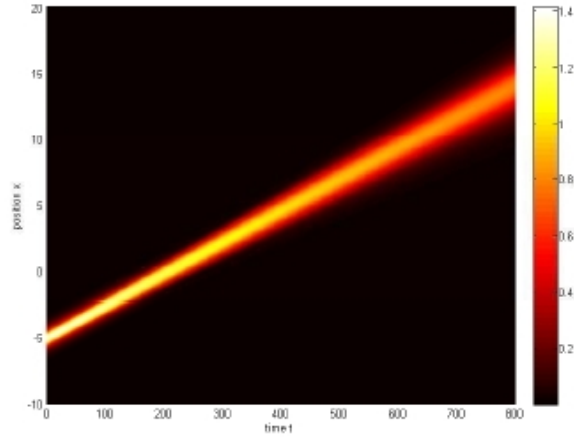
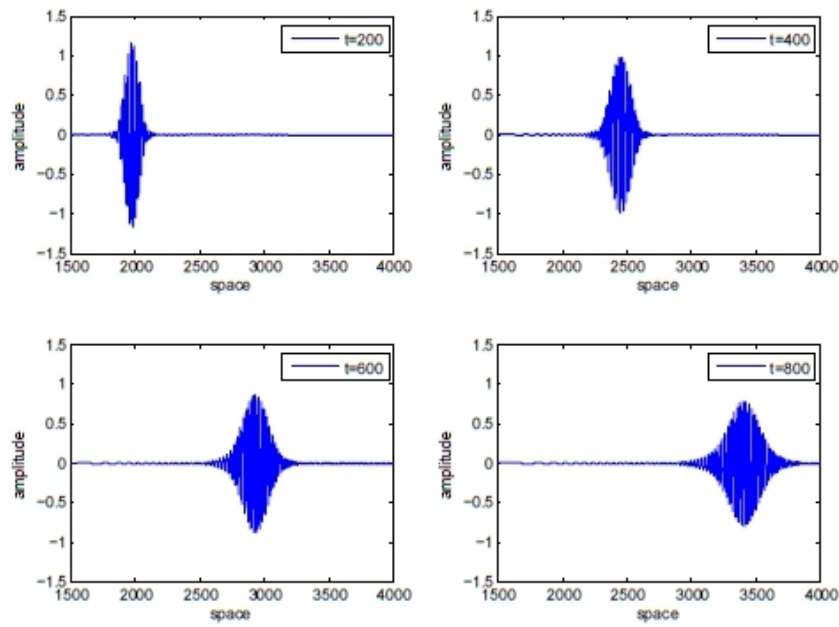


FIG. 18: (Color online) Time evolution and propagation of a breather (bright soliton) on the space-time plane. IC ($\beta = 0.1, \delta = 1, k = 0.1, PQ > 0$), NLSE ($\beta = 0.2, \delta = 1, k = 0.1, PQ > 0$).

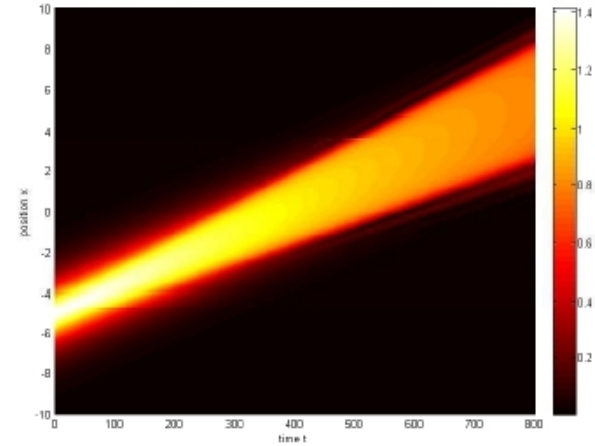
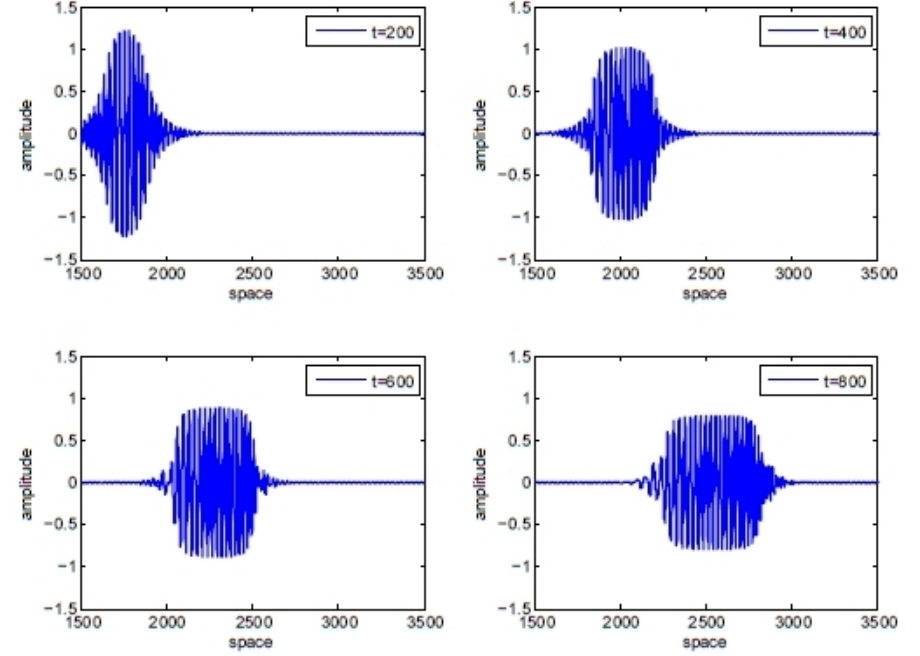
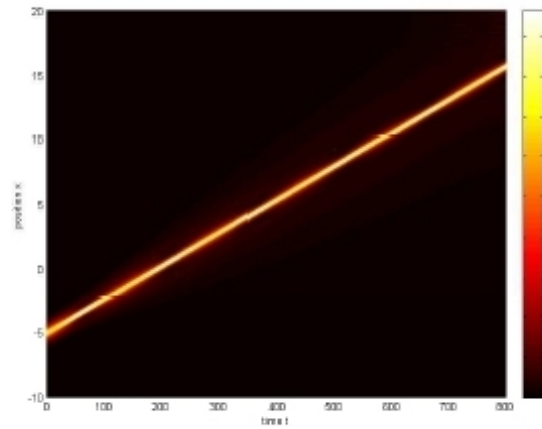
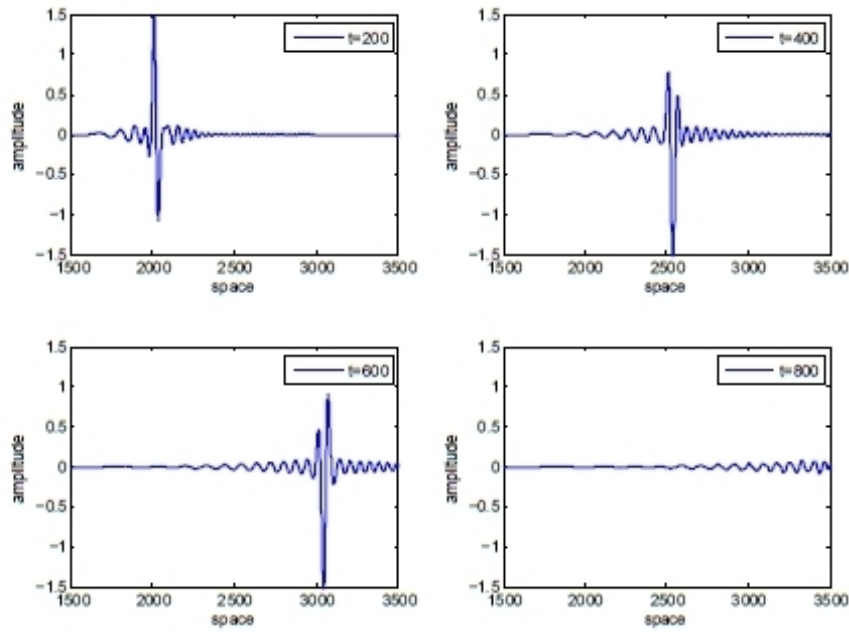
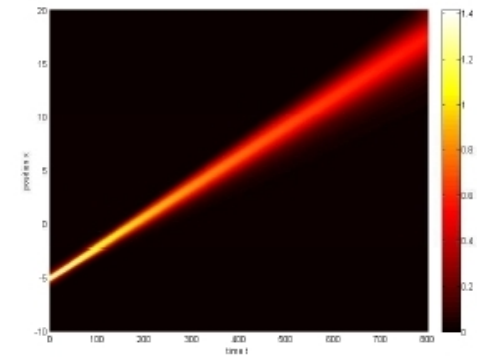
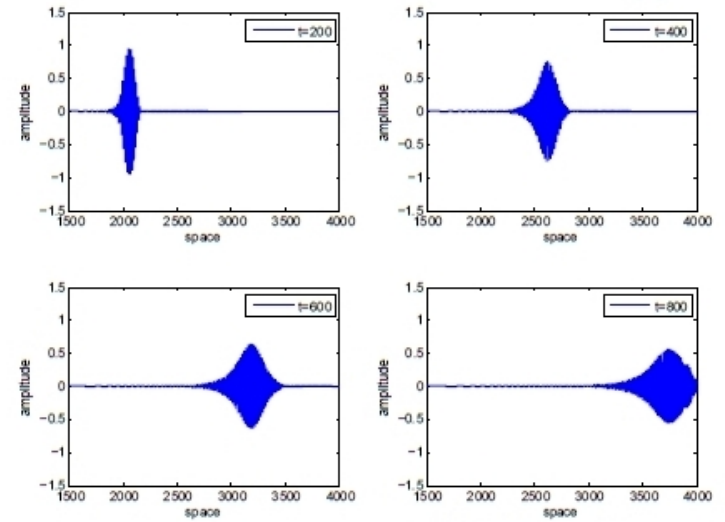


FIG. 19: (Color online) Time evolution and propagation of a breather (bright soliton) on the space-time plane. IC ($\beta = 0.2, \delta = 1, k = 0.1, PQ > 0$), NLSE ($\beta = 0, \delta = 1, k = 0.1, PQ < 0$).



(a)



(b)

FIG. 20: (Color online) Time evolution and propagation of a breather (bright soliton) on the space-time plane. (a) IC ($\beta = 0.2$, $\delta = 1$, $k = 0.1$, $PQ > 0$), NLSE ($\beta = 0.4$, $\delta = 2.1$, $k = 0.7$, $PQ > 0$). (b) IC ($\beta = 0$, $\delta = 1$, $k = 0.1$, $PQ < 0$), NLSE ($\beta = 0.2$, $\delta = 1$, $k = 0.1$, $PQ > 0$).

Analytical models for rogue waves

- The *Peregrine soliton*

[D. H. Peregrine, J. Austral. Math. Soc. B **25**, 16 (1983); K. B. Dysthe, and K. Trulsen, Physica Scripta **T82**, 48 (1999); V. I. Shrira, and V. V. Geogjaev, J. Eng. Math. **67**, 11 (2010); B. Kibler, J. Fatome, et al., Nature Physics **6**, 790 (2010)]

- The *Akhmediev breather*

[N. N. Akhmediev, V. M. Eleonskii, and N. E. Kulagin, Theor. Math. Phys. 72, 809 (1987)];

- The *Kuznetsov-Ma breather*

[Ya C. Ma, Stud. Appl. Math. **60**, 43 (1979)];

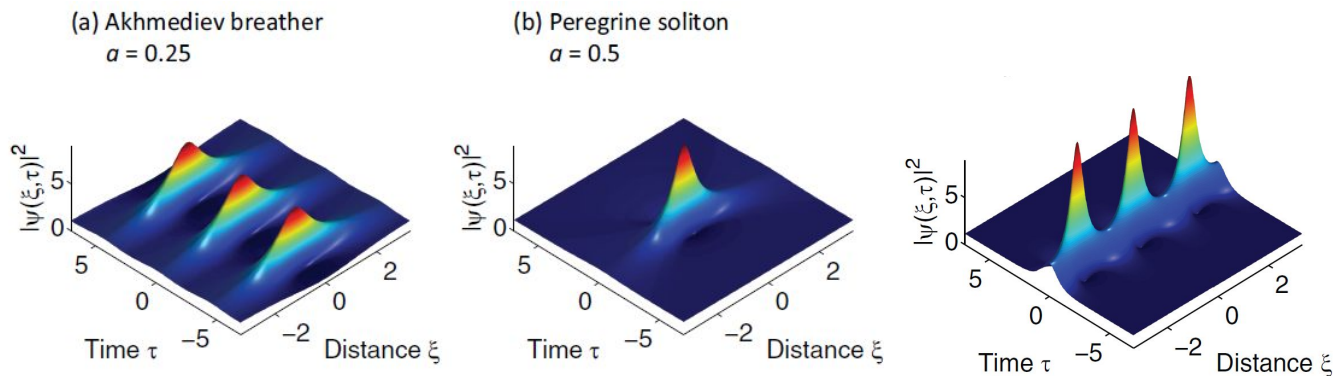


[Figure from: Kibler *et al*, Nat. Phys. (2010) & Nature/Sci.Rep. (2012).]

Parametric analysis: dependence on the negative-ion concentration (β)

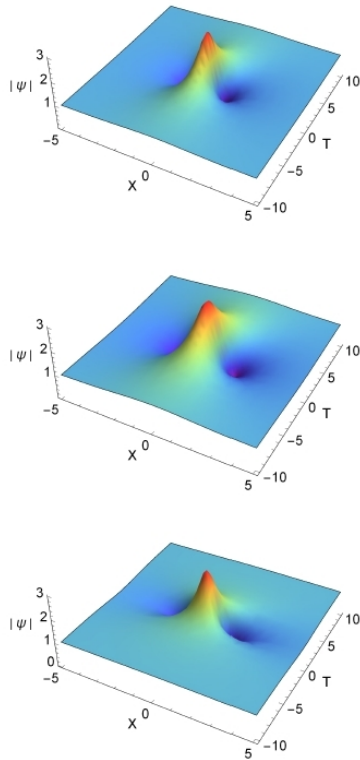


FIG. 15: (Color online) The *Peregrine soliton* is depicted for different values of β ($= 0.2, 0.4, 0.6$), with $k = 0.1$ and $\delta = 1$ (e.g. for H^+/H^- plasma).

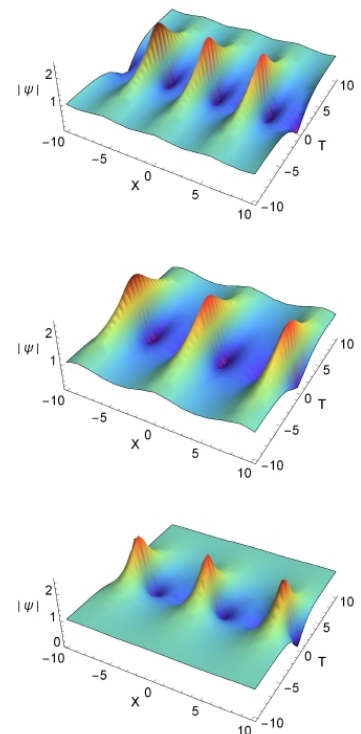


FIG. 16: (Color online) The *Akhmediev breather* is depicted for different values of β ($= 0.2, 0.4, 0.6$), with $k = 0.1$ and $\delta = 1$ (e.g. for H^+/H^- plasma).

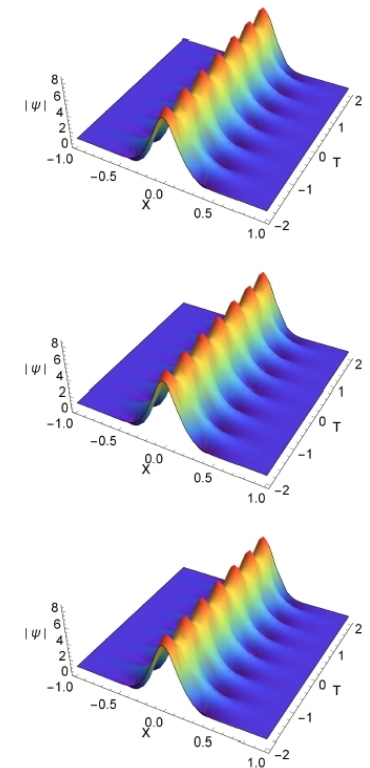


FIG. 17: (Color online) The *Kuznetsov-Ma breather* is depicted for different values of β ($= 0.2, 0.4, 0.6$), with $k = 0.1$ and $\delta = 1$ (e.g. for H^+/H^- plasma).

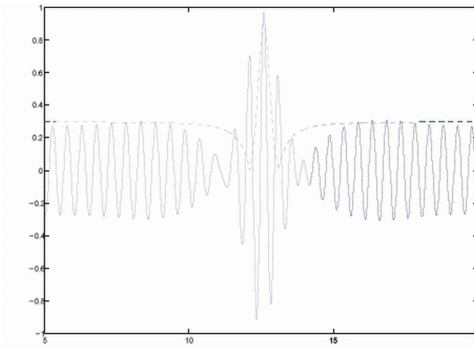
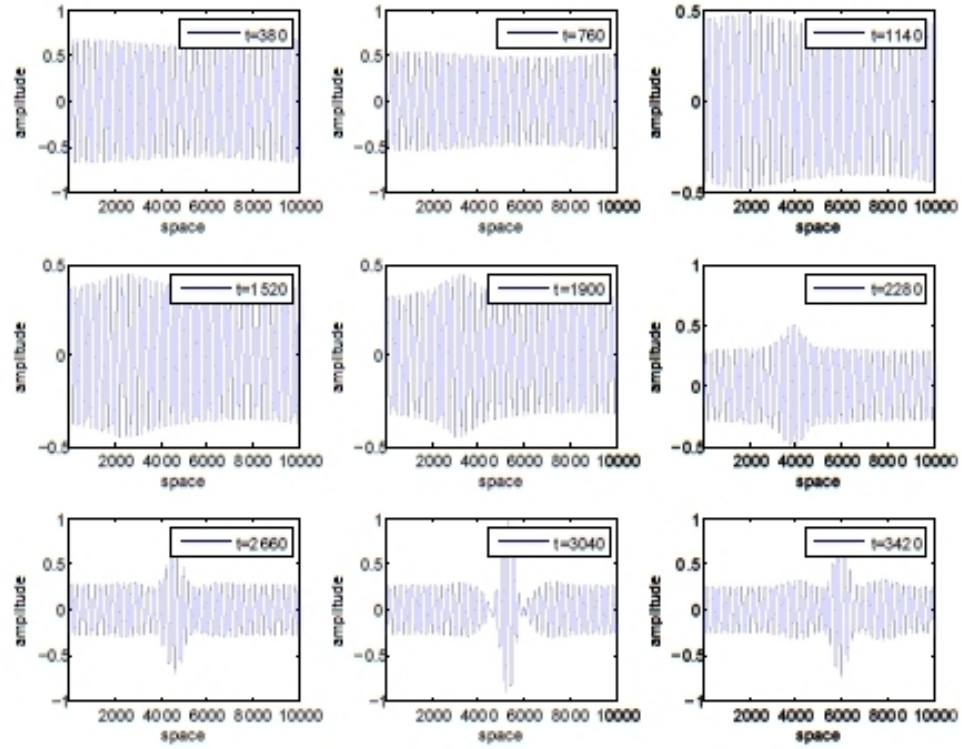


FIG. 21: (Color online) (a) Temporal profiles of the carrier and the growing rogue wave for $PQ > 0$. (b) The envelopes described by the corresponding analytic Peregrine solution of the NLS equation are shown by the dashed (green) curves.

Thanks for listening!

IoannisKourakisSci@gmail.com , ioannis.kourakis@ku.ac.ae

Additional slides for plasma and simulation parameters

Plasma and Simulation Parameters for generation of supersoliton (slides 2&3)

Initial Perturbation Form: Gaussian Potential

$$n_j = n_{j0} + \Delta n \text{Exp} \left[- \left(\frac{x - x_c}{l_0} \right)^2 \right]$$

Here, Δn is the amplitude of the perturbation, x is the position on the x -axis, x_c is the center of the system, and l_0 controls the width of the perturbation.

Simulation Parameters: $\Delta n = 1.9 n_{i0}$ and $l_0 = 10 k \lambda_{dhe}$, Grid spacing: $\Delta x = 0.2 k \lambda_{dhe}$,

time interval: $\Delta t = 0.1 \omega_{pi}^{-1}$, and system length: $Lx = 40000 k \lambda_{dhe}$.

Plasma Parameters: $f = 0.055$, $\tau = 0.12$, $\kappa_{ce} = 10$, and $\kappa_{he} = 10$

(Verheest, Hellberg & Kourakis PoP 2013)

The flow velocities of the plasma species at $t = 0$ are assumed to be zero

Plasma and Simulation Parameters: Head-on collision of supersoliton with regular soliton

Perturbation used: In both densities and in ion velocity

$$n_s(x) = \begin{cases} n_{s0} \left(1 + \Delta n_s \exp \left[- \left(\frac{x-x_{ssw}}{l_{n0}} \right)^2 \right] \right), & \text{if } \omega_{pi} t = 0. \\ n_{s0} \left(1 + \Delta n_s \exp \left[- \left(\frac{x-x_{rsw}}{l_{n0}} \right)^2 \right] \right), & \text{if } \omega_{pi} t = 1100. \end{cases}$$

$$U_i(x) = \begin{cases} \Delta v_s \exp \left[- \left(\frac{x-x_{ssw}}{l_{v0}} \right)^2 \right] & \text{if } \omega_{pi} t = 0. \\ -\Delta v_s \exp \left[- \left(\frac{x-x_{rsw}}{l_{v0}} \right)^2 \right], & \text{if } \omega_{pi} t = 1100. \end{cases}$$

TABLE I. The perturbation parameters used for the generation of SSW and RSW in the simulation.

Perturbation		SSW	RSW	Normalizing unit
Density (s=we, he, i)	Δn_s	0.32	0.2	n_{0i}
	l_{n0s}	31	10	λ_{Dhe}
Velocity (s=i)	Δv_s	0.4	-0.1	C_{IA}
	l_{v0s}	20	20	λ_{Dhe}
Position	x_0	0	-12875	λ_{Dhe}
Time	t	0	1070	ω_{pi}^{-1}

Plasma Parameters: $f = 0.055$, $\tau = 0.12$, $\kappa_{ce} = 10$, and $\kappa_{he} = 10$
(*Verheest, Hellberg & Kourakis PoP 2013*)

Flow velocities of plasma species at $t = 0$ are assumed to be zero

Phase space holes in kinetic simulations

Method: Fully kinetic simulation approach based on the Vlasov-Poisson system:

Vlasov equation:

$$\frac{\partial f_j}{\partial x} + v \frac{\partial f_j}{\partial x} + \frac{q_j}{m_j} E \frac{\partial f_j}{\partial v} = 0$$

Poisson equation :

$$\frac{\partial^2 \varphi}{\partial x^2} = \frac{e}{\epsilon_0} (n_e - n_i)$$

In which f_j is the distribution function, \mathbf{E} and \mathbf{B} represent the electric and magnetic field.

Number densities:

$$n_j = \sum_{j=e,i} n_{0,i} \int f_j dv$$

in which i and e denote electron and ions respectively.

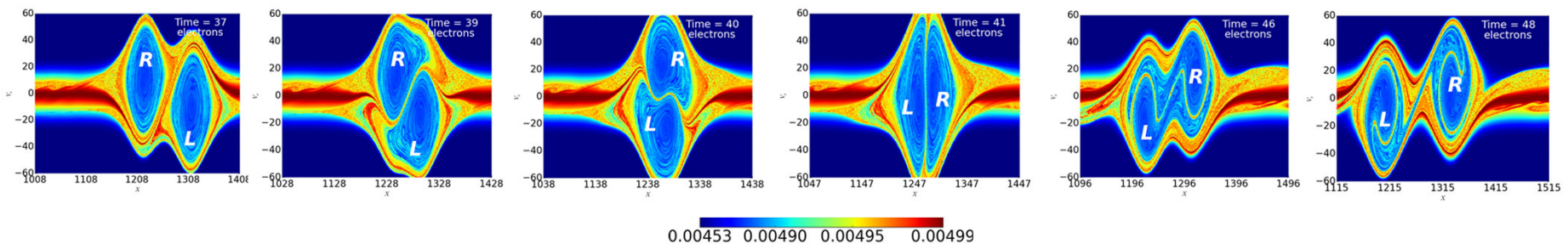
Electron Holes in the kinetic framework

- **Method:**

- Fully kinetic simulation approach based on Vlasov-Poisson equation

- **Findings:**

- 1. Electron holes accompanying solitons show strong resilience against mutual collisions.
- 2. In kinetic simulation is revealed that the internal structure of the electron hole changes after each collision without any traceable impact on the fluid-level characteristics such as density or its electrostatic feature such as electric field or potential

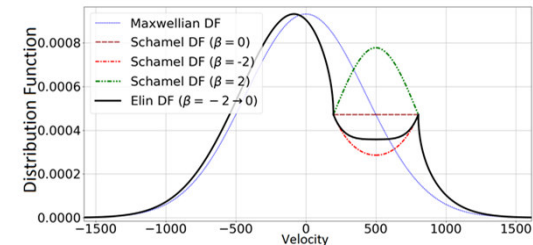


Source: SM Jenab Hosseini and F. Spanier, *Fully kinetic simulation study of ion-acoustic solitons in the presence of trapped electrons*, Physical Review E **95** 5 053201 (2017).

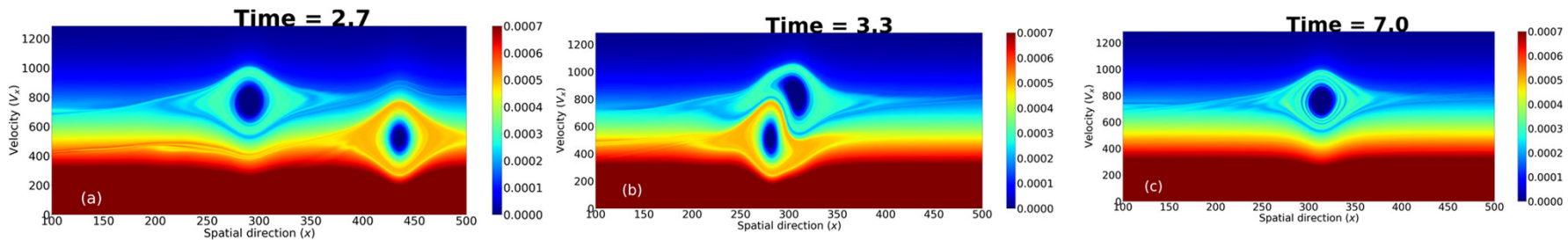
->>> See movies 1 & 2 by Mehdi Jenab

“Elin” Distribution Function for ultrafast electron holes

- Powerful simulation framework to study kinetic effects of hole and solitons
- The *Elin* df is proposed by generalizing the original Schamel df in a recursive manner.
- Adopting the *Elin* df, nonlinear solutions obtained by kinetic simulations with velocities twice the electron thermal speed coined as “Ultrafast electron holes”



Comparison of Elin DF with Maxwellian and Schamel DF



Overtaking collision of two ultrafast electron hole in the phase space

Source: SM Jenab Hosseini, G. Brodin, J. Juno & I. Kourakis, *Ultrafast electron holes in plasma phase space dynamics*, Scientific Reports, **11** (1), 1-9 (2021).

->>> See movies 3 & 4 by Mehdi Jenab

Article

Two-Parametric, Mathematically Undisclosed Solitary Electron Holes and Their Evolution Equation

Hans Schamel 

Physikalisches Institut, Universität Bayreuth, D-95440 Bayreuth, Germany; hans.schamel@uni-bayreuth.de

Received: 11 August 2020; Accepted: 25 September 2020; Published: 30 September 2020



Abstract: The examination of the mutual influence of the two main trapping scenarios, which are characterized by B and D and which in isolation yield the known sech^4 ($D = 0$) and Gaussian ($B = 0$) electron holes, show generalized, two-parametric solitary wave solutions. This increases the variety of hole solutions considerably beyond the two cases previously discussed, but at the expense of their mathematical disclosure, since $\phi(x)$, the electrical wave potential, can no longer be expressed analytically by known functions. Therefore, they belong to a variety with a partially hidden mathematical background, a hitherto unexplored world of structure formation, the origin of which is the chaotic individual particle dynamics at resonance in the coherent wave particle interaction. A third trapping scenario Γ , being independent of (B, D) and representing the perturbative trapping scenarios in lowest order, provides a broad, continuous band of associated phase velocities v_0 . For structures propagating near $C_{SEA} = 1.307$, the *slow electron acoustic speed*, a Generalized Schamel equation is derived: $\varphi_\tau + [\mathcal{A} - B\frac{15}{8}\sqrt{\varphi} + D \ln \varphi]\varphi_x - \varphi_{xxx} = 0$, which governs their evolution. \mathcal{A} is associated with the phase speed and $\tau := C_{SEA}t$ and $\varphi := \phi/\psi \geq 0$ are the renormalized time and electric potential, respectively, where ψ is the amplitude of the structure.

Additional slides for plasma and simulation parameters

Plasma and Simulation Parameters for generation of supersoliton (slides 2&3)

Initial Perturbation Form: Gaussian Potential

$$n_j = n_{j0} + \Delta n \text{Exp} \left[- \left(\frac{x - x_c}{l_0} \right)^2 \right]$$

Here, Δn is the amplitude of the perturbation, x is the position on the x -axis, x_c is the center of the system, and l_0 controls the width of the perturbation.

Simulation Parameters: $\Delta n = 1.9 n_{i0}$ and $l_0 = 10 k \lambda_{dhe}$, Grid spacing: $\Delta x = 0.2 k \lambda_{dhe}$,

time interval: $\Delta t = 0.1 \omega_{pi}^{-1}$, and system length: $Lx = 40000 k \lambda_{dhe}$.

Plasma Parameters: $f = 0.055$, $\tau = 0.12$, $\kappa_{ce} = 10$, and $\kappa_{he} = 10$

(Verheest, Hellberg & Kourakis PoP 2013)

The flow velocities of the plasma species at $t = 0$ are assumed to be zero

Plasma and Simulation Parameters: Head-on collision of supersoliton with regular soliton

Perturbation used: In both densities and in ion velocity

$$n_s(x) = \begin{cases} n_{s0} \left(1 + \Delta n_s \exp \left[- \left(\frac{x-x_{ssw}}{l_{n0}} \right)^2 \right] \right), & \text{if } \omega_{pi} t = 0. \\ n_{s0} \left(1 + \Delta n_s \exp \left[- \left(\frac{x-x_{rsw}}{l_{n0}} \right)^2 \right] \right), & \text{if } \omega_{pi} t = 1100. \end{cases}$$

$$U_i(x) = \begin{cases} \Delta v_s \exp \left[- \left(\frac{x-x_{ssw}}{l_{v0}} \right)^2 \right] & \text{if } \omega_{pi} t = 0. \\ -\Delta v_s \exp \left[- \left(\frac{x-x_{rsw}}{l_{v0}} \right)^2 \right], & \text{if } \omega_{pi} t = 1100. \end{cases}$$

TABLE I. The perturbation parameters used for the generation of SSW and RSW in the simulation.

Perturbation		SSW	RSW	Normalizing unit
Density (s=we, he, i)	Δn_s	0.32	0.2	n_{0i}
	l_{n0s}	31	10	λ_{Dhe}
Velocity (s=i)	Δv_s	0.4	-0.1	C_{IA}
	l_{v0s}	20	20	λ_{Dhe}
Position	x_0	0	-12875	λ_{Dhe}
Time	t	0	1070	ω_{pi}^{-1}

Plasma Parameters: $f = 0.055$, $\tau = 0.12$, $\kappa_{ce} = 10$, and $\kappa_{he} = 10$
(*Verheest, Hellberg & Kourakis PoP 2013*)

Flow velocities of plasma species at $t = 0$ are assumed to be zero